

**Diamond Fly Cutting Applied to Form
Accuracy Improvement by In-process
Measurement and Control on an Ordinary
Milling Machine**

APRIL 2019

GRADUATE SCHOOL OF ENGINEERING
NAGASAKI UNIVERSITY

JINHUI WANG

CONTENTS

Chapter 1 Introduction	1
1.1. Research background	1
1.2. The principle of in-process measurement and control	4
1.3. Purpose	8
1.4. Composition	9
1.5. References	11
Chapter 2 Components and configuration of control cutting system	13
2.1. Micro displacement servo (MDS)	13
2.1.1. Basic characteristic of MDS	13
2.1.2. Structure of MDS	14
2.1.3. Static rigidity of MDS	16
2.2. Optical sensors for in-process measurement	18
2.2.1. Principle of HIPOSS and optical system	18
2.2.2. Characteristics of HIPOSS and LK-H008W used for gap sensor	20
2.3. Diamond tool and fly cutter	23
2.4. Mirror and mirror jig	26
2.5. Displacement detector	26
2.6. PZT amplifier, HIPOSS amplifier and LK-H008W controller	29
2.7. Machine Tool and surface roughness tester	30
2.8. Control system for MDS	33
2.9. AD/DA conversion board	33
2.10. Software development by LabVIEW	35
2.10.1. LabVIEW	35
2.10.2. Control program	35
2.11. Calibration	38
2.12. The method of gain adjustment	39
2.13. Transient characteristics	43
Chapter 3 Noise suppression of controlled cutting	47
3.1. Control system for fly cutting	47
3.1.1. Fly cutting part configuration	47
3.1.2. Principle of control system	49
3.1.3. Fly cutting system and correcting system for hysteresis	49

3.2. Experimental conditions	50
3.3. Non-controlled cutting experiment	52
3.4. Noise suppression of controlled cutting experiment.....	58
3.4.1. The order of controlled cutting	58
3.4.2. Factors causing noise in control system.....	59
3.4.3. Results and discussion	62
3.4.4. Conclusions.....	69
Chapter 4 Feed rate experiment	70
4.1. Experimental condition.....	70
4.2. Experimental results and discussion	70
4.3. Conclusions.....	91
Chapter 5 Disturbance removal experiment	94
5.1. Experimental condition.....	94
5.2 Experimental results and discussion	95
5.3. Conclusions.....	99
Chapter 6 Experiment for improving precision of circular machining.....	101
6.1. Configuration and principle	101
6.2 Experiment result and discussion.....	104
6.3. Conclusions.....	108
Chapter 7 Summary and future work.....	109
7.1 Conclusions of each chapter	109
7.2 Future work.....	112
Acknowledgments.....	114

Chapter 1 Introduction

1.1. Research background

It is widely appreciated that the development of precision manufacturing has greatly changed our lives in terms of increased living standards. High precision manufacturing not only offers quality and reliability for conventional products, but also makes possible entirely new products, especially where mechatronics, miniaturization and high performance are important. Impressive examples are digital cameras, mobile phones, minimal invasive medical equipment as well as biotechnological or chemical processing equipment. The high function density and reduced size and weight will make the miniature and micro products more competitive.

With the development of science and technology in the 21st century, the surface of microstructure function becomes more and more intensive and diversified. It shows more and more important application value and broad application prospect in all fields [1-2]. In optical field, optical microstructures are small-scale topologies which are important part in flat-panel displays used in hand-held devices such as mobile phone, digital camera and other electronic devices. The light module enables the display screen to obtain a brighter and more uniform display effect with a smaller light source energy [3]. The use of micro-optical elements such as Fresnel lens, diffraction optical element and fan element is convenient for optical designers to optimize optical system, reduce weight, reduce volume, achieve integration, etc. [4]. It is the realization of the broad application of ultra-precision machining technology in micro structural functional surface processing. In the past few years, many countries have been strengthening this research. The application of the corresponding ultra-precision machining technology in the processing of micro optical elements is increasing [5-6]. There are many kinds of super precision machining methods for functional surfaces of microstructures. In general, single point diamond turning or milling are used. Single point diamond is the

ideal material for super precision machining as it has a sub-micrometric tool contour geometry and a nanometric cutting tool edge. In addition, it has many outstanding properties, such as super hardness, high thermal conductivity, a nanometric tool edge, and high wear resistance with low friction.

But for some complex microstructural functional surfaces that are used in special environments, due to the geometrical shape limitation of the structure and the limitation of the tool machining trajectory, other machining methods are used, such as diamond fly cutting [7]. Diamond fly cutting processing technology has been successfully used in contact lenses, prism, aspheric lens, micro lens array, pyramid microstructure surface, deceleration reflection grating microstructure surface. **Fig. 1.1** and **Fig. 1.2** shows the microstructures machined by diamond fly cutting.

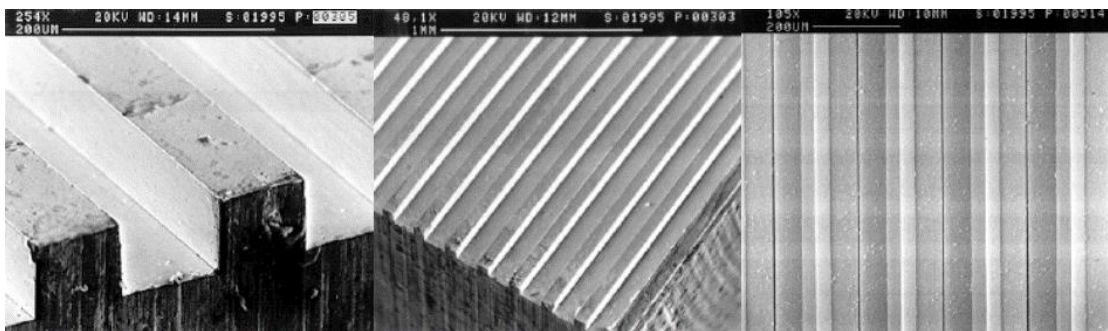


Fig. 1.1 Micro-grooves fly-cutting by Fraunhofer IPT.

(Weck, M.,Hennig, J.,Hilbing, R., Precision cutting processes for manufacturing of optical components)

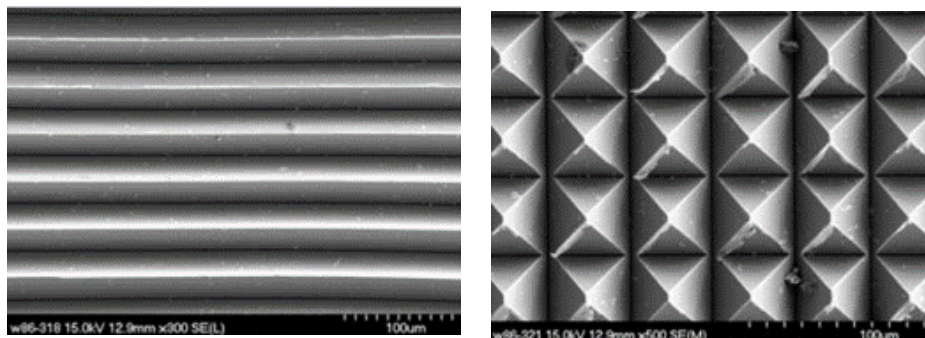


Fig. 1.2 SEM photographs of micro-structures by diamond fly-cutting.

(Zhao Qing-liang, Center for Precision Engineering, Harbin Institute of Technology)

Compared with other diamond machining methods, diamond flying cutting can produce more complex surface structures. Diamond fly cutting machining plays an extremely important role especially in the field of processing linear groove microstructure and micro groove structure composed of multiple intersecting line array, the repeatability of the prismatic matrix, pyramid matrix and microstructures for special reflective surface coatings, thin films, and magnetic tape [8]. Those microstructures process some special functions including light guiding, anti-reflective and self-clean, etc. The microstructures will further improve the performance of miniature and micro products. In addition, for the processing of planar non-rotational symmetric surface structures, diamond flying cutting is the most economical diamond processing method, because tool is not necessary to be made big adjustment in the machining process and it can directly process microstructure surface with nanometer surface quality and submicron surface shape precision without later polishing [9]. Because of the advantages in manufacturing microstructural functional surfaces, diamond fly cutting is widely used in manufacturing communications equipment, medical equipment, micro-optics element, obtaining enormous economic benefits. Therefore, it is of great significance to improve the technology level of surface manufacturing for structural functions and promote the progress of machinery manufacturing technology.

However, the high form accuracy of microstructures are just achieved on the ultra-precision milling machine and as we know the cost is very high. In ultra-precision machining, the accuracy of the machined surface is determined by the so-called copying principle. Therefore, it is important to improve the accuracy and stiffness of the machine tool and to improve the measurement accuracy of size, shape or surface roughness. Furthermore, the machining environment also affect the machining accuracy greatly. So it is the necessary condition for ultra-precision machining to suppress the influence of temperature change and vibrations of machine itself or affected from outside. Besides, for ultra-precision machining technology, the basic way to improve an accuracy of ultra-precision machine is to improve more efficient mechanical parts such as spindle,

slide, driving-unit, etc. On the other hand, some researchers are underway aimed at achieving higher accuracy by an in-process measurement and control on ordinary machines. As we know, machining and measurement were almost separated in time and space before and it is not suitable from view point of the efficiency and cost of machining. Therefore, the integration of machining and measurement in time and space named in-process measurement and control was proposed in previous research and then the effectiveness of a system named workpiece-referred form accuracy control system (WORFAC) was confirmed on a waviness improvement in experiments [10-16].

1.2. The principle of in-process measurement and control

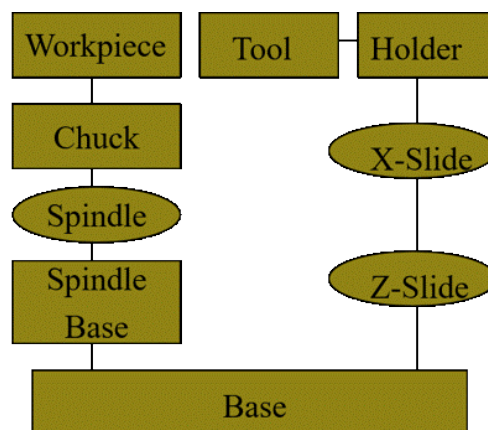


Fig. 1.3 Normal mechanical element chain.

For ordinary lathe, it has normal mechanical elements, spindle, x-axis z-axis motion elements, all of which are error factors for relative position. As shown in **Fig. 1.3**, the mechanical element chain is very long.

In in-process measurement control, as shown in **Fig. 1.4**, the mechanical element chain is short-cut by using displacement gauge and virtually minimized the mechanical element chain to eliminate error mixing. So due to the few number of components, it is difficult to be affected by disturbance and it is possible to deal with random error and

realize high precision processing. Meanwhile, for in-process measurement, because the location and time of processing and measurement are consistent, the processing ends at the same time the measurement ends, so it can greatly shorten the processing time.

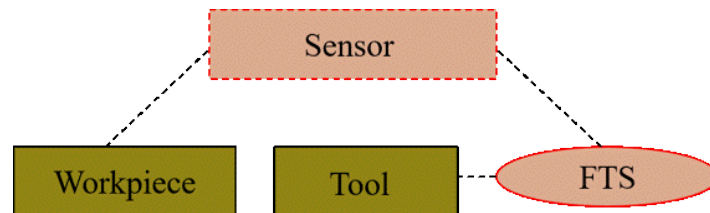


Fig. 1.4 Mechanical element chain of WORFAC.

As mentioned above, some researchers aimed at achieving higher accuracy by in-process measurement and control and they proposed a system named workpiece-referred form accuracy control system (WORFAC).

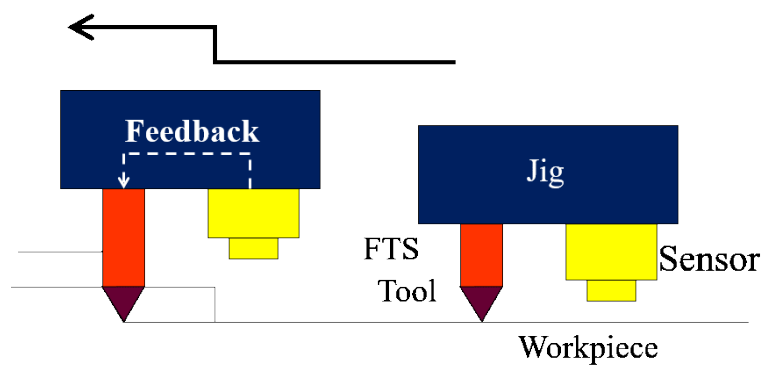


Fig. 1.5 The principle of in-process measurement and control.

Fig. 1.5 shows the principle of in-process measurement and control. A displacement gauge attached to the tool base measures the relative displacement between the tool base and the processing surface. This measured data is immediately fed back to the minute cutting device attached to the tool base so that the relative position between the tool and the processed surface is always constant even if the relative position between

the tool table and the processed surface changes processing is performed by controlling the minute cut amount. As a result, high precision machining can be realized without being influenced by errors existing in the spindle or the feed table.

So far, the method of WORFAC almost applied to lathe to improve the accuracy of machined surface by diamond turning. The cylinder surface precision of workpiece is improved by eliminating x-axis z-axis motion error. Even if we can change the tool with different shape of nose to manufacture different microstructures by the method on lathe. However, non-rotational symmetric surface structures such as V-groove, pyramid structures, F-theta lens and other freeform surfaces cannot be machined by diamond turning.

To manufacture microgroove on ordinary lateral milling machines, the controlled cutting with reference surface (CCRS) [17], which is based on WORFAC, was used to improve the form accuracy in previous research [18]. **Fig.1.6** shows the CCRS principle. Displacement sensing is based on the reference surface on the support jig fixed directly on the workpiece holder. Both the micro tool servo (MTS) for controlling the micro depth of cut and the gap sensor are fixed on the tool table to satisfy the Abbe' s principle, so table motion error is assumed to be negligible except in the depth-of-cut direction. Sensing relative displacement between the sensor and the reference surface is equivalent to measuring the relative displacement between the cutting tool and workpiece. The feedback signal from the sensor is led to MTS, and micro depth of cut is controlled by the MTS, so relative displacement between the cutting tool and workpiece is kept constant.

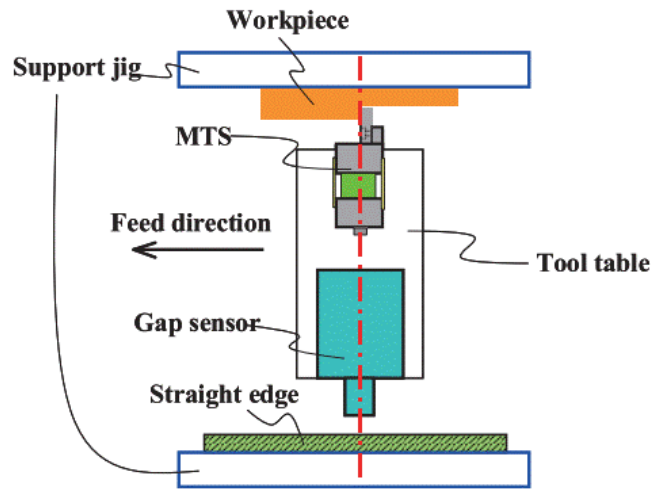


Fig. 1.6 controlled cutting with reference surface.

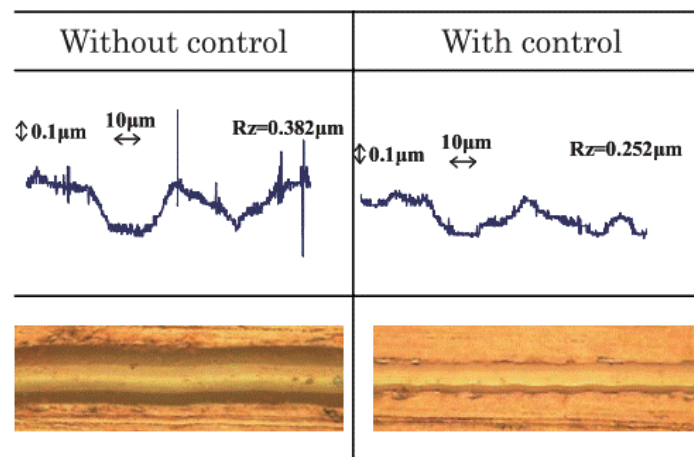


Fig. 1.7 example of microgroove shaping without/with CCRS.

Fig. 1.7 shows the example of microgroove shaping without CCRS and with CCRS. The research showed that accuracy can be improved if digital control sampling time is enough shorter than the error motion determined by feed rate. However, the surface roughness became worse when slow down the feed rate because the feed rate equals cutting speed in shaping. Consequently, fly cutting with CCRS was proposed since fly cutting can work at a high cutting speed and a low feed rate. As illustrated in **Fig. 1.8**, fly cutting is a typical intermittent cutting process, whereby the diamond tool rotates

with high speed, cutting into and out of the workpiece surface intermittently and we can see that the cutting speed and feed rate are independent. By every rotary cut, a crater is formed while the piece and piece of crater cutting generate the desired surface structures.

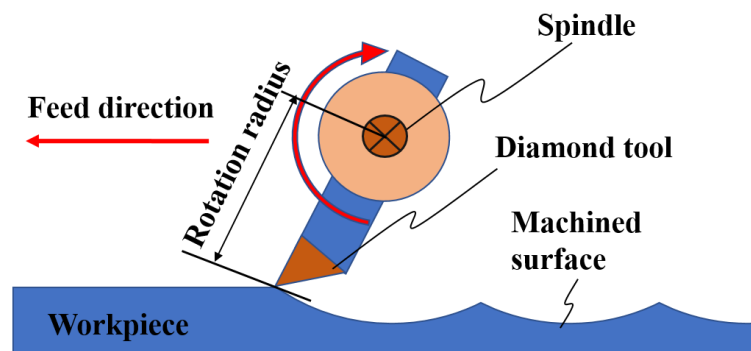


Fig. 1.8 Schematic of fly cutting.

1.3. Purpose

Fly cutting usually applied to manufacture ultra-precision microstructures with nanometric surface roughness and sub-micrometric form accuracy, without the need for any subsequent polish. Nevertheless, the high level of accuracy was just achieved on the ultra-precision milling machine.

In this study, fly cutting was utilized to improve the form accuracy of machined surface on an ordinary milling machine by using controlled cutting with reference surface (CCRS), which is a processing method by in-process measurement and control. This study will prove that the form accuracy can be improved on an ordinary milling machine by this control cutting system.

1.4. Composition

In order to set forth the research, the flowchart of each chapter as shown in **Fig.1.9**

- 1) Chapter 2: This chapter will introduce the components and configuration used in control cutting system, including micro displacement servo (MDS), optical sensors for in-process measurement, diamond tool and fly cutter, mirror and mirror jig, displacement detector, PZT amplifier, HIPOSS amplifier and LK-H008W controller. Machine tool and surface roughness tester used for experiment are also be introduced. The software part and the configuration of control cutting system were introduced.
- 2) Chapter 3: The noise in the control cutting system has a bad influence on machined surface. Therefore, noise suppression experiments were carried out. Low-pass filter was used for suppressing noise. And the machined surface machined with and without controlled cutting were discussed.
- 3) Chapter 4: The relationship between feed rate and machined surface with and without controlled cutting were discussed and how to machine a good quality surface by changing feed rate with controlled cutting was elucidated
- 4) Chapter 5: By the control cutting system, not only the machine error but also the disturbance form outside should be suppressed. Therefore, disturbance removal experiments were carried out and the effectiveness of this control system on suppressing disturbance was confirmed.
- 5) Chapter 6: Based on the mechanism of the control cutting, the precision of circular machining using an ordinary milling machine should be improved by a cylindrical concave mirror used as reference surface. To prove it, experiments for improving precision of circular machining were carried out and the results were discussed.
- 6) Chapter 7: The researches until now will be summarized, and what will do from now on.

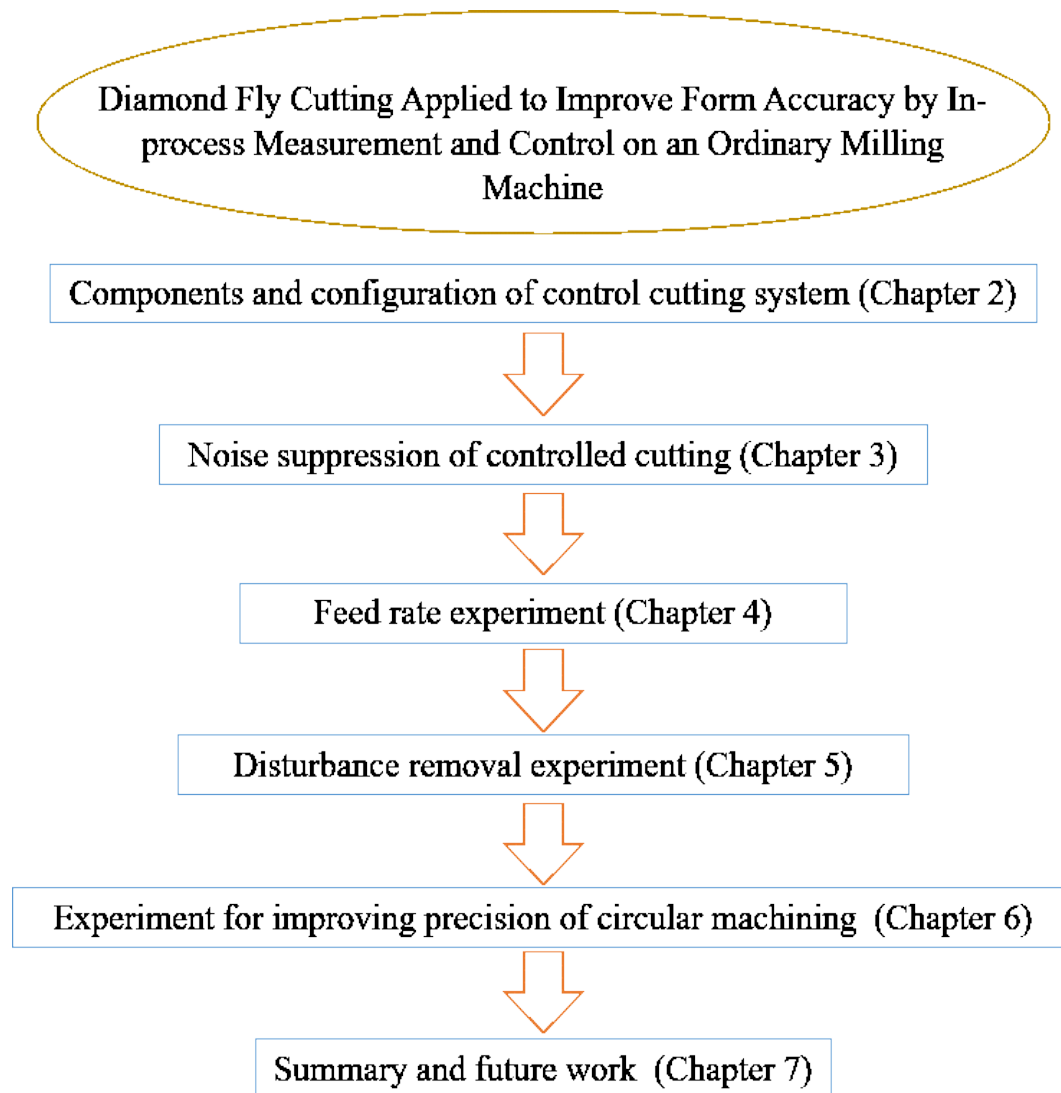


Fig. 1.9 Flowchart of each chapter.

1.5. References

- [1] K.H. Brenner, M. Kufner, S. Kufner, J. Moisel, A. Müller, S. Sinzinger, M. Testorf, J. Göttert. Application of Three-dimensional Micro-optical Components Formed by Lithography, Electroforming, and Plastic Molding. *Applied Optics*. 1993, 32: 6464~6469.
- [2] G. Sotgiu, L. Schirone. Microstructured Silicon Surfaces for Field Emission Devices. *Applied Surface Science*. 2005, 240: 424~431.
- [3] W. Lee, S. To, C. Cheung, D. Gao, and W. Chiu, Ultra-precision machining of optical microstructures, *Nanotechnology and precision engineering*, 2003.
- [4] M. Weck and S. Fischer, Manufacturing of Microstructures Surfaces Using Ultraprecision Turning, Milling and Shaping. *Proceedings of the 1st International Conference and General Meeting of the European Society for Precision Engineering and Nanotechnology (euspen)*. 1999, 420~423.
- [5] N. Ikawa, R. Donaldson, R. Komanduri, W. König, P. McKeown, T. Moriwaki, I. Stowers, Ultraprecision metal cutting—the past, the present and the future, *CIRP Annals-Manufacturing Technology*, 40 (1991) 587-594.
- [6] E. Paul, C.J. Evans, A. Mangamelli, M.L. McGlaufflin, R.S. Polvani, Chemical aspects of tool wear in single point diamond turning, *Precision Engineering*, 18 (1996) 4-19.
- [7] L. Autschbach, E. Brinksmeier, W. Preuß, O. Riemer, Manufacturing of micro structured molds for an operating light system, *HTM – Haertere-Technische Mitteilungen*, Volume 60, Issue 3, 2005, Pages 183~189.
- [8] M. Weck, J. Hennig, R. Hilbing, Precision cutting processes for manufacturing of optical components, *Proceedings of SPIE – The International Society for Optical Engineering* 4440, 2001:145~151.
- [9] M. Cheng, C.F. Cheung, W.B. Lee, S. To, A study of factors affecting surface quality in ultra-precision raster milling, in: *Key Engineering Materials*, Trans Tech Publ, 2007, pp. 400-406.

- [10]T. Kohno, Y. Okazaki, N. Ozawa, K. Mitui, M. Omoda, In-process measurement and a workpiece-referred form accuracy control system (WORFAC): concept of the method and preliminary experiment, *Precision engineering*, 11 (1989) 9-14.
- [11]Y.Uda, et al, In-process measurement and a workpiece-referred form accuracy control-The servo control of cylindrical turning for an ordinary lathe, *Int. J. Japan Soc. Prec. Eng.*, p.385, Vol.27, No.4, 1993.
- [12]T. Yazawa, Y. Uda, T. Kohno, Accuracy improvement of machine tool by workpiece-referred control-Simulation of sensor position for plain turning, in: *Advancement of Intelligent Production*, Elsevier, 1994, pp. 233-240.
- [13]Y. Uda, T. Kohno, T. Yazawa, In-process measurement and workpiece-referred form accuracy control system (WORFAC): application to cylindrical turning using an ordinary lathe, *Precision engineering*, 18 (1996) 50-55.
- [14]Y. Uda, T. Kohno, T. Yazawa, T. Suzuki, A. Soyama, Concept and basic study of improvement system of surface roughness, waviness and figure accuracy by WORFAC, *Journal of materials processing technology*, 62 (1996) 423-426.
- [15]T. Yazawa, T. Kohno, Y. Uda, N. Ohno, In-Process Measurement and Workpiece-Referred Form Accuracy Control (6th Report), *Journal of the Japan Society for Precision Engineering*, 64 (1998) 1806-1810. (in Japanese)
- [16]T. Kohno, T. Yazawa, D. Saito, S. Kohno, Figure error control for diamond turning by in-process measurement, *Precision engineering*, 29 (2005) 391-395.
- [17]T. Yazawa, T. Yamazaki, and T. Kohno, In-Process Measurement and Workpiece-Referred Form Accuracy Control (7th Report), *Journal of the Japan Society for Precision Engineering*, vol. 64, no. 11, pp. 1689-1693, 1998. (in Japanese)
- [18]T. Yazawa, Y. Hattori, Y. Ogiya, and T. Kojima, Figure Error Control for Microgrooving on Ordinary Lateral Milling Machines Using a Reference Surface to Control Cutting, *International Journal of Automation Technology*, vol. 3, no. 4, pp. 428-432, 2009.

Chapter 2 Components and configuration of control cutting system

2.1. Micro displacement servo (MDS)

2.1.1. Basic characteristic of MDS

In a machining experiment based on controlled cutting with reference surface (CCRS), a micro displacement servo (hereinafter referred to as MDS) is required to control the minute displacement amount. The following functions are required for this PZT part.

- High positioning resolution of displacement.
- Have high speed responsiveness.
- Have high rigidity so that the position of the displacement is not affected by the variation of the cutting resistance.
- Compact and lightweight.

Piezoelectric elements (PZT), as shown in **Fig.2.1**, are considered most suitable as actuators in terms of high resolution, high driving force, small size and light weight, low power consumption, high speed response, impact resistance and so on. However, there is a disadvantage that the amount of generated displacement is small and hysteresis is present. However, for the former, those which are quite good and inexpensive as multilayered piezoelectric elements are commercially available, and for

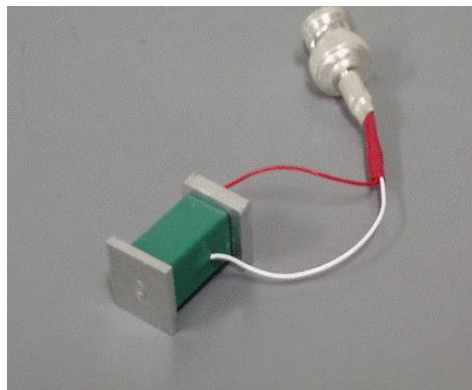


Fig. 2.1 PZT actuator.

the latter, it does not become a problem in control loop. The method of eliminating hysteresis will be mentioned later. **Table 2.1** shows the specification of PZT actuator.

Table 2.1 Specification of PZT actuator

Standard operating temperature range [°C]	-25 ~ + 85
Max. operating voltage [V _{DC}]	150
Open-loop travel [μm]	18.4±3.5
Pushing force [N]	3500
Unloaded resonant frequency [kHz]	69
Size [cm]	11.5×11.5×20

2.1.2. Structure of MDS

Fig. 2.2 and **Fig. 2.3** show the structure of MDS. The structure of the MDS adopts a mechanism in which a total of four leaf springs of phosphor bronze are installed as an elastic supporting and guiding mechanism, and a laminated piezoelectric element (PZT) is used as a driving source.

The fixing base for fixing the tool, PZT and leaf spring are divided into the Head part and the Base part, the Head part is designed to be lightweight because the micro displacement generated by the PZT actuator is transmitted directly to the workpiece that glued to head side rigidly by hot melt adhesive. So the head part material is aluminum alloy A5052. In addition, since the base part is integrated with the tool base, it is required not to be influenced by micro displacement generated by the PZT actuator, so it is required to be rigid, and the material is carbon steel S45C.

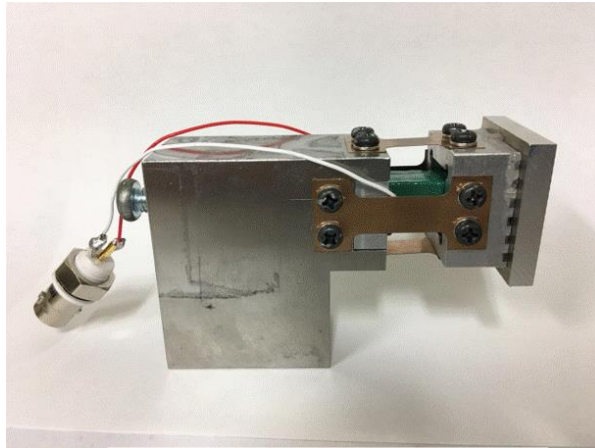


Fig. 2.2 Picture of MDS.

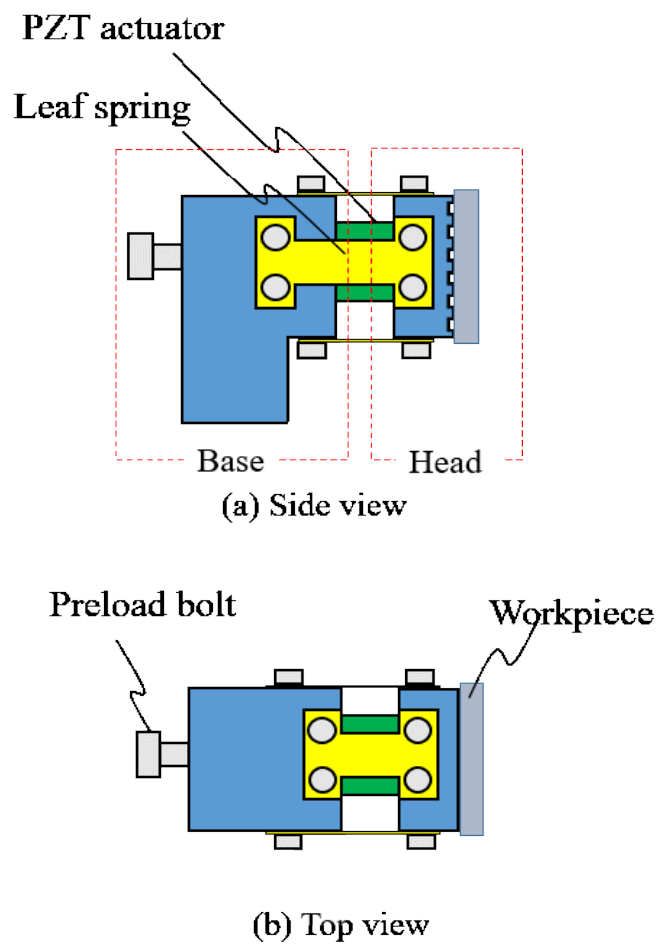


Fig. 2.3 External view of MDS.

Table 2.2 shows the property of Leaf Spring and **Table 2.3** shows the property of materials for Head part and Base part.

Table 2.2 Property of Leaf Spring

Material	Phosphor bronze
Young's modulus[GPa]	110
Density [g/cm ³]	8.8
Elongation[%]	11
Spring limit[MPa]	460

Table 2.3 Property of materials for Head part and Base part

	Material	Young's modulus[GPa]	Tensile strength[MPa]	Density [g/cm ³]
Head part	Aluminum ally A5052	69	243	2.68
Base part	Carbon steel S45C	206	569	7.86

2.1.3. Static rigidity of MDS

The static rigidity and transient characteristics of MDS were confirmed. For confirmation of static rigidity, as shown in **Fig. 2.4**, a force was applied to the A point of MDS in the direction of the arrow by a tension gauge, and the amount of displacement at points B and C was measured using an electric micrometer. As an experimental condition, at the time of measurement, a voltage of 80 V was added to PZT and control was not carried out. Since the strength of the applied force is adjusted by reading the scale of the tension gauge, it is considered that some errors occur. Under

the above conditions, the amount of displacement with respect to the applied force is as shown in **Fig.2.5**. The static stiffness value obtained from this result is $0.12 \text{ N}/\mu\text{m}$. This shows that it is sufficiently rigid to the cutting resistance generally called several percentage N. As for the PZT, since a force of 3500 N is generated while voltage is being applied, it is considered that the distortion is negligible compared to cutting

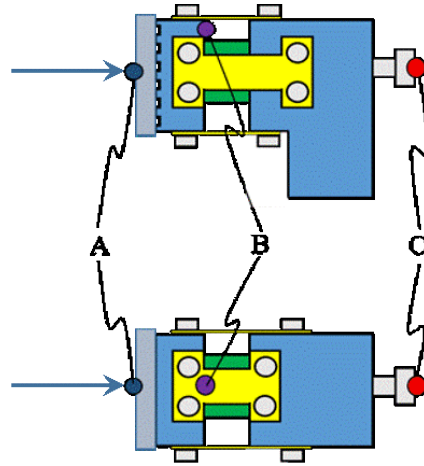
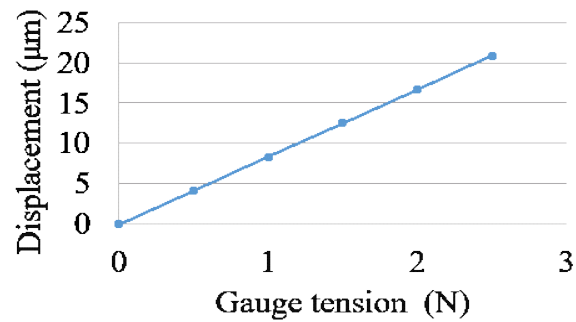
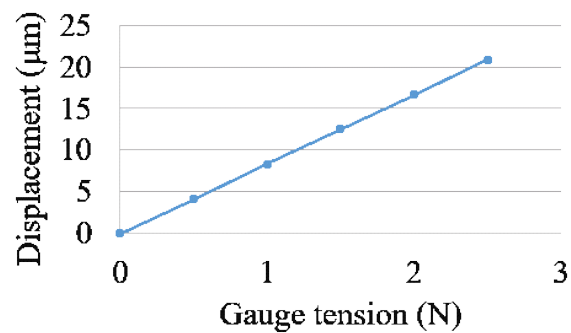


Fig. 2.4 Measurement point for checking static stiffness.



(a) Head section



(b) Base section

Fig. 2.5 Static stiffness of MDS.

resistance.

2.2. Optical sensors for in-process measurement

2.2.1. Principle of HIPOSS and optical system

HIPOSS (high-precision optical surface sensor) is a photochromic needle type micro-displacement meter using a critical angle method utilizing a sudden change in light quantity near the critical angle of the critical angle prism. **Fig. 2.6** shows the principle of the critical angle method.

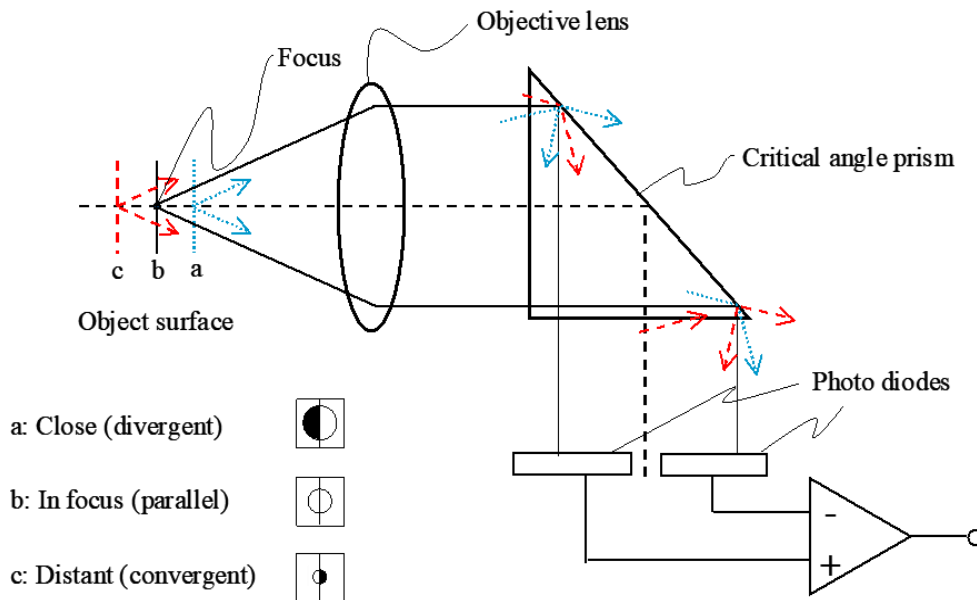


Fig. 2.6 Principle of critical angle method.

When the measurement surface is at the focal position (b) of the objective lens, the light passing through the objective lens becomes a parallel light flux and is incident on the prism set at the critical angle. Since the luminous flux is totally reflected by the prism, the same quantity of light is incident on the two photodiodes. On the other hand, in the case (a) where the measurement surface is a surface closer than the focal position, the light beam becomes divergent light and the incident angle becomes smaller in the

upper half of the optical axis, so that it is not totally reflected. Similarly, in the case (c) where the measurement surface is a surface farther than the focal position, the luminous flux becomes convergent light and the incident angle becomes small at the lower half of the optical axis, so that it is not totally reflected. As a result, a difference in light amount occurs between the two photodiodes. This light quantity difference can be output as the displacement amount of the surface. This is the principle of the critical angle method.

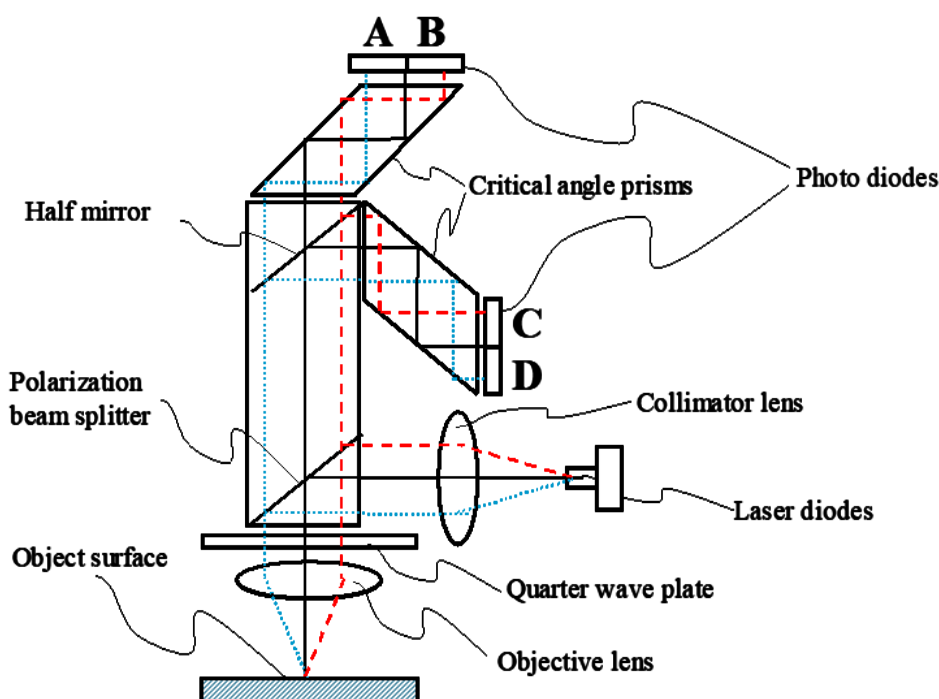


Fig. 2.7 Optical system of HIPOSS.

Fig. 2.7 shows the optical system of HIPOSS. The beam emitted from the laser diode passes through the collimator lens, becomes parallel light, passes through the polarization beam splitter and the quarter wave plate, and focuses on the measurement surface. The reflected light again passes through the quarter-wave plate and the polarization beam splitter, and the light beam is divided in two directions by the half mirror. The divided luminous flux is reflected twice by the critical angle prism and is

incident on the two division diodes. The sensitivity is raised by reflecting twice in the prism.

Let signals A, B, C and D be the signals of the light receiving elements.

$$(A - B) + (C - D) \quad (2.1)$$

A displacement signal is obtained by the calculation of equation (2.1). As a result, even if inclination occurs on the measurement surface, it can be corrected to ± 5 degrees.

$$E = \frac{(A - B) + (C - D)}{A + B + C + D} \quad (2.2)$$

An output signal is obtained by the calculation of equation (2.2). By dividing by the sum of the whole, it can be made dimensionless, and it is possible to eliminate the influence of the temperature change of the light source and the change of reflectance of the measurement surface.

2.2.2. Characteristics of HIPOSS and LK-H008W used as gap sensors

Fig. 2.8 and **Fig. 2.9** shows the appearance of HIPOSS and LK-H008W respectively. **Table 2.4** shows the characteristics of HIPOSS and LK-H008W.

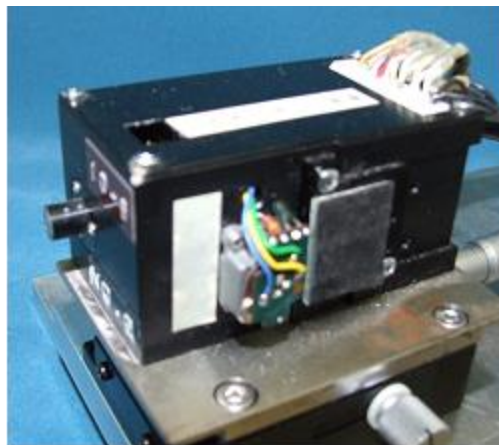


Fig. 2.8 Picture of HIPOSS.



Fig. 2.9 Picture of LK-H008W.

Table 2.4 Specifications of HIPOSS and LK-H008W

	HIPOSS	LK-H008W
Limit of resolution [nm]	0.2	5
Dynamic range [μm]	2	1000
Response frequency [kHz]	10	5
Working distance [mm]	0.6	8
Spot diameter [μm]	1.6	20
Size [mm]	$51 \times 38 \times 86$	$66 \times 73.5 \times 27.5$

As shown in **Table 2.4**, HIPOSS has a very short working distance of 0.6 mm, and it is necessary to pay close attention so that the lens does not come into contact with the measuring surface at the time of measurement. Therefore, when applied to in-process measurement and near to the processing side, chips and the like are sandwiched between the workpiece and the objective lens, which also causes a measurement error. Moreover, since the dynamic range is as narrow as $2\mu\text{m}$, when roughness and straightness of the workpiece exceed this value, it may deviate from the measurement area and the control system will cannot be controlled. While LK-H008W has a long working distance of 8 mm which is much farer than that of HIPOSS and the dynamic range is so wide that it

is not easily interfered in the cutting process. For those reasons, LK-H008W was chosen to work at fly cutting side.

Before controlled cutting, it is necessary to warm up the machine and devices for control cutting system. Among these, HIPOSS and LK-H008W always take a long time. **Fig.2.10** and **Fig.2.11** show that the time spent reaching a relatively stable state of HIPOSS and LK-H008W. Both them will take about 30 minutes to reach a relatively stable state and then gap sensors drift (measurement error) will be less than $0.02\ \mu\text{m}$ in 2 minutes, which calculated by sensitivity of HIPOSS (sensitivity : $5\mu\text{m}/\text{V}$) and LK-H008W (sensitivity : $1\mu\text{m}/\text{V}$). It is quite small along machined length of 10 mm when feed rate is 5 mm/min.

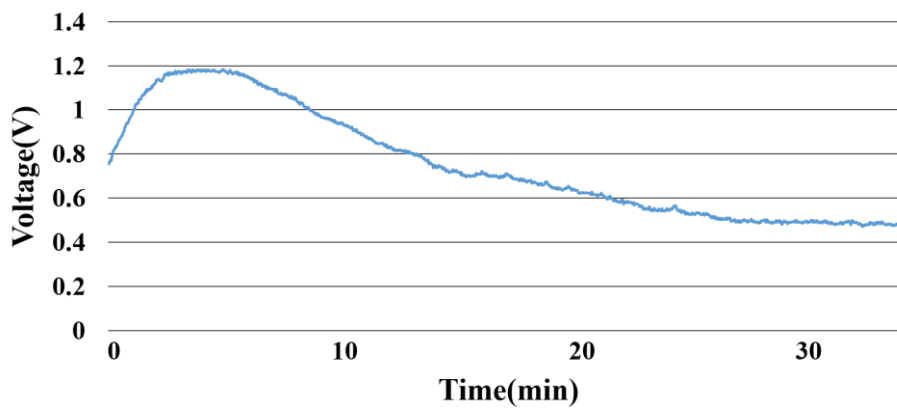


Fig. 2.10 Time spent reaching a relatively stable state of HIPOSS.

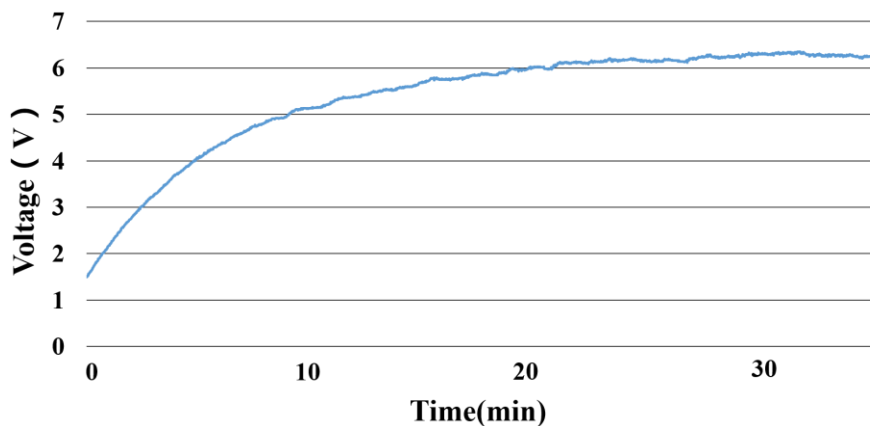


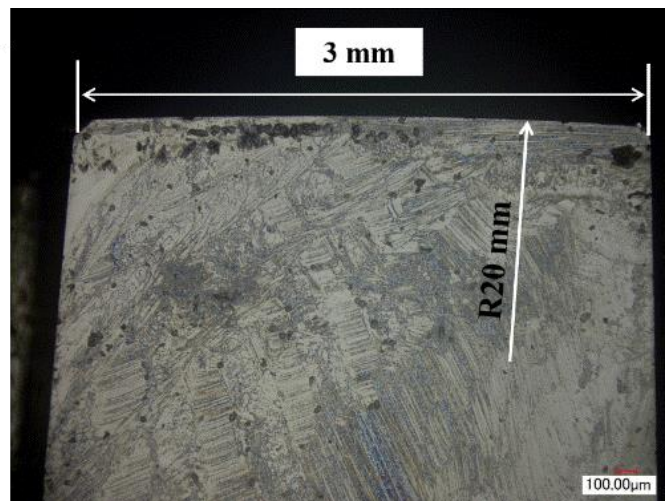
Fig. 2.11 Time spent reaching a relatively stable state of LK-H008W.

2.3. Diamond tool and fly cutter

Almost maternal principle holds for cutting work of diamond tool and the geometry of diamond cutting edge can imprint into machined surface. **Fig.2.12** shows the cutting edge of single crystal diamond tool used for control processing experiments. The nose of this diamond tool is R20mm. **Table 2.5** shows the specifications of diamond tool.



(a) Top view of single crystal diamond tool.



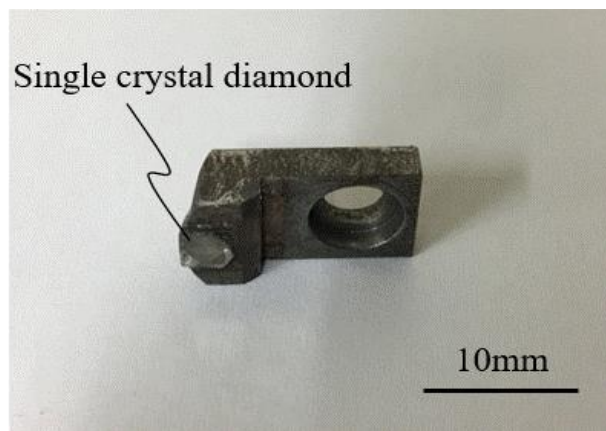
(b) Front view of single crystal diamond tool.

Fig. 2.12 Single crystal diamond tool.

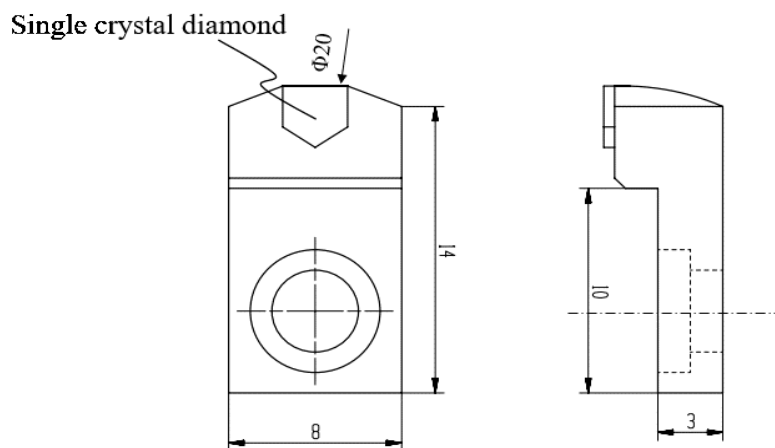
Table 2.5 Specifications of diamond tool

material	Single crystal diamond
Rake angle	5
Clearance angle	2500
Noise radius [mm]	20

Fig. 2.13 shows the single crystal diamond holder. It is fixed rigidly in fly cutter as shown in **Fig. 2.14**.

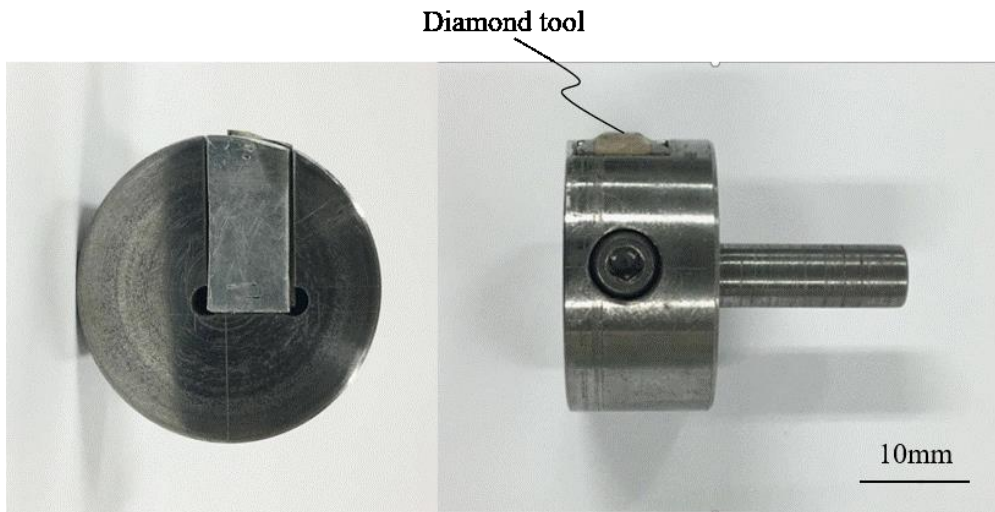


(a) Picture of single crystal diamond holder

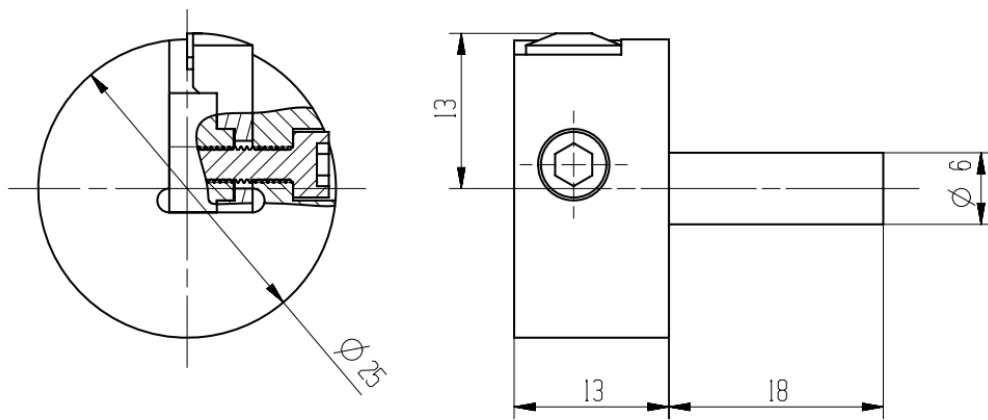


(b) Schema of single crystal diamond holder

Fig. 2.13 Single crystal diamond holder.



(a) Picture of fly cutter



(b) Schema of fly cutter

Fig. 2.14 Fly cutter.

2.4 Mirror and mirror jig

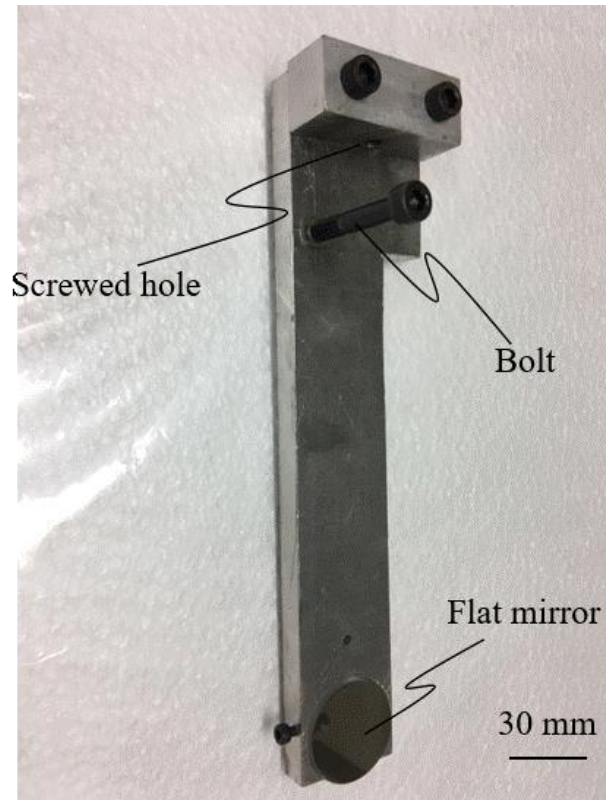


Fig. 2.15 mirror and mirror jig.

Fix mirror jig onto machine body using a bolt through the screwed hole. And then beat the bolt as shown in **Fig. 2.15** to adjust the mirror angle to ensure that the mirror is parallel to feed direction.

2.5. Displacement detector

Conventionally, we measured the amount of displacement of the PZT built into the MTS (used in previous experiments) with a strain gauge affixed to the leaf spring to detect the minute cut amount of the tool. However, this time we prepared another pair of the same mechanisms as PZT and MDS of the same type, and we made the same movement theoretically by giving the same signal to the two PZTs. Then, the movement

amount of PZT is measured by HIPOSS in the displacement amount detection section, and the result is fed back as the control amount.

The advantage of adopting this method is that it eliminates the need for a strain gauge, so that it was possible to remove the bridge box that was previously installed and to make the tool stand smaller. Also, in measuring the displacement of PZT, selecting and installing a place with less disturbance makes it difficult for the control signal to be affected by noise, which improves measurement accuracy. On the other hand, the problem is whether the measured amount of displacement of PZT is actually equal to the amount of displacement of MDS. This is to prepare screws for preloading PZT in the BASE section of MDS and calibrating beforehand to compensate so that the displacements of the two PZTs become equal.

Here, since the processing force generated in ultra-precision cutting is as small as several percentage N, it is considered that there is no problem even if another PZT actuator is prepared and the displacement is used as the state quantity. Therefore, the displacement amount is measured by another PZT actuator under another similar specification and condition, and it is used as a control amount to form a feedback loop. Since the dynamic range of HIPOSS is as narrow as $2\ \mu\text{m}$, in this study, it is used as gap sensor of displacement detector, as shown in **Fig. 2.16**.

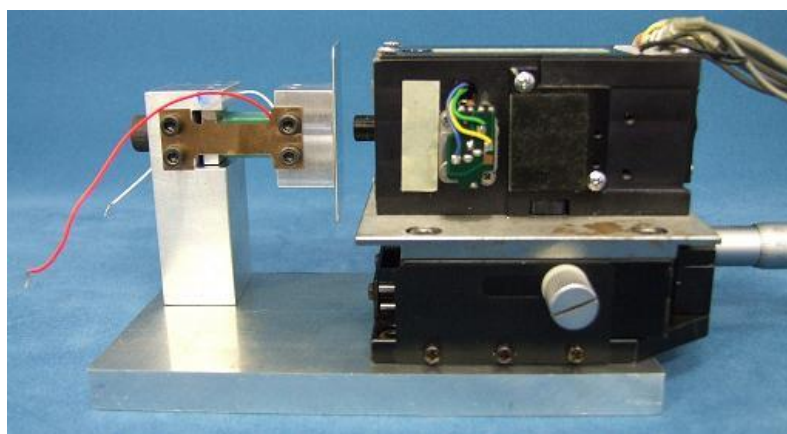
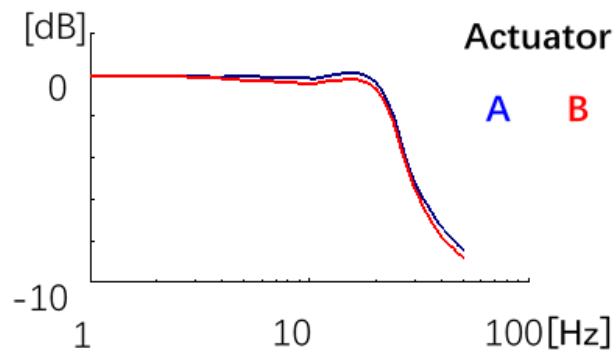
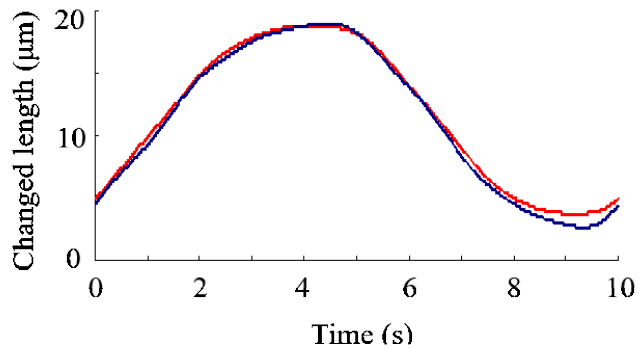


Fig. 2.16 Picture of displacement detector.

This device is required to operate in the same way as the actuator on the MDS side in order to accurately know the position of the cutting edge. The graph of **Fig. 2.17 (a)** shows the gain curves of the frequency characteristics of the two actuators. From the graph, you can see that there is little difference. The graph of **Fig. 2.17 (b)** shows the motion when a sine wave input is given. From here it is understood that there is almost no difference. Therefore, it can be said that state quantity detection by this method is possible. As a merit of this method, since it is possible to isolate the equipment from the stage, MDS can be miniaturized and robust against disturbance can be obtained.



(a) Gain curves comparison of two actuators



(b) Waveform comparison of two actuators

Fig. 2.17 Comparison of two actuators.

2.6. PZT amplifier, HIPOSS amplifier and LK-H008W controller

The PZT amplifier, HIPOSS amplifier and LK-H008W controller used in control system are shown in **Fig. 2.18**, **Fig. 2.19** and **Fig. 2.20**.



Fig. 2.18 Photographs of PZT amplifier.



Fig. 2.19 Photographs of HIPOSS amplifier.



Fig. 2.20 LK-HD500 used as LK-H008W controller.

2.7. Machine Tool and surface roughness tester

In this research, we use an ordinary milling machine installed in an environment not performing vibration isolation and temperature control. The appearance and specification of the milling machine used for the experiment are shown in **Fig.2.21** and **Table2.6**. The profile of machined surface was measured by the digital microscope ACCRETECH SURFCOM130A as shown in **Fig.2.22**.



Fig. 2.21 Picture of milling machine (Osakakiko rakuraku-mill 3V).

Table 2.6 Specifications of milling machine

Model name		Osakakiko rakuraku-mill 3V
Company		OKK Ltd.
Table size		1650x380mm
Feeding direction	X-direction	920 (mm)
	Y-direction	380 (mm)
	Z-direction	450 (mm)



(a) Detector



(b) Operator

Fig. 2.22 Photographs of surface roughness tester (ACCRETECH SURFCOM130A).

2.8. Control system for MDS

In control, closed loop control is performed in order to eliminate the hysteresis characteristic of the multilayered piezoelectric element which is an actuator incorporated in the MDS. The control method is I-PD control. Since this I-PD control works as an I operation for the target value input and a PD operation for the disturbance, there is no offset with respect to the target value input, and it is possible to respond appropriately to disturbance. However, as compared with PID control, the differentiation operation is not added to the target value input, so the control speed is slow. For this reason, it can be said that it is not suitable for true follow-up control, but it is suitable for suppressing overshoot with respect to target value input.

2.9. AD/DA conversion board

There are two kinds of AD/DA conversion boards in my hand, USB-6008 and AIO-163202FX-USB as shown in **Fig. 2.23** and **Fig. 2.24**. The specifications of them are shown in **Table 2.7**.



Fig. 2.23 Picture of USB-6008.



Fig. 2.24 Picture of AIO-163202FX-USB.

Table 2.7 Specifications of USB-6008 and AIO-163202FX-USB

	USB-6008	AIO-163202FX-USB
Bus	USB	USB
Analog inputs	8	32
Input resolution[bit]	12	16
Max sampling rate[kS/s]	10	500
Input range[V]	0 to ± 10	0 to ± 10
Analog outputs	2	2
Output resolution[bit]	12	16
Output rate[Hz]	150	100000
Output range[V]	0 to 5	0 to ± 10

In this study, the software LabVIEW was used for control cutting system. When use USB-6008 for AD input and DA output, the system response frequency is about 1300Hz in I-PD simulation. Actually, in in-process measurement and control cutting process, a certain positive voltage should be input to PZT actuator by PZT amplifier so that the PZT actuator can start at a certain stretched length. And then when control start, by DA output relevant negative voltage or positive voltage into PZT actuator through PZT

amplifier, the PZT actuator can retract or stretch. Nevertheless, USB-6008 cannot output negative voltage. So it cannot be used for AD input and DA output simultaneously. While, when use AIO-163202FX-USB for AD input and DA output, the system response frequency is about 33.3Hz in I-PD simulation and it is much slower than AIO-163202FX-USB for AD input and DA output. Maybe AIO-163202FX-USB is not very compatible with LabVIEW.

Considering that, when use USB-6008 for AD input and use AIO-163202FX-USB for DA output, the system response frequency is about 77Hz in I-PD simulation and it is faster than that when use AIO-163202FX-USB for AD input and DA output. So this method was adopted in my study.

2.10. Software development by LabVIEW

2.10.1. LabVIEW

In this research, we created a control program using LabVIEW. LabVIEW is a programming language realizing the virtual instrument developed by NATIONAL INSTRUMENTS INC. In 1986, and it is possible to carry out the entire process from acquisition, analysis and display of data on a personal computer. Also, LabVIEW is a programming language that allows you to work with visual operations like Visual Basic and Visual C++, rather than programming languages with descriptive expressions using character strings such as traditional C and Fortran languages. Yes, programming can be done easily by placing objects and wiring. In this research, in order to perform reference plane reference control processing, LabVIEW creates control programs and acquires data to construct a control system.

2.10.2. Control program

A flow chart of the control program created by LabVIEW for control processing is shown in **Fig. 2.25**.

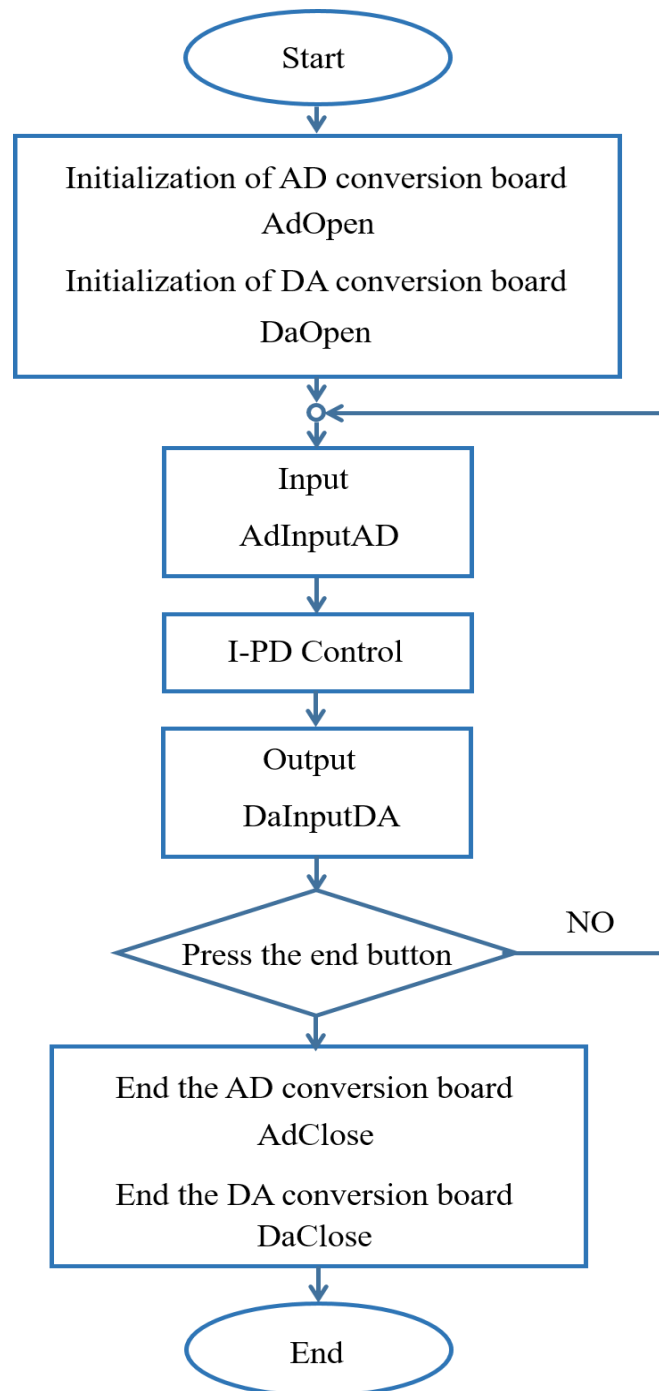
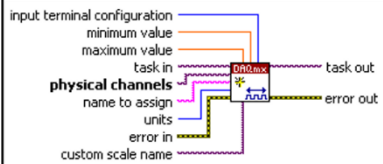
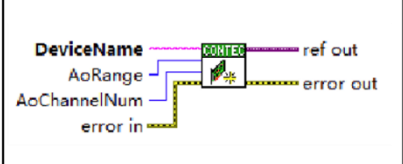
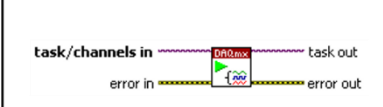
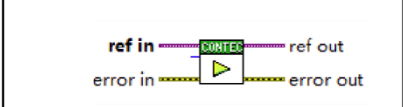
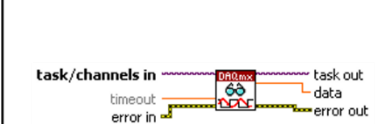
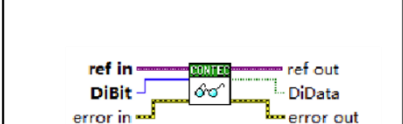
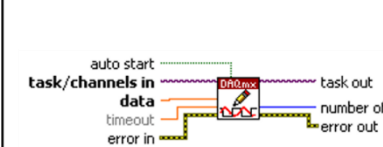
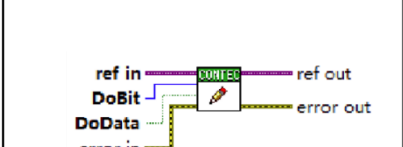




Fig. 2.25 Flow chart of control system.

The control program is attached to the appendix. We have created a program using VI (Diagram) which provides interface to use AD/DA conversion board under LabVIEW environment of NATIONAL INSTRUMENT.

Table 2.8 DAQmx - Data Acquisition VIs and Functions.

USB-6008	AIO-163202FX-USB	Functions of VI
 <p>input terminal configuration minimum value maximum value task in physical channels name to assign units error in custom scale name</p> <p>task out error out</p>	 <p>DeviceName AoRange AoChannelNum error in</p> <p>ref out error out</p>	<p>Creates a virtual channel or set of virtual channels and adds them to a task.</p>
 <p>task/channels in error in</p> <p>task out error out</p>	 <p>ref in error in</p> <p>ref out error out</p>	<p>Transitions the task to the running state to begin the measurement or generation. Using this VI is required for some applications and is optional for others.</p>
 <p>task/channels in timeout error in</p> <p>task out data error out</p>	 <p>ref in DiBit error in</p> <p>ref out DiData error out</p>	<p>Reads samples from the task or virtual channels you specify. The instances of this polymorphic VI specify what format of samples to return, whether to read a single sample or multiple samples at once, and whether to read from one or multiple channels.</p>
 <p>auto start task/channels in data timeout error in</p> <p>task out number of error out</p>	 <p>ref in DoBit DoData error in</p> <p>ref out error out</p>	<p>Writes samples to the task or virtual channels you specify. The instances of this polymorphic VI specify the format of the samples to write, whether to write one or multiple samples, and whether to write to one or multiple channels.</p>
 <p>task/channels in error in</p> <p>task out error out</p>	 <p>ref in error in</p> <p>error out</p>	<p>Stops the task and returns it to the state the task was in before the DAQmx Start Task VI ran or the DAQmx Write VI ran with the autostart input set to TRUE.</p>

Data Acquisition VIs used in the created LabVIEW control program is shown in **Table 2.8**. Because two kinds of AD / DA conversion board were used in LabVIEW control program, there are two kinds of Data Acquisition VIs for each other.

2.11. Calibration

In this study, as mentioned above, the displacement of another PZT actuator is measured by HIPOSS during controlled cutting for hysteresis. So there are two signals measured by two gap sensors, HIPOSS and LK-H008W.

As shown in **Fig. 2.26**, although the voltage input to PZT1 and PZT2 through PZT Amp. are the same, the voltage values measured by HIPOSS and LK-H008W may differ, due to the different sensitivity of the two gap sensors and different scalability of the two PZT actuators. Therefore, those two signals need to be calibrated for control cutting system.

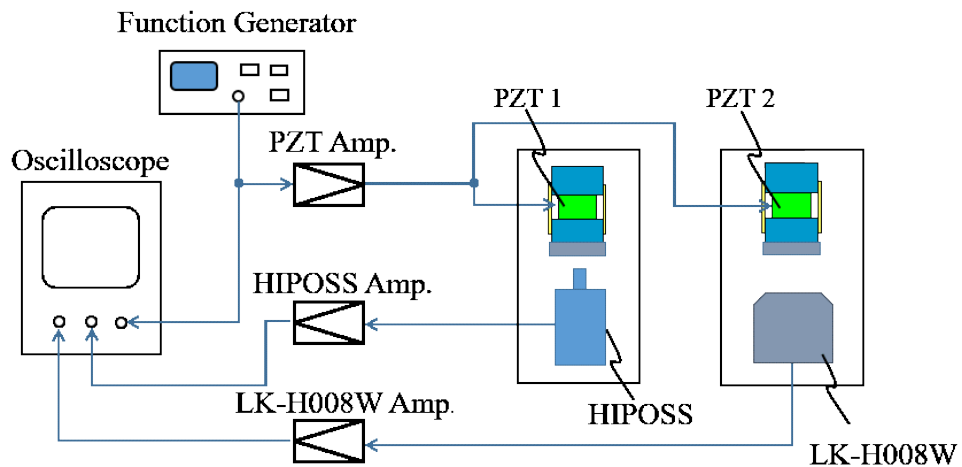


Fig. 2.26 Block diagram of calibration system.

The order of correction is as follows:

- Connect the devices as shown in **Fig. 2.26** and warm up devices.

- Adjust HIPOSS and LK-H008 to focus.
- Input step wave to PZT1 and PZT2 by Function Generator (FG) through PZT Amp.
- Obtain transformation coefficient, amplitude of voltage measured by HIPOSS/ amplitude of voltage measured by LK-H008W.

In control cutting process, by multiplying the signal value of LK-H008W by the transformation coefficient obtained in control program, accurate feedback control becomes possible.

2.12. The method of gain adjustment

In order to avoid the damage caused by overshoot to the diamond tool, I-PD control method is adopted. Therefore, before controlled cutting, gain of I-PD need to be adjusted. The method is shown in Fig. 2.27.

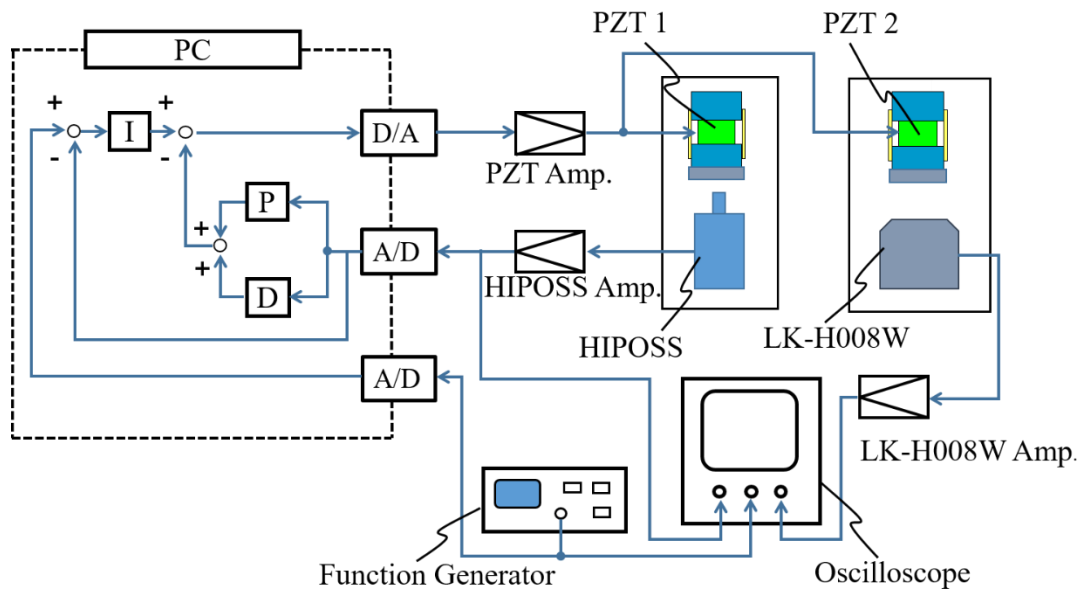


Fig. 2.27 Block diagram of gain adjustment system.

I-PD control includes Proportional control, Integral control and Differential control :

Proportional control

An operation of adjusting the operation amount in proportion to the magnitude of the deviation

→ Increase output

Integral control

An operation for performing a correction operation proportional to time integration of past deviations

→ Reduce vibration and reduce offset amount.

Differential control

Operation to operate in proportion to the speed of change of deviation

→ Increase response speed.

The front panel of LabVIEW for control program is shown in **Fig. 2.28**.

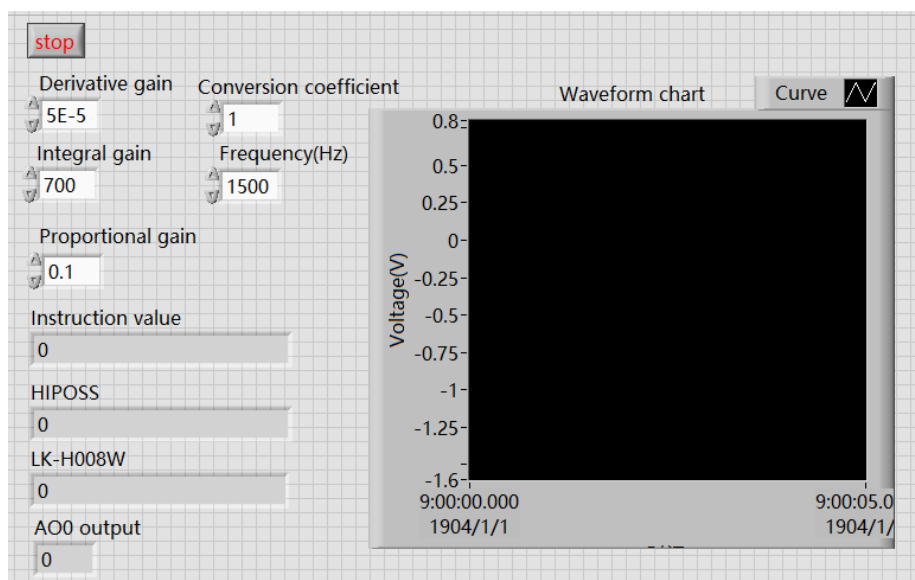


Fig. 2.28 Front panel.

Actually, in control cutting processing, the instruction value of the control system is signal value measured by LK-H008W, but in order to adjust the gain value of I-PD, the signal value output by FG is taken as the instruction value.

The limit sensitivity method is adopted for the gain adjustment of the control program. With the sine wave applied as the target command value, the differential gain and the integral gain are set to 0, and the value of the proportional gain is gradually increased while looking at the waveform of the output signal. The limit value at which the output signal is stable is determined as a proportional gain, after which integral gain and differential gain are determined.

The order of gain adjustment is as follows:

- Connect the devices as shown in **Fig. 2.27** and warm up devices.
- Adjust HIPOSS and LK-H008 to focus.
- Set gain values of I-PD preliminarily.
- Input step wave by FG as the instruction value.
- Start control and compare the waveform of instruction value with that measured by HIPOSS as shown in **Fig. 2.29**. If each gain value is appropriate, the waveform of these two signals should be almost the same, and overshoot doesn't appear on the waveform measured by HIPOSS.
- If the waveform measured by HIPOSS is not appropriate, change the value of each gain value of I-PD by limit sensitivity method and control again.

Fig. 2.30 shows the VI program for gain adjustment and **Fig. 2.31** shows the I-PD VI program.

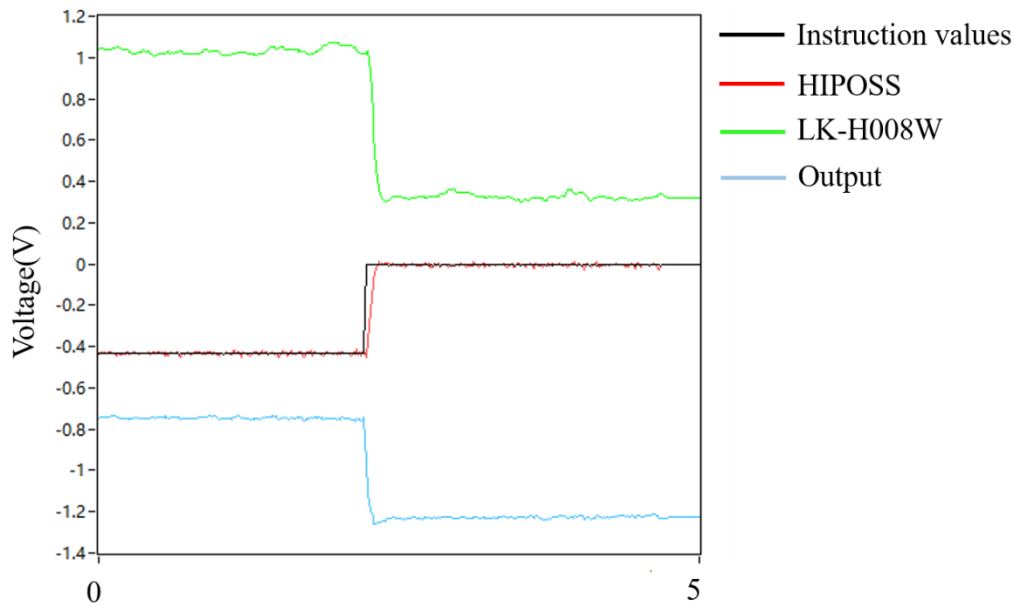


Fig. 2.29 Control signal.

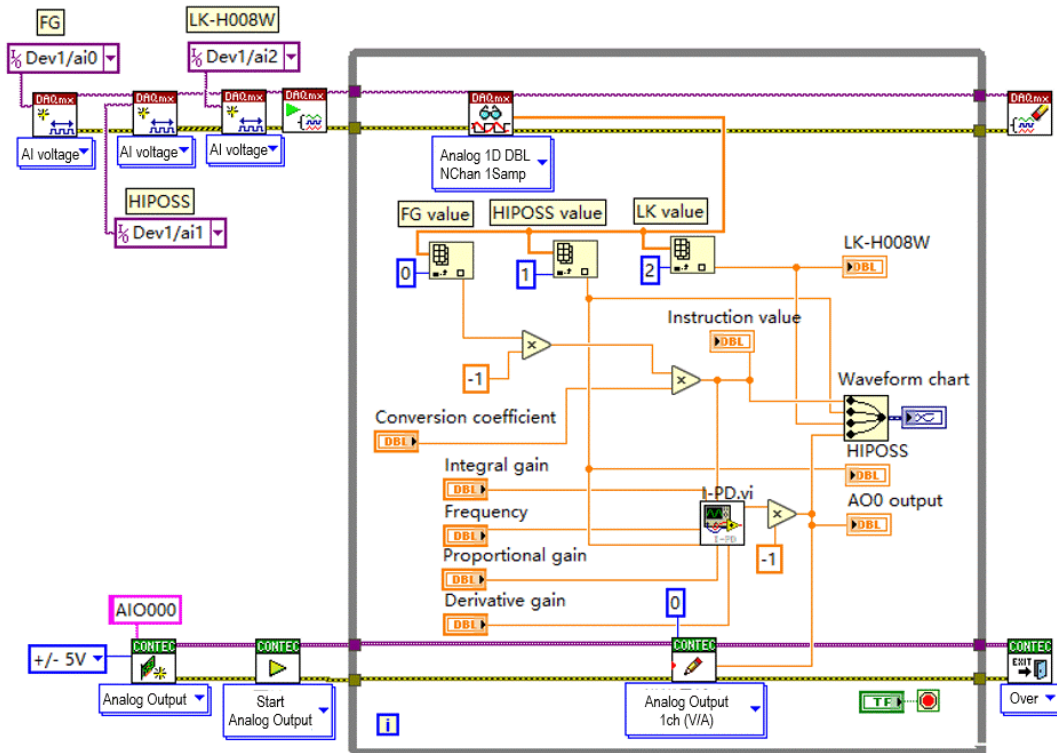


Fig. 2.30 VI program for gain adjustment.

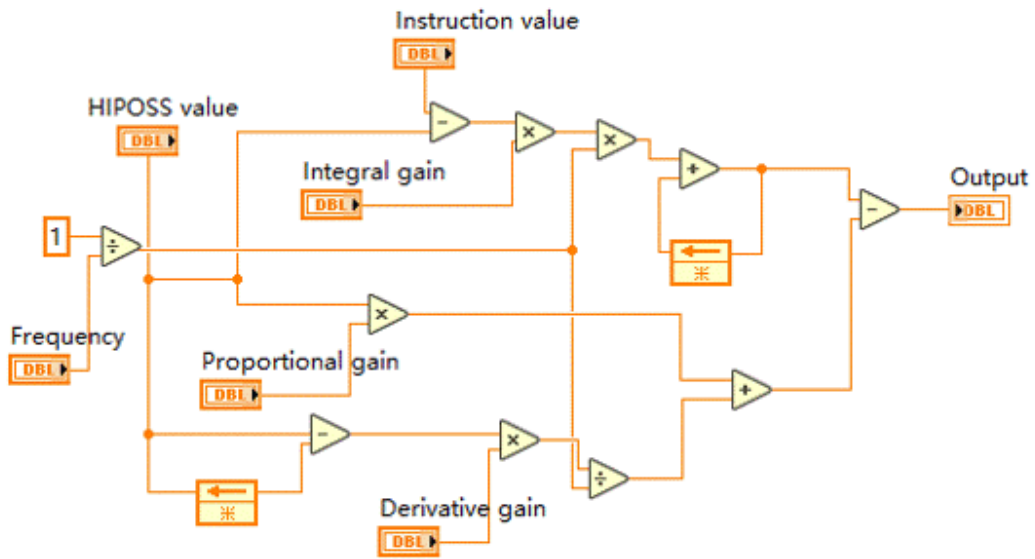


Fig. 2.31 I-PD VI program.

2.13. Transient characteristics

Confirmation of the transient characteristics is tested by comparing the output of HIPOSS (MDS tip displacement measured by the gap sensor when the output from the function generator (FG) is controlled as the target command value) and the output signal from the original FG. The gain and the phase difference at the time of control and the time of non-control were determined from the two signal.

(1) The method to obtain the gain

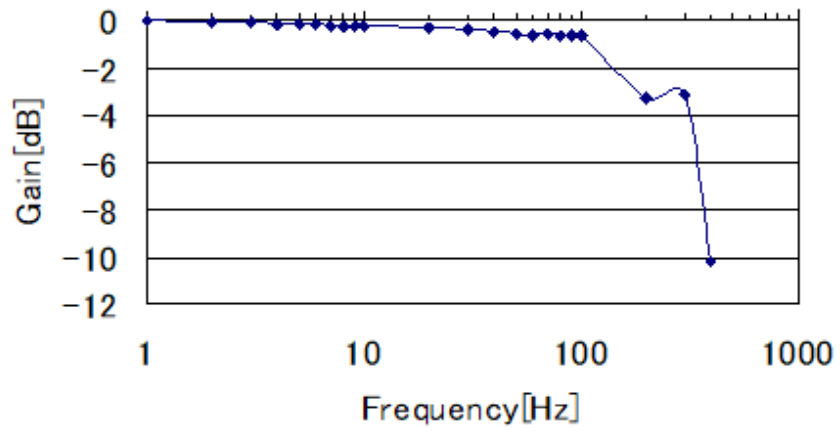
Calculate the amplitude of the signal of FG as Input and the amplitude of the signal of HIPOSS as Output and calculate from the following formula.

$$- 20 \log \left(\frac{Output}{Input} \right) [dB] \dots \dots (1)$$

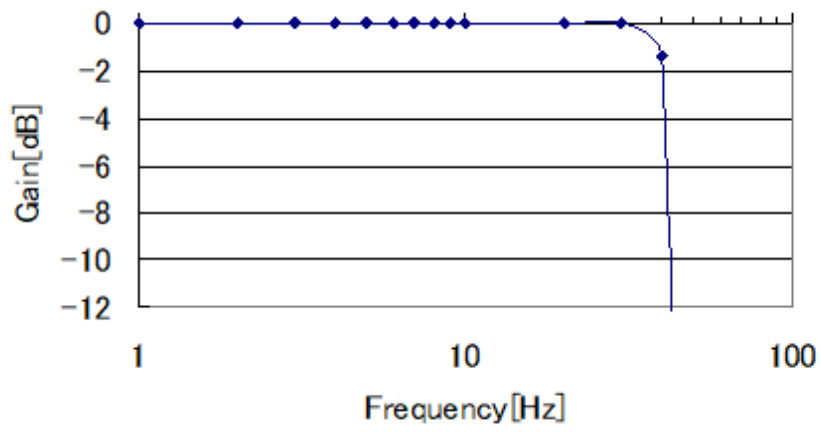
(2) The method to obtain the gain determine the phase difference

One cycle of the signal is set to 360° , and the deviation of the signal of FG and HIPOSS is calculated by converting it into an angle.

Fig. 2.32 and **Fig.2.33** show the gain and phase difference obtained by using the above method. The frequency at which the gain is -3 [dB] is the limit of responsiveness, and the amplitude ratio is about 70%. Although the quantitative value of the phase difference is not decided, it is thought that the limit where the difference sharply increases in the graph is the limit. It can be said that it responds to over 40 Hz during control and to 200 Hz strong at non-control. By controlling, the divergence of the signal occurred and the response frequency dropped.

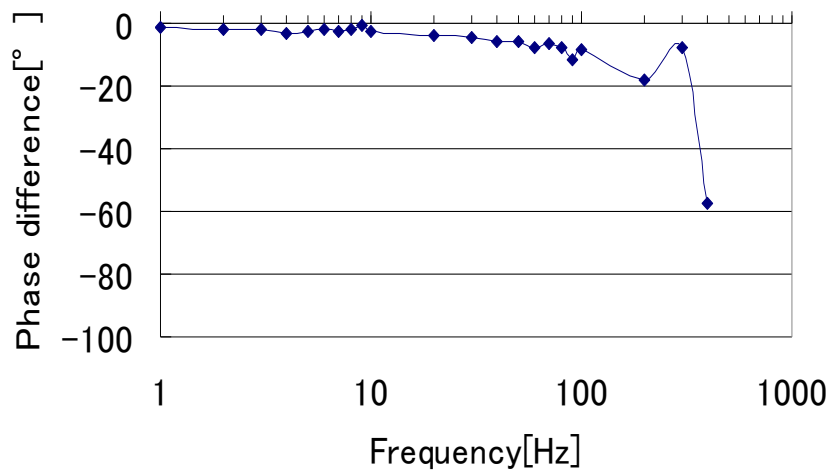


(a) Non-controlled

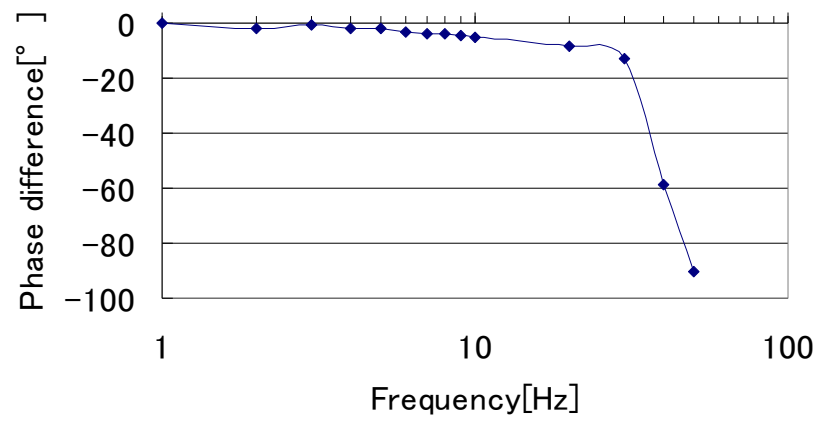


(b) Controlled

Fig. 2.32 Gain.



(a) Non-controlled



(b) Controlled

Fig. 2.33 Phase difference.

Chapter 3 Noise suppression of controlled cutting

3.1. Control system for fly cutting

3.1.1. Fly cutting part configuration

The fly cutting part is shown in **Fig. 3.1** and **Fig. 3.2**. In the fly cutting process, the workpiece that fixed on the PZT actuator is mounted vertically on the table of the milling machine while the fly cutter, in which the diamond tool was installed, rotates circularly with high speed around the spindle axis.

The PZT actuator and LK-H008W used as gap sensor are both mounted rigidly on machine table and the fly cutter and reference surface are placed between them. All of them are fixed to satisfy the Abbe's principle. Spindle and support jig of reference surface are both fixed to machine body. The relative displacement between the sensor and reference surface is considered to be the same as the relative displacement between the fly cutter and workpiece. Down cut was employed for fly cutting and horizontal cutting strategy was adopted in feed direction.

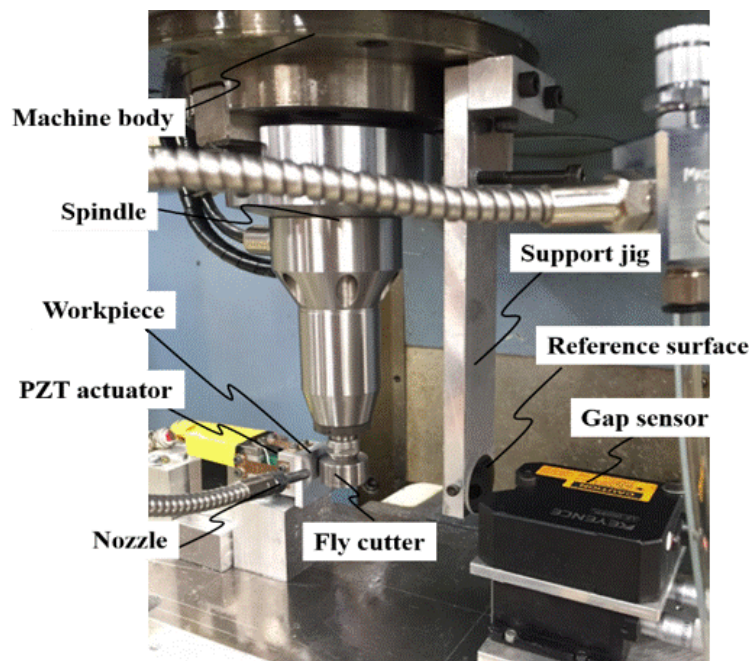
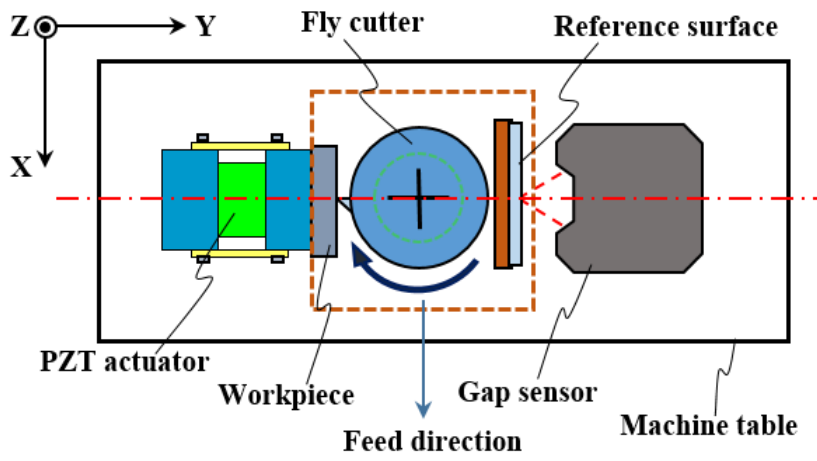
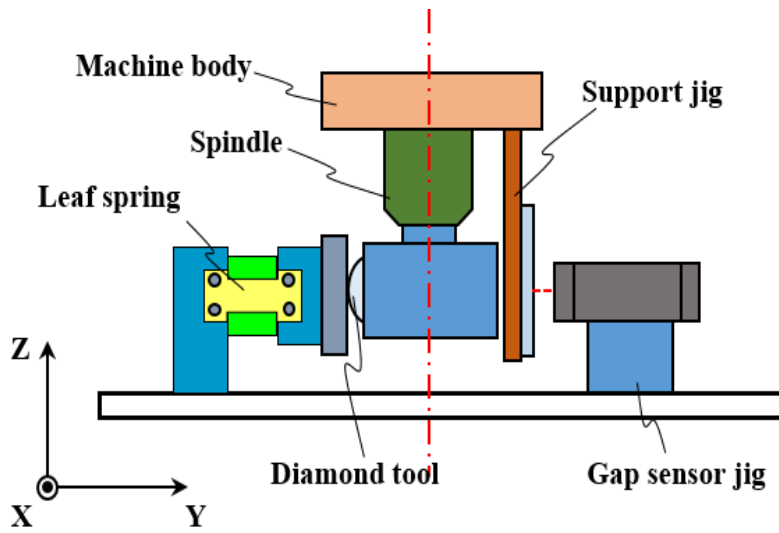


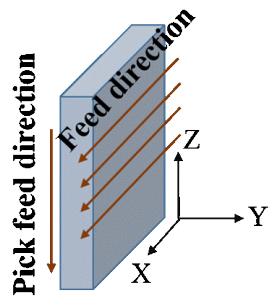
Fig. 3.1 Photograph of experimental setup of fly cutting part.



(a) Top view of fly cutting part.



(b) Side view of fly cutting part.



(c) Cutting strategy on workpiece.

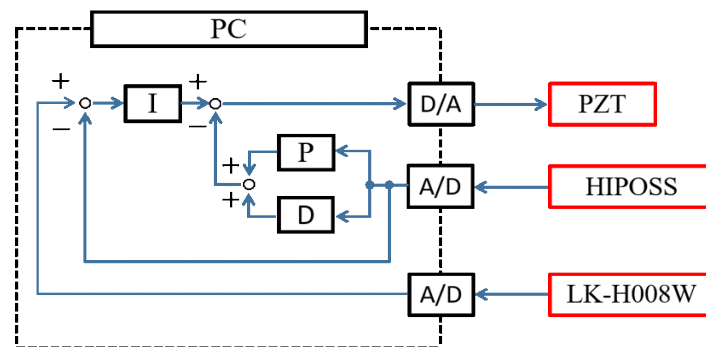
Fig. 3.2 Fly cutting part.

3.1.2. Principle of control system

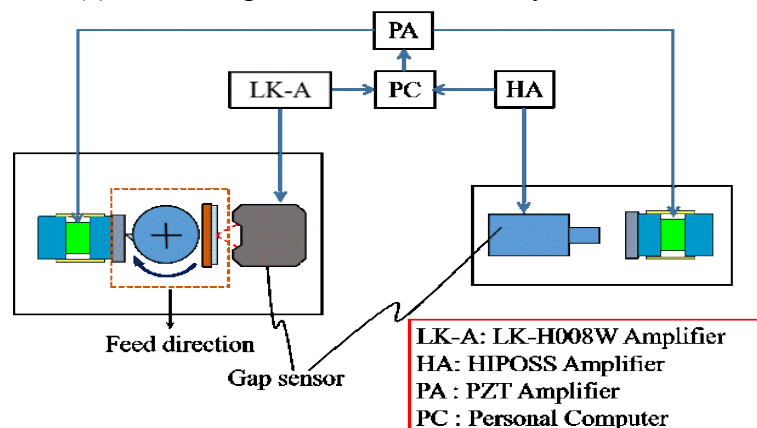
Fig. 3.2 (a) and (b) shows the principle of CCRS. When the workpiece surface moves away from or toward the fly cutter, the gap sensor detects the relative displacement between reference surface and gap sensor and then feedback the signal to the PZT actuator to compensate a same relative displacement between workpiece and fly cutter. Therefore, the control system compensates for the movement to keep a same distance between workpiece and fly cutter in real time.

3.1.3. Fly cutting system and correcting system for hysteresis

Fig. 3.3 shows fly cutting control system. The displacement of another PZT actuator is measured by HIPOSS during controlled cutting for hysteresis.



(a) Block diagram of I-PD control system.



(b) Correcting system for hysteresis.

Fig. 3.3 Fly cutting control system.

Fig. 3.4 shows the VI program for fly cutting control system.

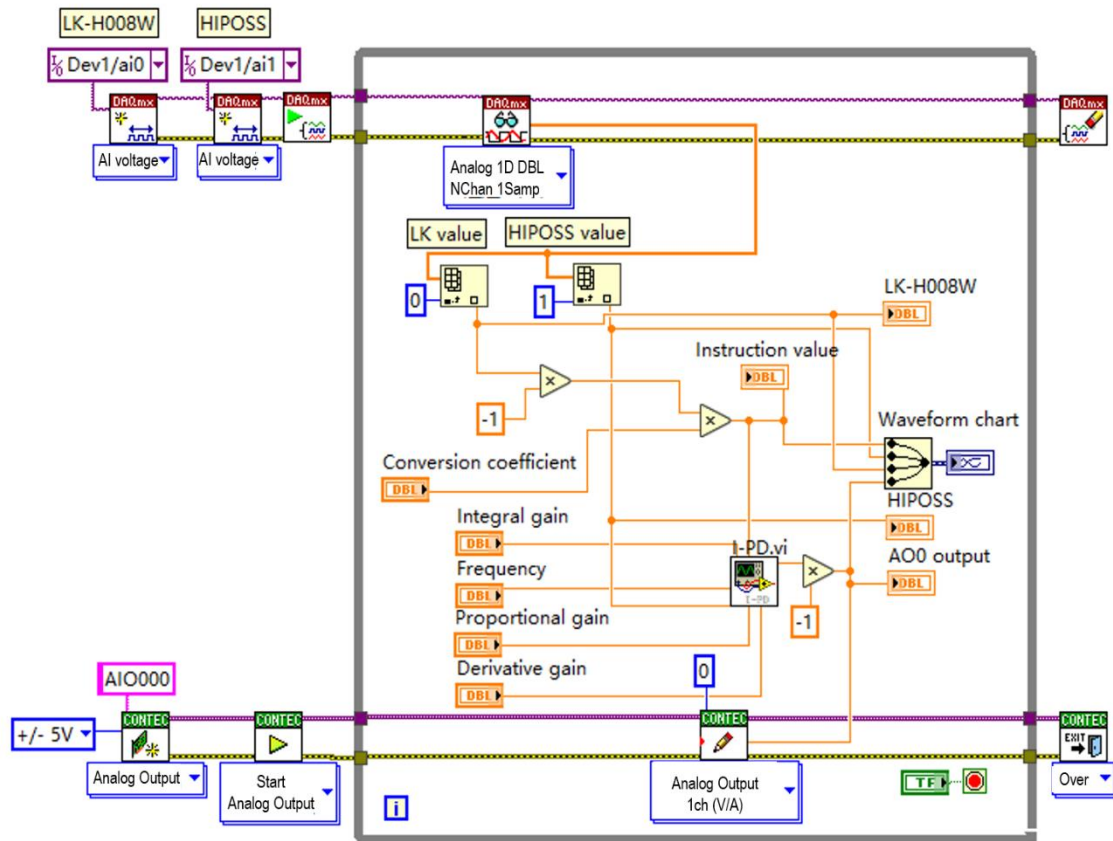


Fig. 3.4 VI program for fly cutting control system.

3.2. Experimental conditions

The commonly used Aluminum alloy AlMg2.5 for ultra-precision machining was used as the workpiece material, which has good diamond-machinable properties and appropriate hardness.

For aluminum materials diamond cutting, the minimum cutting speed is 60 to 100m/min, and the most economical cutting speed is 200 to 300m/min. Because the rotation radius(r) of fly cutter is 13mm. When Spindle speed(n) is 2500 rev/min, cutting speed is $2 \pi r n = 2 \times 3.14 \times 0.013 \times 2500=204$ (m/min) and this cutting speed meet the conditions of aluminum material diamond cutting.

Feed rate make sure that digital control sampling time is enough shorter than the error motion period.

The selected parameter used to evaluate the machined surface is maximum height of the scale-limited surface (S_z).

In feed direction, the formula of theoretical S_z is

$$S_z = \frac{fz^2}{8Rt} \quad (3.1)$$

, where, fz is the feed per revolution and Rt means rotation radius of fly cutter.

When feed rate (F) is 5 mm/min, $fz = F/n = 5 \div 2500 = 0.002$ (mm) and the theoretical $S_z = \frac{fz^2}{8Rt} = \frac{0.002^2}{8 \cdot 13} = 0.04$ (nm) in feed direction.

While, in pick feed direction, the formula of theoretical S_z is

$$S_z = \frac{fz^2}{8Rn} \quad (3.2)$$

, where fz is the pick feed and Rn means the tool nose radius (20mm).

In this study, pick feed 0.5mm and 0.1mm were selected for experiments. When pick feed is 0.5mm, 0.1mm, the theoretical S_z equals 1.5 (μm), 0.05 (μm) respectively.

To machine an ultra-precision microstructure, an ultra-precision plane surface is necessary as reference surface.

Since aluminum has a high coefficient of thermal expansion, it expands simultaneously with cutting and rubs the front flank of the cutting tool. This is a phenomenon called burnishing process, but if burnishing is strong, aluminum will burn blue. For ultra-precision cutting process, white kerosene is often used as cutting fluid. Some people use alcohol (ethyl / methyl), but ignition is afraid, so white kerosene is mainstream. Moreover, when impurities are contained in cutting fluid after ultra-precision cutting, it is difficult to remove cutting fluid and have a bad influence on diamond tool and machined surface. Due to few impurities in white kerosene and good volatilization, only washed by alcohol or acetone, the machined surface becomes beautiful without touching the surface.

Based on above, the experimental conditions are shown in **Table 3.1**.

Table 3.1. Experimental conditions

Feed rate [mm/min]	5
Spindle speed [rev/min]	2500
Rotation radius [mm]	13
Tool	Single crystal diamond
Noise radius [mm]	20
Depth of cut [μm]	5
Pick feed [mm]	0.5, 0.1
Lubricant	White kerosene, dry
Material	AlMg2.5(A5052)
Reference surface	Aluminum Mirrors (Circle)
Surface Flatness	$\lambda/10$

3.3. Non-controlled cutting experiment

Unlike high-speed cutting and single point diamond turning. Fly cutting is a cutting process whereby the diamond tool is flying during the cutting. Since the intermittent cutting mechanism and low feed rate, very small chips were observed just like dust as shown in **Fig. 3.5** and fly easily in the air in my experiment when in a lubricant-off cutting environment.

Owing to that, the chips attach to the workpiece, as shown in **Fig. 3.6**, and the diamond tool easily and caused a bad influence on machined surface as is shown in **Fig. 3.7**. Therefore, chip evacuation is a key component to producing a good surface finish.

For ultra-precision cutting, white kerosene always be used as lubricant because of its low impurities and after cutting the machined surface does not need to be cleaned again due to the volatilization of white kerosene. When in a lubricant-on cutting environment, a better quality machined surface was obtained when using white kerosene as we can see in **Fig. 3.8**.

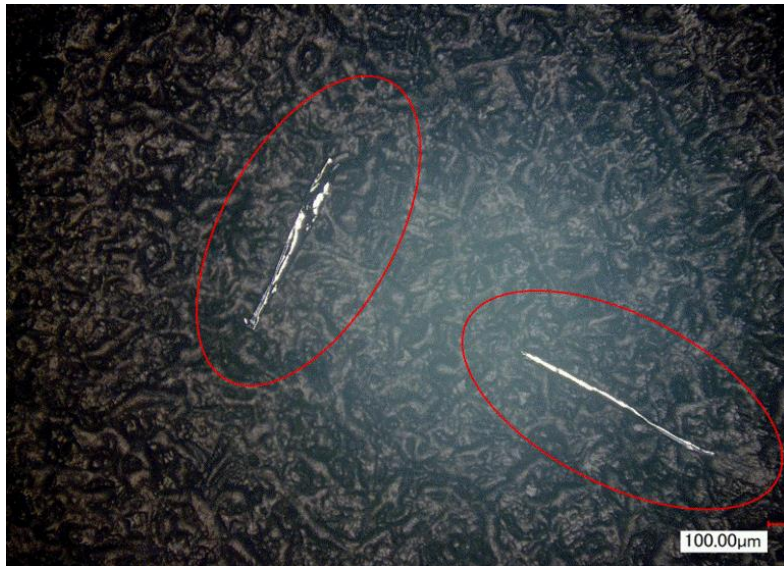


Fig. 3.5 Fly cutting chips.

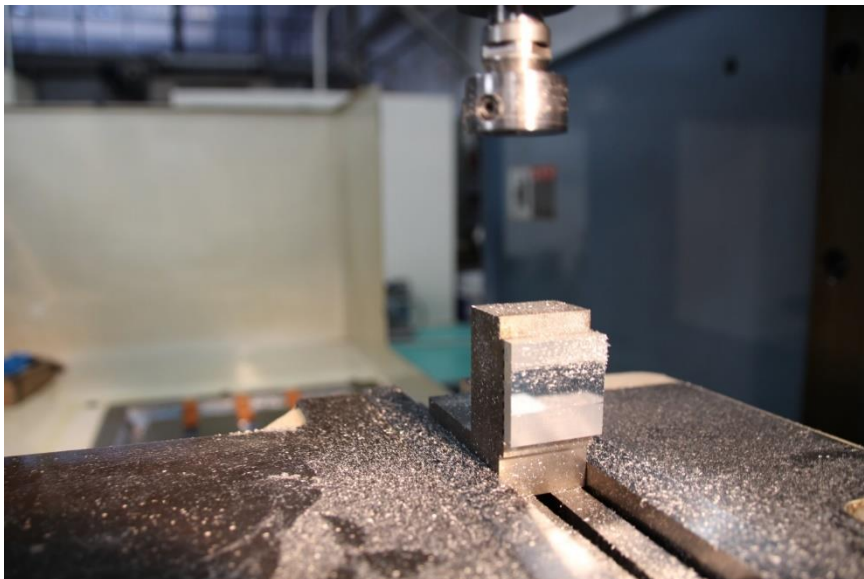
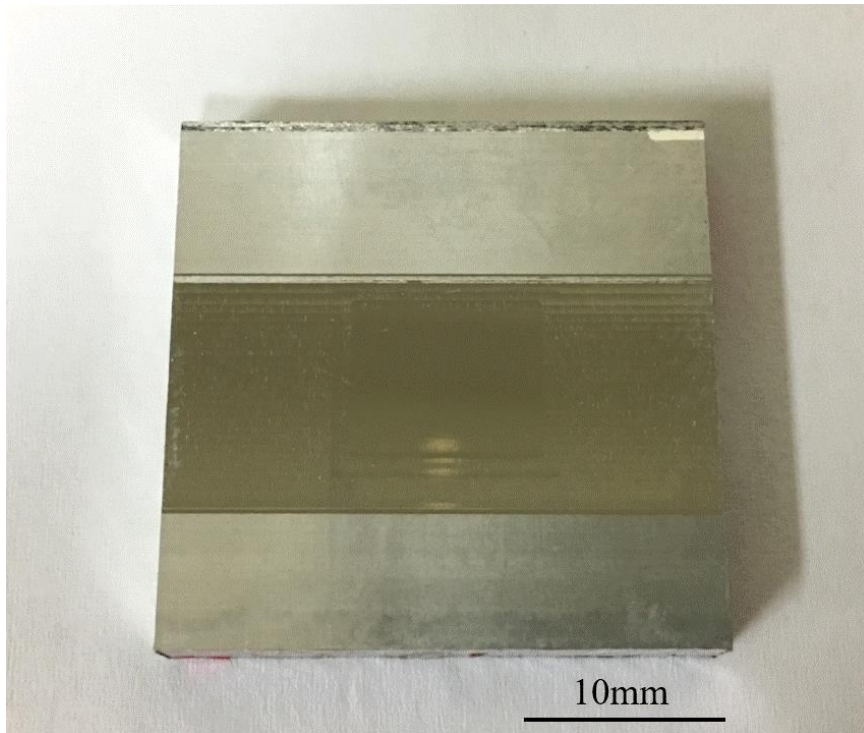
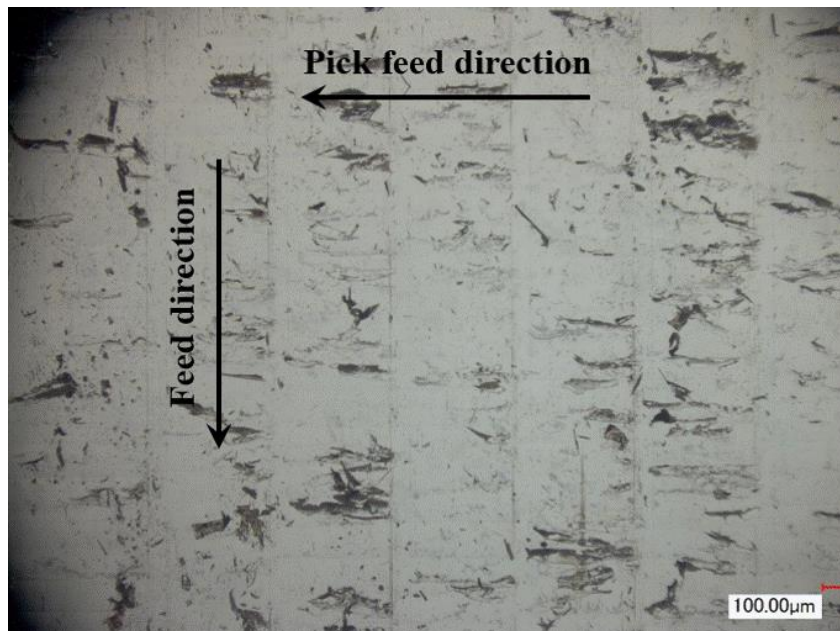


Fig. 3.6 Picture of after cutting with Lubricant-off.

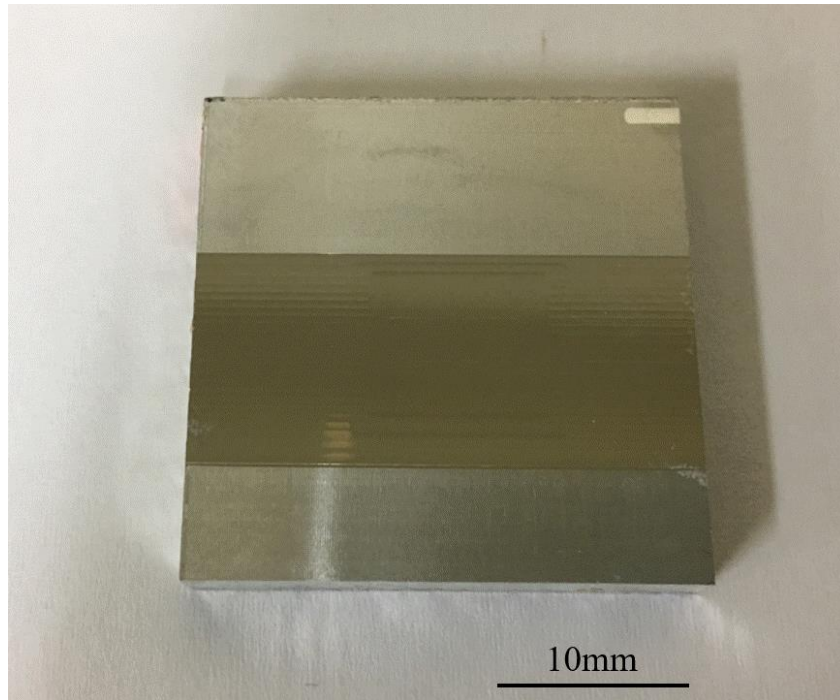


(a) Picture of machined surface on workpiece.

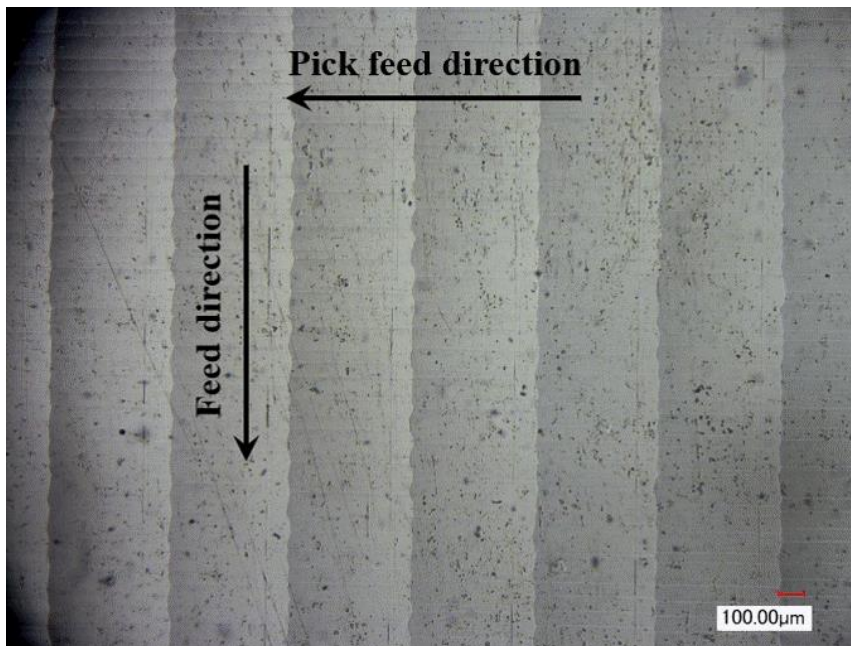


(b) Partial enlarged detail of (a).

Fig. 3.7 Machined surface with Lubricant-off.



(a) Picture of machined surface on workpiece.



(b) Partial enlarged detail of (a).

Fig. 3.8 Machined surface with Lubricant-on.

In pick feed direction

Fig. 3.9 and Fig. 3.10 shows the profile of machined surface in pick feed direction when pick feed is 0.5mm and 0.1mm respectively. Both of the form accuracy of them showed the table motion error of this milling machine.

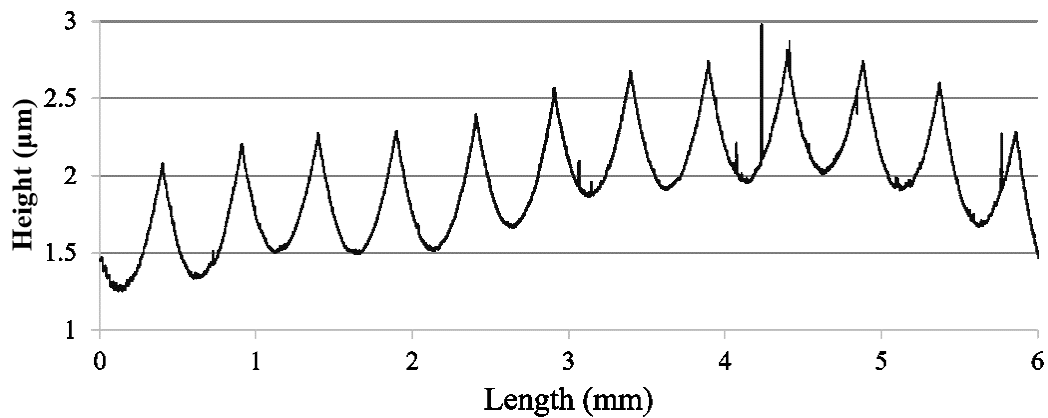


Fig. 3.9 Profile of machined surface without control in pick feed direction.
(pick feed : 0.5mm)

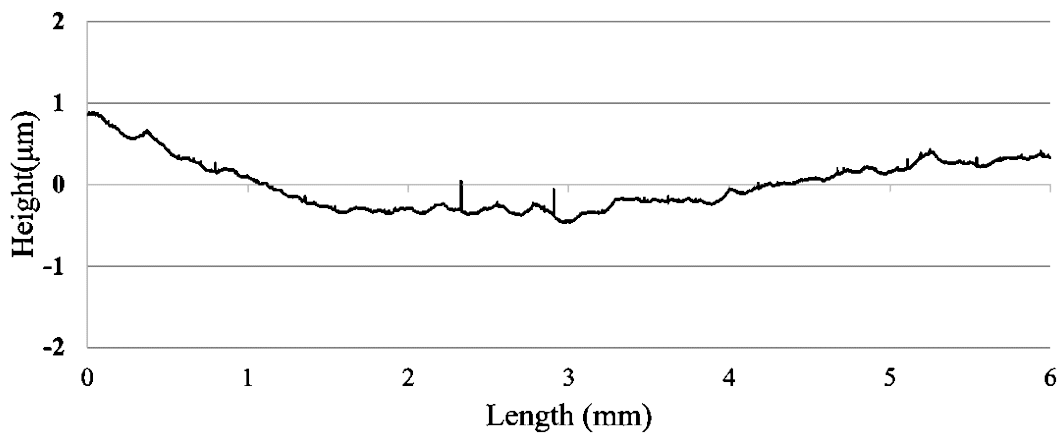
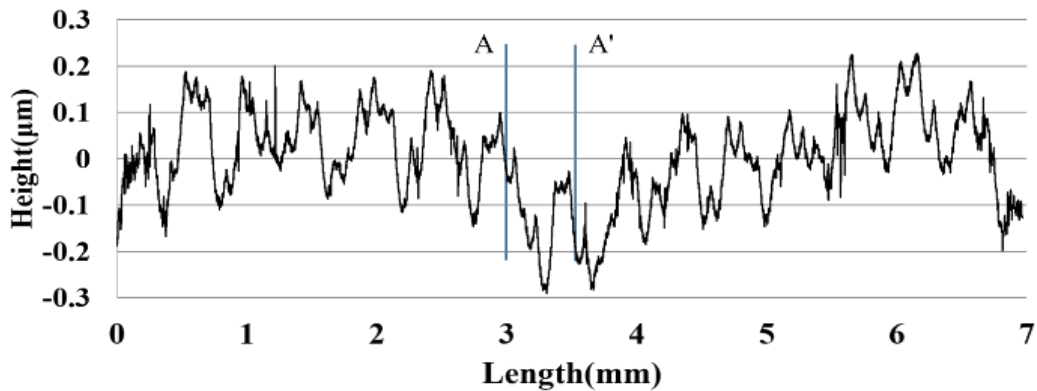


Fig. 3.10 Profile of machined surface without control in pick feed direction.
(pick feed : 0.1mm)

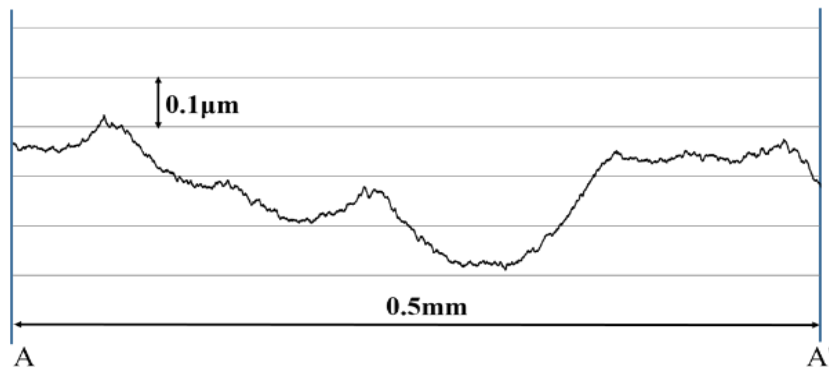
In **Fig. 3.9**, the geometry contour of diamond tool nose can be observed obviously and we can see the pick feed is 0.5mm just like used in cutting conditions. The theoretical S_z is $1.56\ \mu\text{m}$ as mentioned above, when pick feed is 0.5 mm. However, the measured S_z , the depth of each arc-shape, is about $0.8\ \mu\text{m}$. It is smaller than the theoretical S_z value. Probably it was caused by spring back of workpiece due to diamond tool cutting into workpiece through down cut. Although, the quality of machine surface become better when the pick feed is changed to 0.1 mm as shown in **Fig. 3.10**, we can still see that the form accuracy is determined by table motion error of this milling machine.

In feed direction

Fig. 3.11 shows the profile of the machined surface without control in feed direction.



(a) Profile of machined surface.



(b) Partial enlarged detail of (a).

Fig. 3.11 Profile of the machined surface without control in feed direction.

The S_z in **Fig. 3.11 (a)** is about $0.5\mu\text{m}$ that affected by two kinds of waviness induced by table motion error, short period waviness (pitch: 0.5mm ; amplitude: about $0.3\mu\text{m}$; frequency: about 0.17Hz) and long period waviness (pitch: about 3.5mm ; amplitude: about $0.2\mu\text{m}$; frequency: about 0.02Hz)

From the profile of the machine surface along the measured length of 0.5mm as shown in **Fig. 3.11 (b)**, we can see there was no high frequency component at sub-micrometric level appeared if neglect the part of table motion error.

In the previous research, the surface roughness became worse when slow down the feed rate because the feed rate equals cutting speed in shaping and cause high frequency chatter vibration. However, in this experiment, feed rate and cutting speed were independent by fly cutting, slowing down the feed rate, keeping a high cutting speed. The result showed that the high frequency component which deteriorate the machined surface finish in shaping was suppressed by fly cutting. On the other hand, the low frequency waviness induced by table motion error, which impact on accuracy of machined surface at sub-micrometric level, can be theoretically improved by control cutting system.

3.4. Noise suppression of controlled cutting experiment

3.4.1. The order of controlled cutting

- Connect the devices and warm up devices over half an hour.
- Input 70V to PZT through PZT Amp.
- Mill the workpiece to make sure the surface vertically with lubricant-on.
- Fix fly cutter into high speed spindle and mirror support jig onto machine body.
- Adjust the angle of mirror, ensure it is parallel to cutting trace measured by LK-H008W.
- Open the cutting fluid.

- Start controlled cutting.
- Stop controlled cutting program when cutting is finished.

3.4.2. Factors causing noise in control system

Fig. 3.12 shows the experimental setup. The noise detected by the gap sensor (LK-H008W), whose output convert to instruction values (setpoint), easily affects the machined surface. **Fig. 3.13** shows that the wave height of noise measured by LK-H008W only when the fly cutter is rotating (not cutting) is about 0.1 μm , which directly influences the accuracy of machined surface by about 0.1 μm . Moreover, the noise wave height becomes bigger than 0.1 μm when tool is cutting the workpiece and the machine table is moving. Therefore, the form accuracy cannot be controlled by less than 0.1 μm theoretically. In this study, a low-pass filter was used to control the noise.

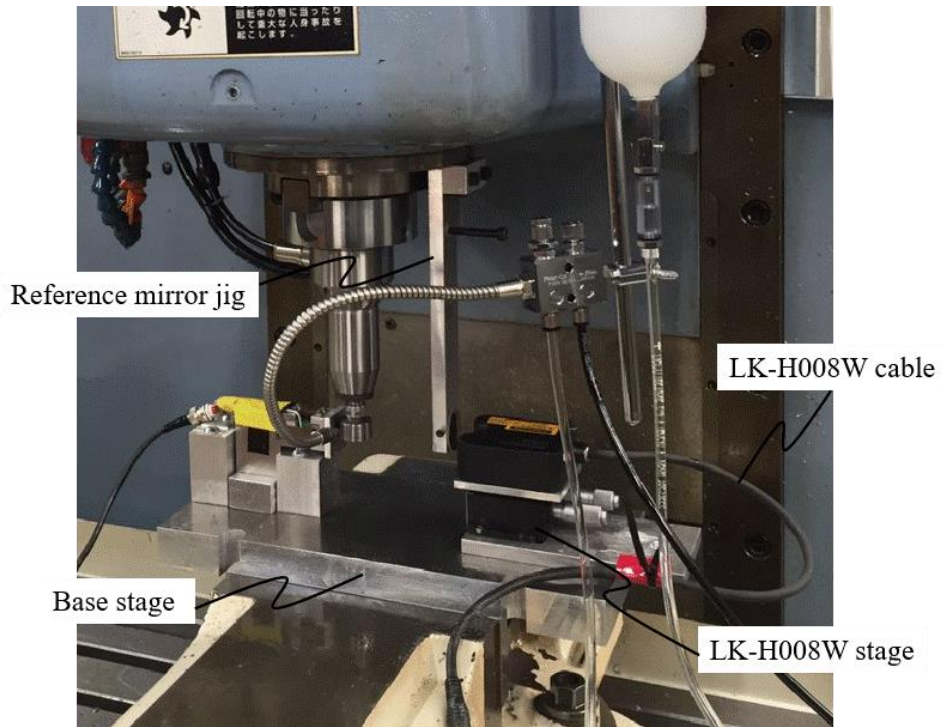


Fig. 3.12 experiment setup.

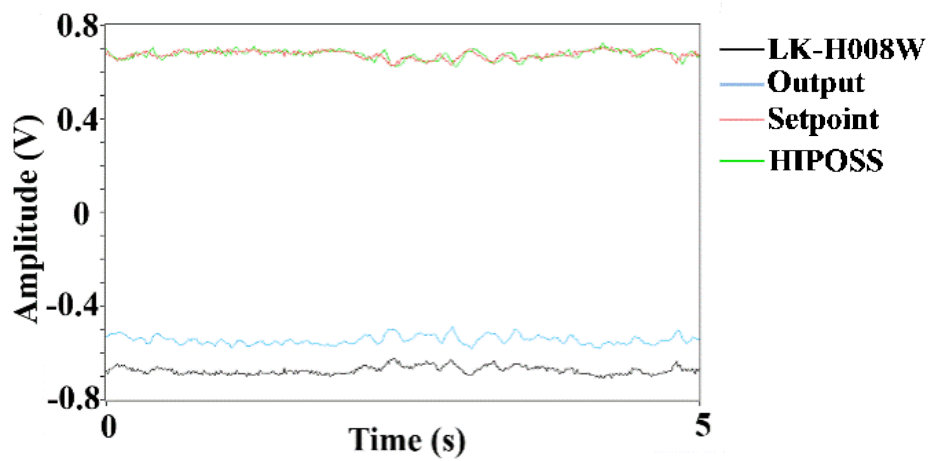


Fig. 3.13 Signal before cutting without low pass filter.

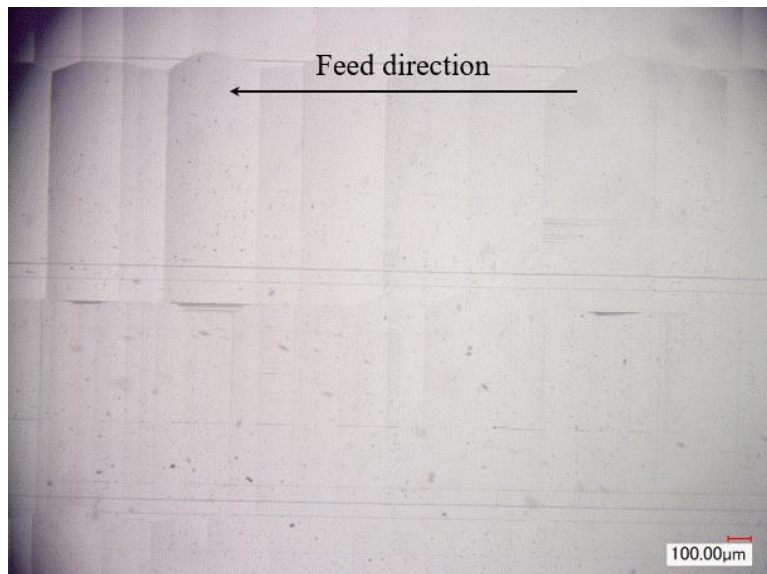


Fig. 3.14 Picture of machined surface with noise influence.

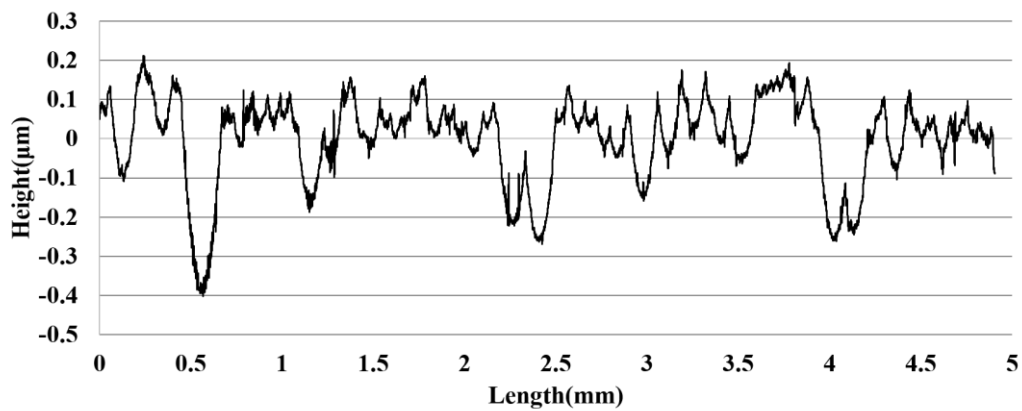


Fig. 3.15 Noise influence left on machined surface.

The another major reason, need to be careful, is that the LK-H008W cable should be fixed on the base stage and LK-H008W stage should be fastened after just adjust the distance between LK-H008W and reference surface. If not, when the table move in cutting process the LK-H008W cable will drag LK-H008W fitfully, and this noise will

mix into instruction values and give a bad influence on machined surface, as shown in **Fig. 3.14** and **Fig. 3.15** (Although the form accuracy was improved, noise influence left on machined surface).

In order to reduce the influence of noise measured by LK-H008W, the low pass filter was used. **Table 3.2** shows the experimental conditions.

Table 3.2. Experimental conditions

Feed rate [mm/min]	5
Spindle speed [rev/min]	2500
Rotation radius [mm]	13
Tool	Single crystal diamond
Noise radius [mm]	20
Depth of cut [μm]	6
Pick feed [mm]	1
Lubricant	White kerosene
Material	AlMg2.5(A5052)
Reference surface	Aluminum Mirrors (Circle)
Surface Flatness	$\lambda/10$
Cutoff frequency of low pass filter [Hz]	0.3, 1, 2, 3, 10

3.4.3. Results and discussion

The results are shown in **Fig. 3.16- Fig. 3.25**.

Cutoff frequency 0.3 Hz :

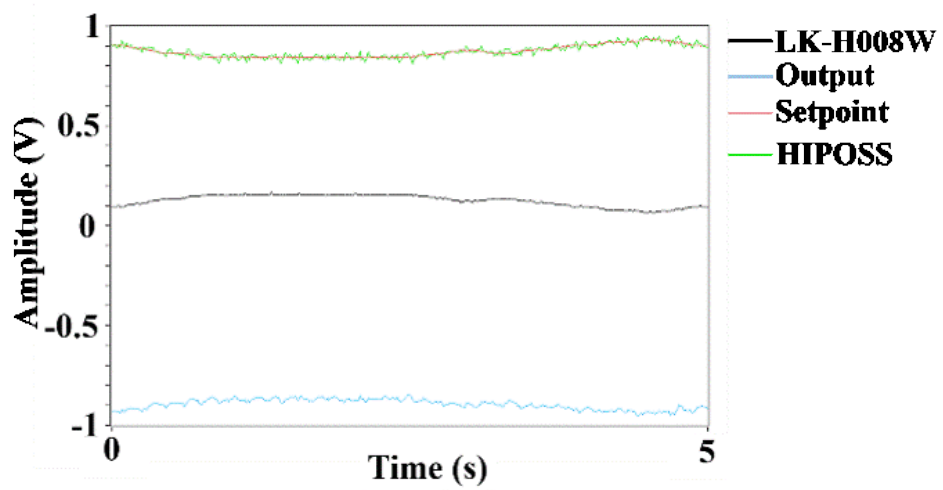


Fig. 3.16 Signal before cutting (Cutoff frequency 0.3 Hz).

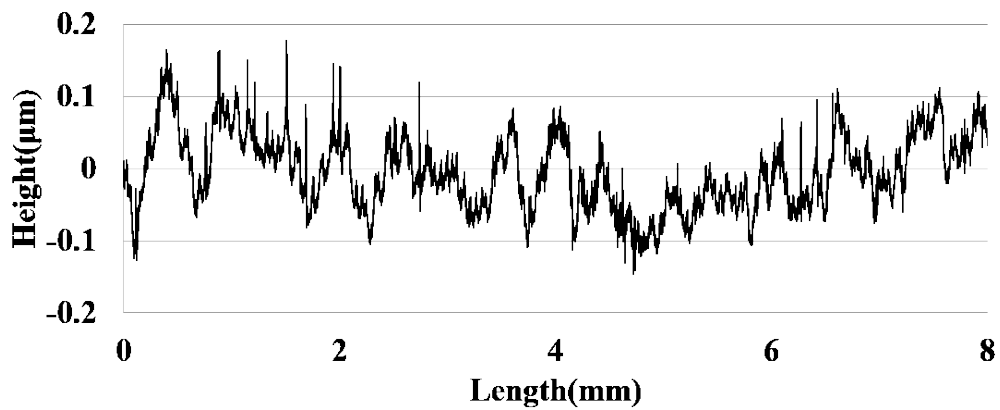


Fig. 3.17 Profile of the machined surface with control in feed direction (cutoff frequency 0.3 Hz).

Cutoff frequency 1 Hz :

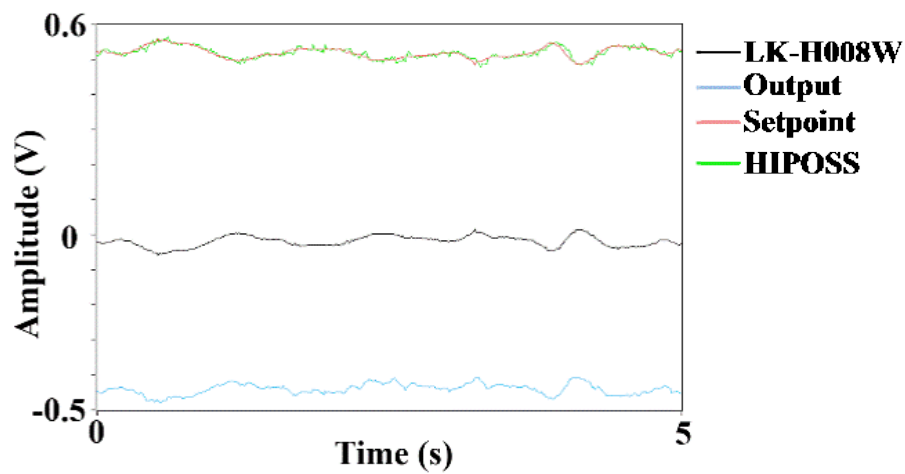
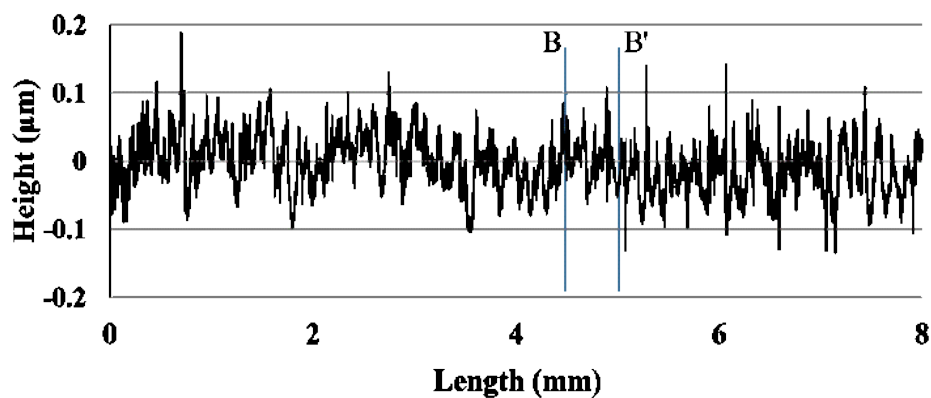
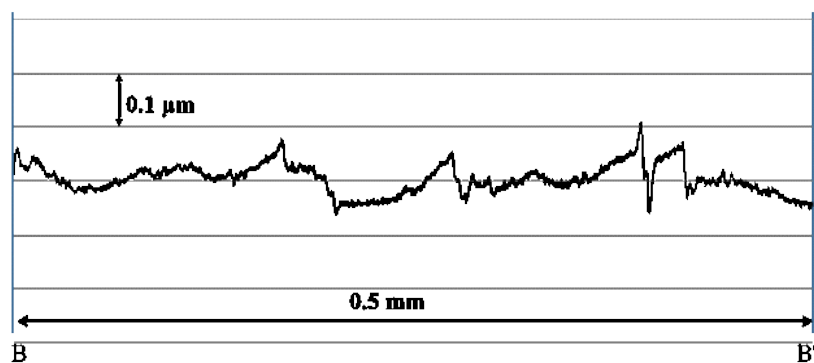


Fig. 3.18 Signal before cutting (Cutoff frequency 1 Hz).



(a) Profile of machined surface.



(b) Enlargement of B-B' in panel (a).

Fig. 3.19 Profile of the machined surface with control in feed direction (cutoff frequency 1 Hz).

Cutoff frequency 2 Hz :

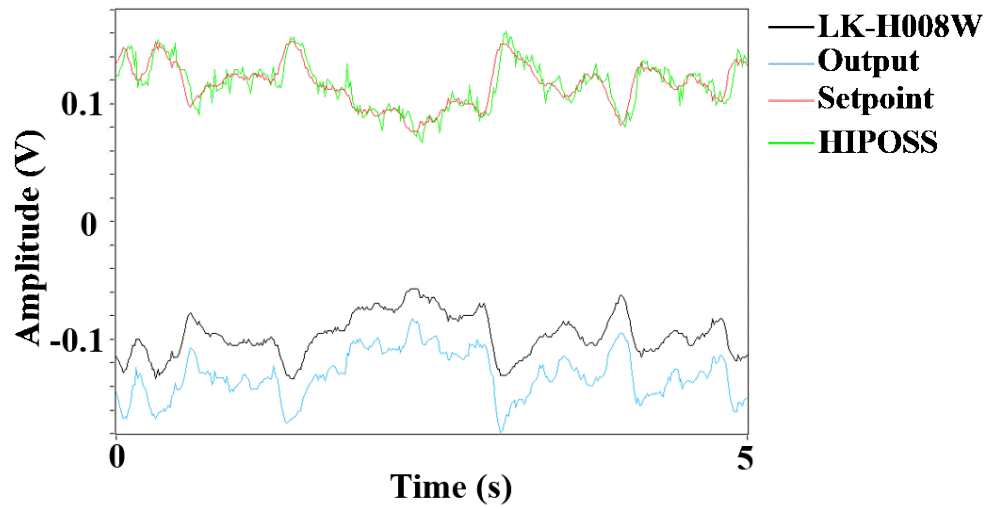


Fig. 3.20 Signal before cutting (Cutoff frequency 2 Hz).

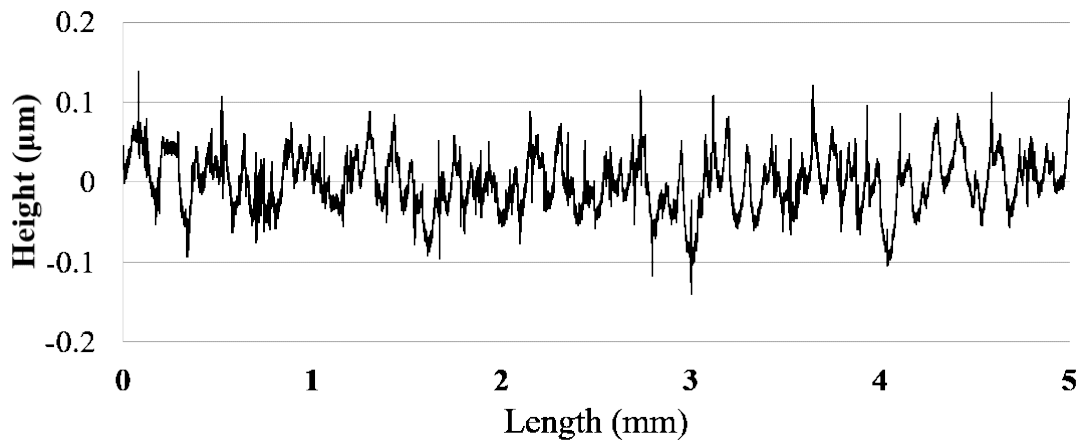


Fig. 3.21 Profile of the machined surface with control in feed direction (Cutoff frequency 2 Hz).

Cutoff frequency 3 Hz :

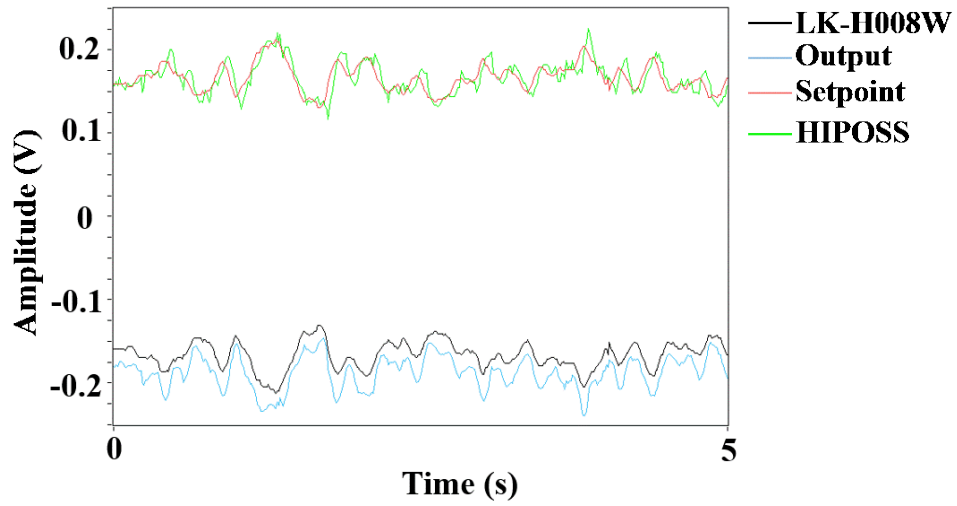


Fig. 3.22 Signal before cutting (Cutoff frequency 3 Hz).

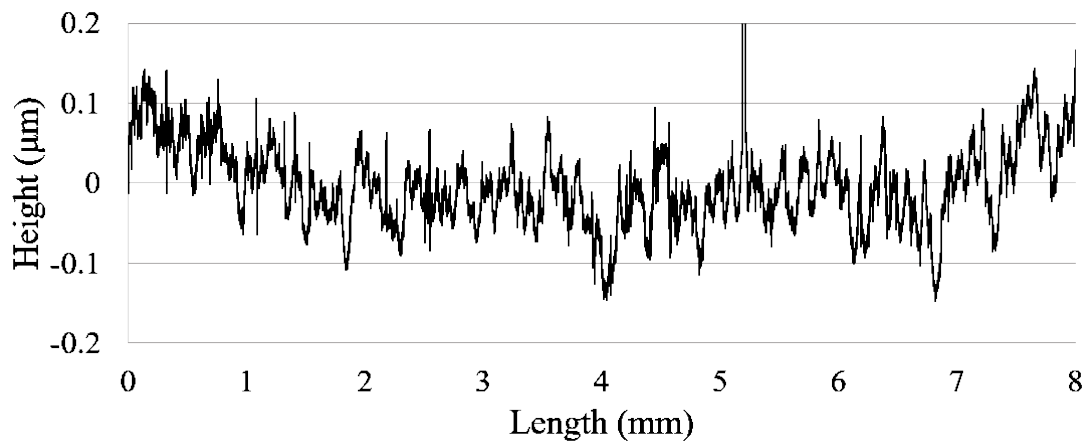


Fig. 3.23 Profile of the machined surface with control in feed direction (cutoff frequency 3 Hz).

Cutoff frequency 10 Hz :

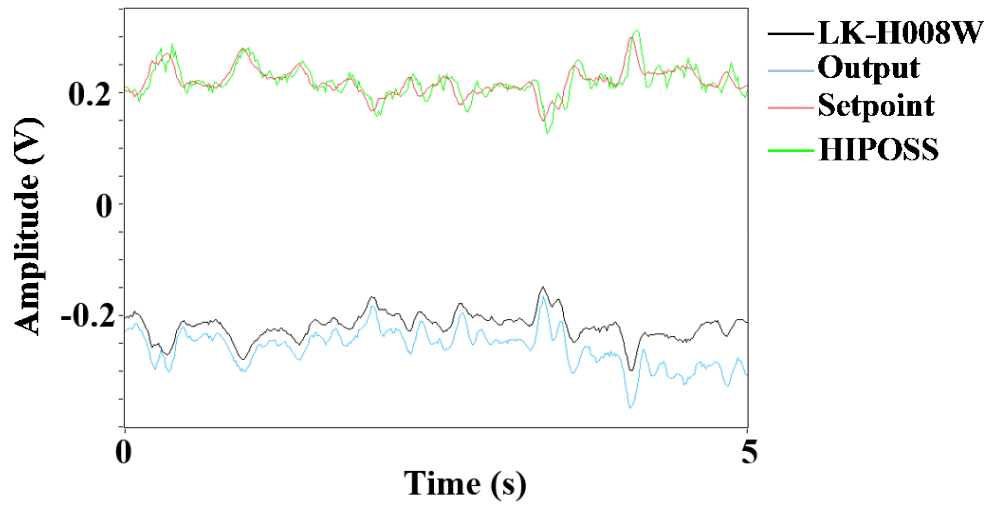


Fig. 3.24 Signal before cutting (Cutoff frequency 10 Hz).

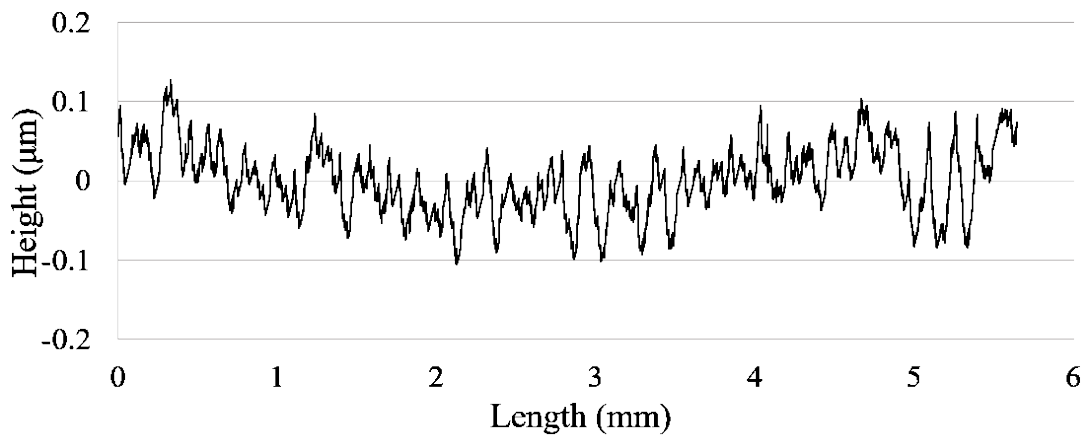


Fig. 3.25 Profile of the machined surface with control in feed direction (cutoff frequency 10 Hz).

When set the cutoff frequency of low pass filter to 0.3 Hz, the wave height of noise measured by LK-H008W before control cutting was reduced to less than $0.05\mu\text{m}$ as shown in **Fig. 3.16**. Although the S_z was improved from $0.5\mu\text{m}$ to less than $0.25\mu\text{m}$ as shown in **Fig. 3.17**, the short period waviness whose frequency is about 0.17Hz, which is useful signal and near to the cutoff frequency 0.3 Hz, was attenuated by low pass filter and left on the machined surface. This result also proved the usefulness and principle of CCRS. To get a better quality of machined surface, the cutoff frequency should change much bigger than 0.17Hz. (Of course, the control result also influenced by gains of HIPOSS and LK - H008W, the control delay of this control system and different kinds of vibrations)

Fig. 3.18 shows the noise when cutoff frequency is 1Hz, the S_z was improved from about $0.5\mu\text{m}$ to less than $0.2\mu\text{m}$, as shown in **Fig. 3.19**. This result shows the short period waviness and long period waviness were both controlled by this control cutting system effectively even though the influence of noise in control cutting process was left on the machined surface. In addition, as mentioned above, the S_z cannot be controlled under $0.1\mu\text{m}$ theoretically since the amplitude of noise is about $0.1\mu\text{m}$ before control cutting as shown in **Fig. 3.18**.

Since all the wave height of noise is about $0.1\mu\text{m}$ when set cutoff frequency to 1Hz, 2Hz, 3Hz, 10Hz, all the S_z of machined surface are about $0.2\mu\text{m}$, as shown in **Fig. 3.18-Fig. 3.25**. But small dent shape appeared on the machined surface became bigger, when the cutoff frequency was set bigger. This is maybe due to that the wave height of high frequency appeared and became bigger when cutoff frequency is bigger. The relationship between them needs to be verified in future work.

As shown in **Fig. 3.11** (uncontrolled cutting) and **Fig. 3.19, Fig. 3.21, Fig. 3.23, Fig. 3.25** (controlled cutting), the accuracy of machined surface with controlled cutting is better than that with non-controlled cutting and no high frequency component at sub-micrometric level appeared on machined surface with controlled cutting, though the noise mixed into control signal. Therefore, by improving the design of the experimental

setup to reduce the effect of noise that majorly impact on machined surface or by other ways, the machined surface quality will become better.

According to the above experiments, it is possible that the accuracy of machined microstructure can be improved on an ordinary milling machine by this control system.

3.4.4. Conclusions

In the experimental study, the machined surface of ultra-precision microstructure by fly cutting using an ordinary milling machine with controlled cutting and with non-controlled cutting are discussed. The conclusive remarks are found as following:

1. The high frequency component that deteriorate the machined surface finish in shaping cutting process can be suppressed by fly cutting (Non-controlled cutting in feed direction).
2. The form accuracy of machined surface can be improved on an ordinary milling machine by this control cutting system (to obtain S_z less than $0.2 \mu\text{m}$).

Chapter 4 Feed rate experiment

4.1. Experimental condition

In this experiment, the relationship between feed rate and machined surface with controlled cutting and uncontrolled cutting were discussed. The experiment conditions are shown in **Table 4.1**.

Table 4.1. Experimental conditions

Feed rate [mm/min]	5, 10, 20, 40, 65, 80
Spindle speed [rev/min]	2500
Rotation radius [mm]	13
Tool	Single crystal diamond
Noise radius [mm]	20
Depth of cut [μm]	6
Pick feed [mm]	1
Lubricant	White kerosene
Material	AlMg2.5(A5052)
Reference surface	Aluminum Mirrors (Circle)
Surface Flatness	$\lambda/10$
Cutoff frequency of Low pass filter [Hz]	1

4.2. Experimental results and discussion

Fig. 4.1-Fig. 4.4 show the photos of machined surface machined at different feed rate.

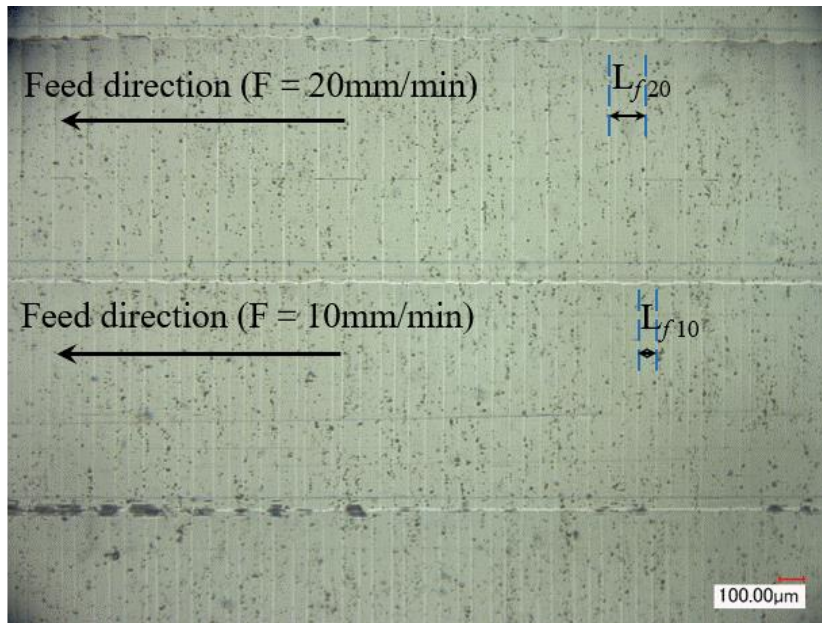


Fig. 4.1 Picture of the machined surface (feed rate : 10 mm/min, 20 mm/min).

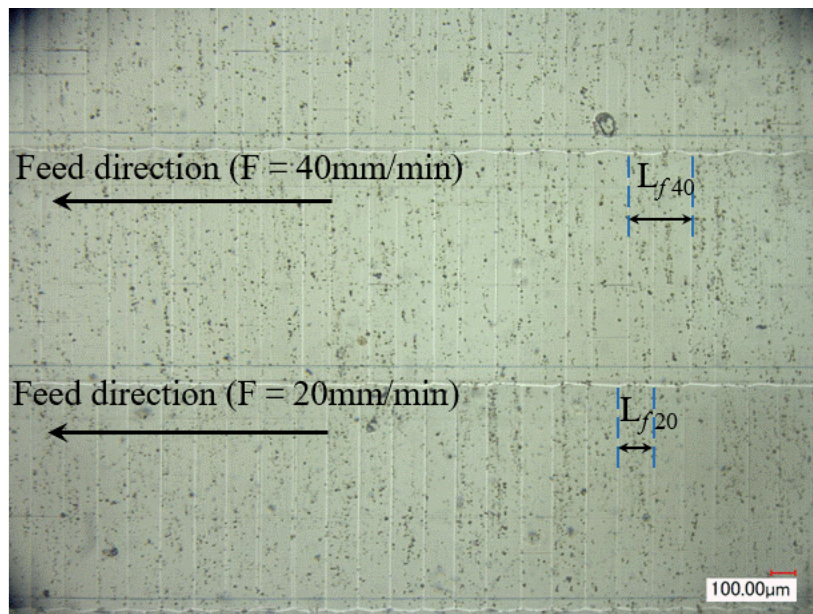


Fig. 4.2 Picture of the machined surface (feed rate : 20 mm/min, 40 mm/min).

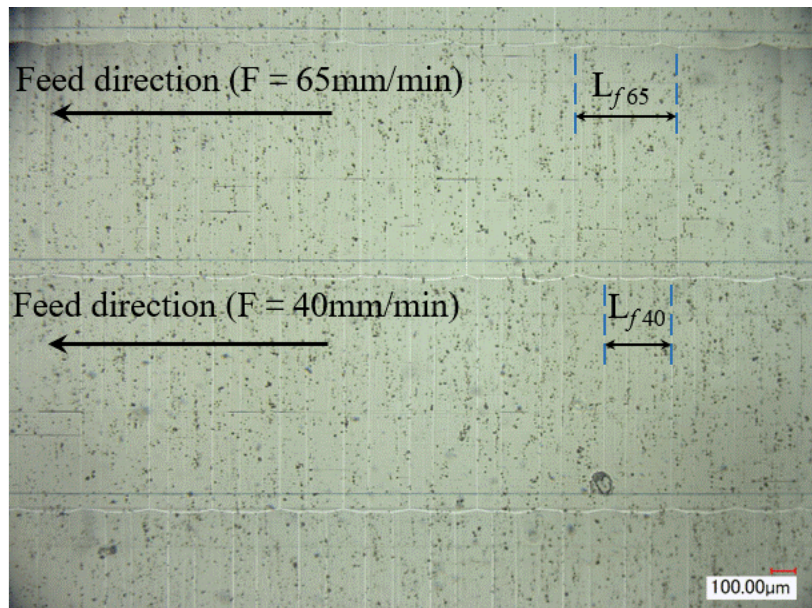


Fig. 4.3 Picture of the machined surface (feed rate : 40 mm/min, 65 mm/min).

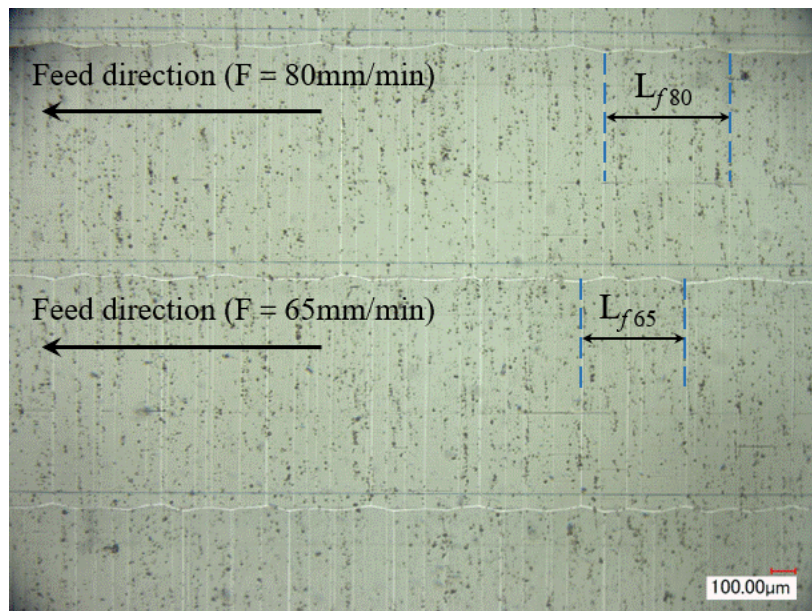
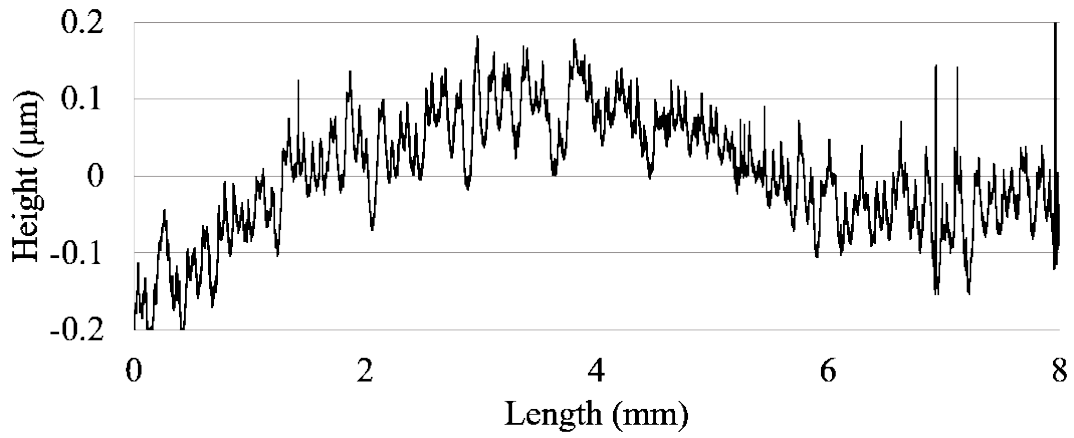
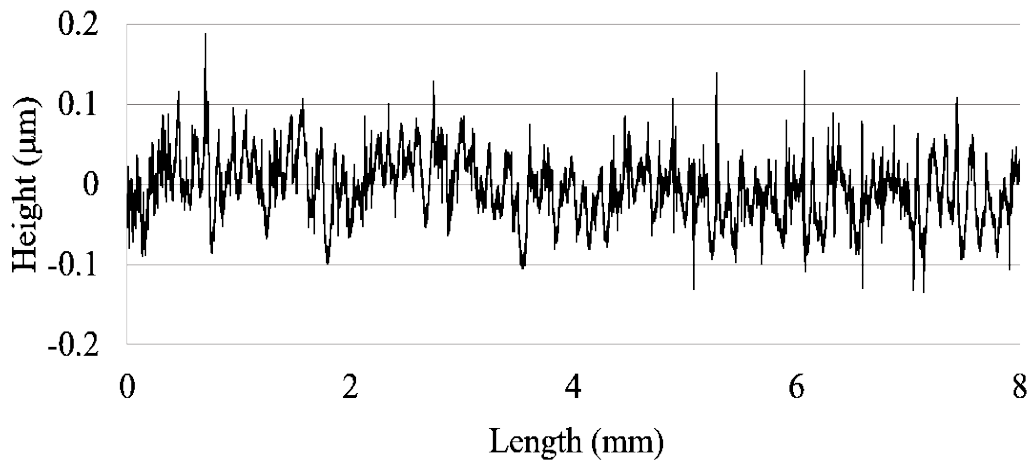


Fig. 4.4 Picture of the machined surface (feed rate : 65 mm/min, 80 mm/min).

F = 5 mm/min :



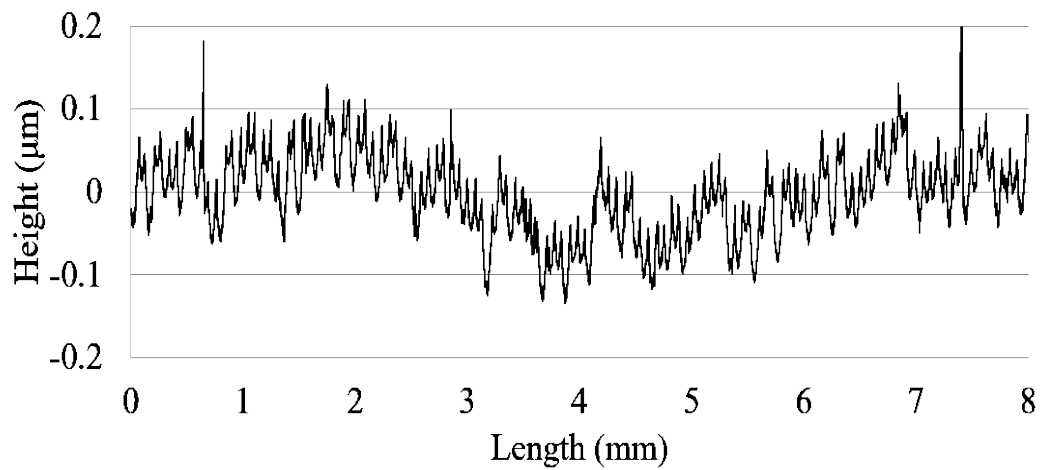
(a) Uncontrolled



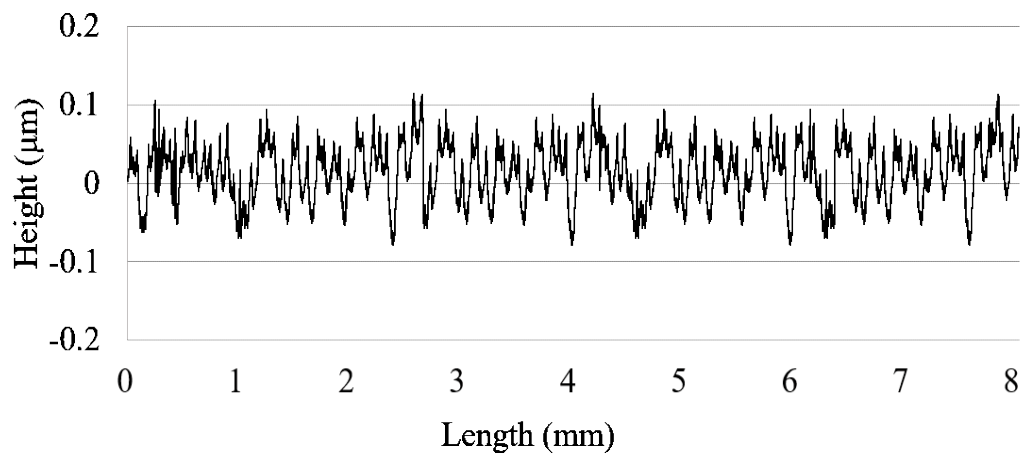
(b) Controlled

Fig. 4.5 Profile of the machined surface when feed rate is 5 mm/min.

F = 10 mm/min :



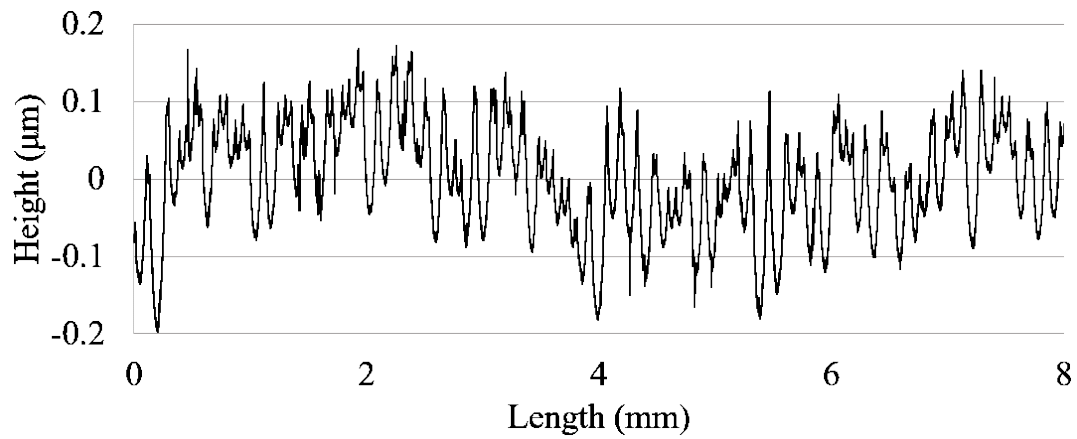
(a) Uncontrolled



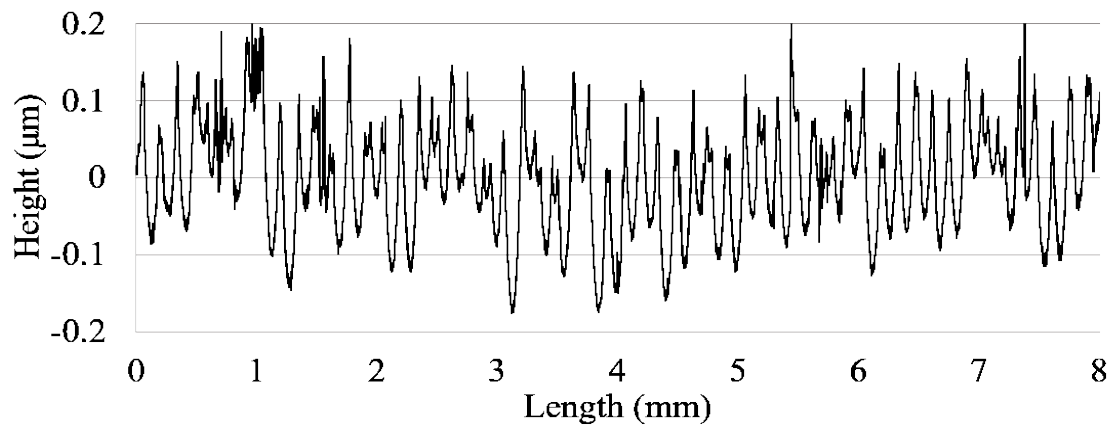
(b) Controlled

Fig. 4.6 Profile of the machined surface when feed rate is 10 mm/min.

F = 20 mm/min :



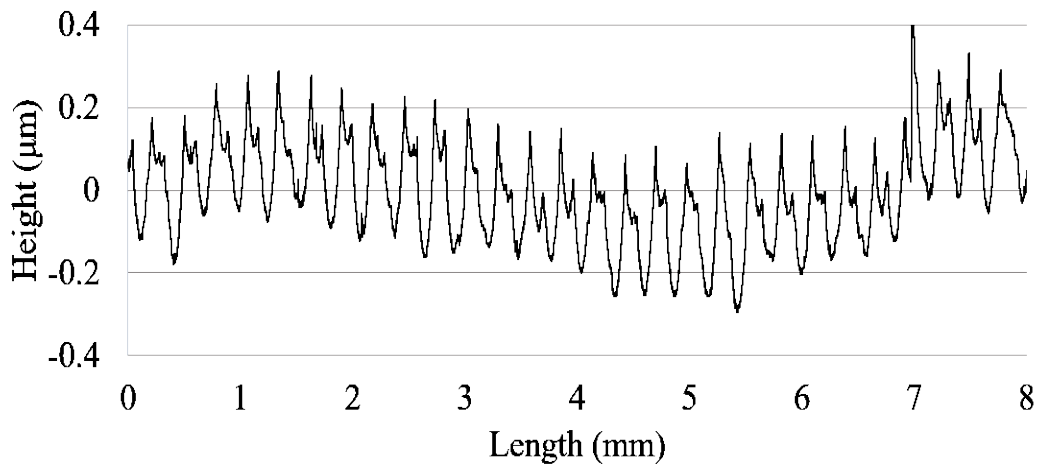
(a) Uncontrolled



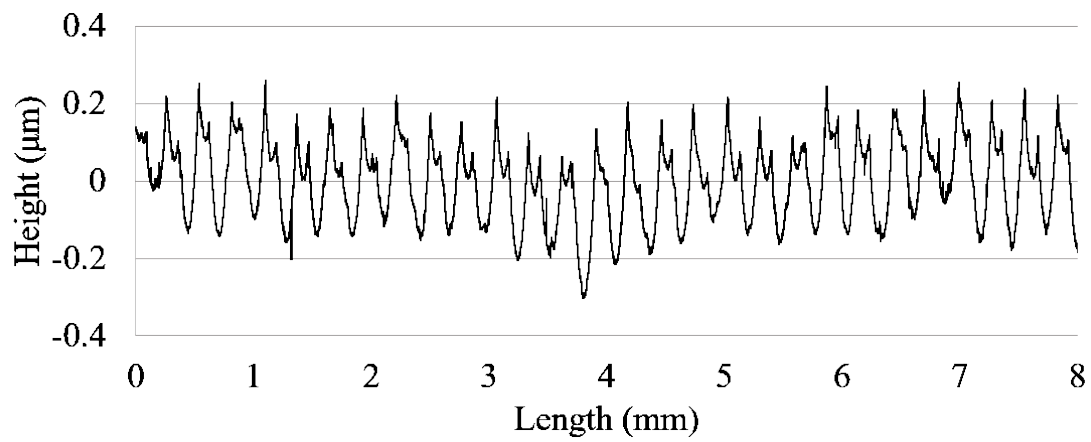
(b) Controlled

Fig. 4.7 Profile of the machined surface when feed rate is 20 mm/min.

F = 40 mm/min :



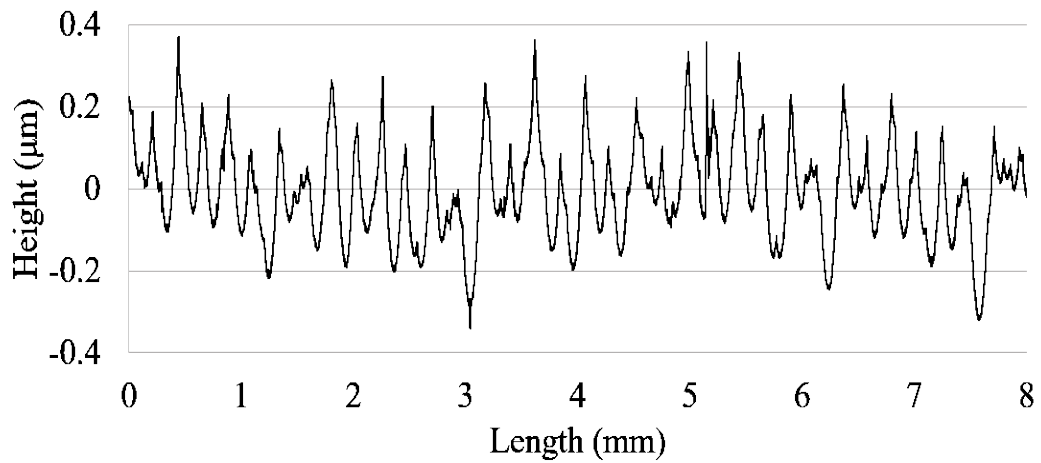
(a) Uncontrolled



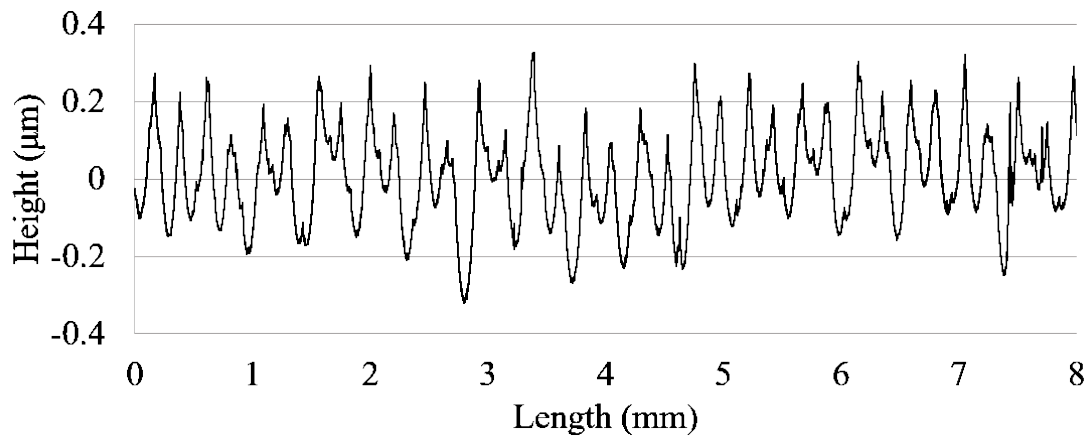
(b) Controlled

Fig. 4.8 Profile of the machined surface when feed rate is 40 mm/min.

F = 65 mm/min :



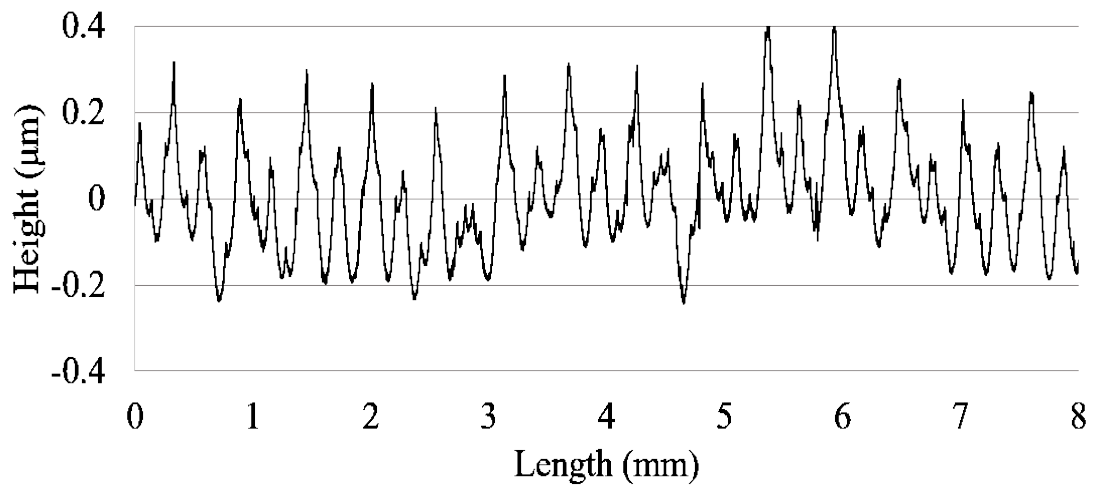
(a) Uncontrolled



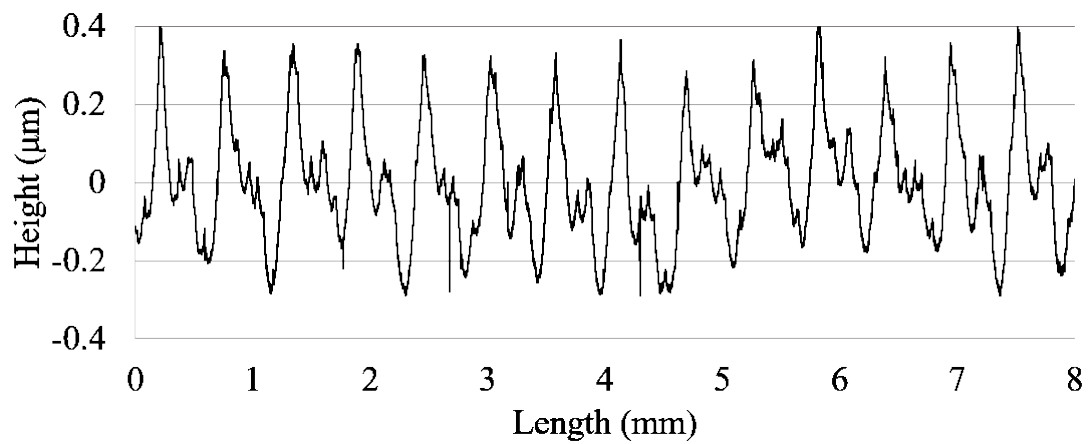
(b) Controlled

Fig. 4.9 Profile of the machined surface when feed rate is 65 mm/min.

F = 80 mm/min :



(a) Uncontrolled



(b) Controlled

Fig. 4.10 Profile of the machined surface when feed rate is 80 mm/min.

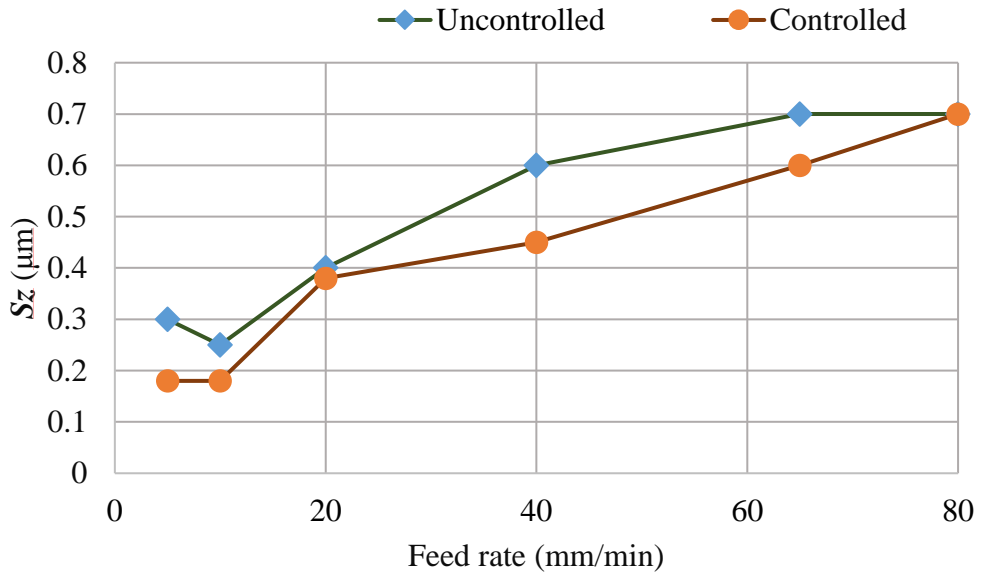


Fig. 4.11 S_z at different feed.

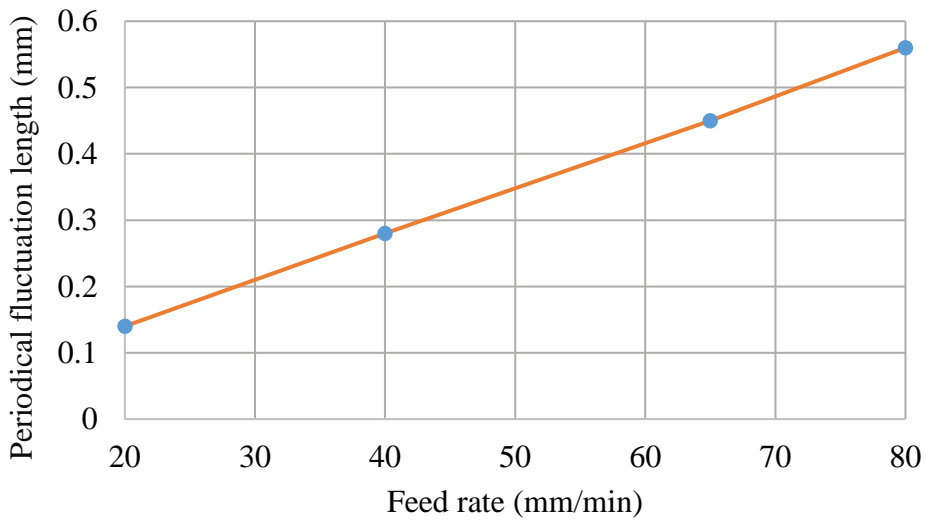


Fig.4.12 Periodical fluctuation length at different feed rate.

The results from **Fig. 4.5-Fig. 4.10** were summarized in **Fig. 4.11** and **Fig. 4.12**. As shown in **Fig. 4.5-Fig. 4.10**, we can see almost all the form accuracy were improved at different feed rate with controlled cutting, and periodical regular fluctuations appeared on machined surface became more and more obvious with the increasing of feed rate whether using controlled cutting or not. As shown in **Fig. 4.12**, the regular fluctuations length is proportional to the feed rate. Those regular fluctuations were not affected by feed per revolution since the theoretical S_z is much smaller than the period of regular fluctuation at each feed rate.

For example, when feed rate is 80 mm/min, $fz = F/N = 80 \text{ (mm/min)}/2500\text{(rev/min)} = 0.032 \text{ (mm)}$, which is smaller than the length of fluctuation about 0.57mm. The theoretical S_z is

$$S_z = \frac{fz^2}{8Rt} = \frac{0.032^2}{8 \times 13} = 0.00985 \text{ (}\mu\text{m)} \quad (4.1)$$

, where fz is the feed per revolution and Rt is rotation radius of fly cutter in feed direction.

However, the peak to valley of fluctuation is about 0.6 μm when feed rate is 80 mm/min. It is much bigger than the theoretical S_z . So feed per revolution is not the cause of forming the regular fluctuations.

As we know, the table motion error of machine is not affected by feed rate and left on machined surface. However, the period of regular fluctuations is proportional to the feed rate. In addition, the peak-to-valley height of the regular fluctuations should be suppressed to less than 0.2 μm when use this control cutting system, but the peak-to-valley height is above 0.2 μm when feed rate is faster than 20 mm/min even with controlled cutting. Based on above, the regular fluctuations are formed by different kinds of vibrations.

In order to analyze the cause of the fluctuations, we performed an FFT analysis based on the feed speed, and the errors frequency influencing the fluctuations were about 2.4 Hz and 4.8 Hz. **Fig.4.13** shows the FFT analysis results for the example of $F = 40$

mm/min. As shown in the **Fig.4.13**, the errors frequency were about 0.1Hz, 2.4Hz, 4.8Hz on the machined surface, the 0.1Hz error, which is the low frequency component, was suppressed to half or less by controlled cutting. While the error of 2.4Hz, 4.8Hz cannot be suppressed.

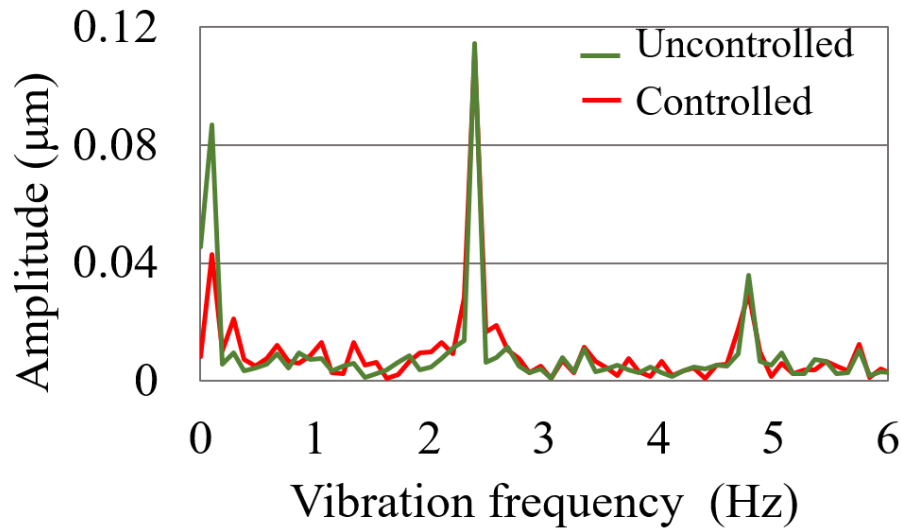


Fig.4.13 Result of FFT analysis of machined surface when feed speed is 40 mm /min.

To prove the vibrations influence on forming the regular fluctuations, simulation was carried out. According to the shape characteristics of the regular fluctuations, simulation formulas were obtained.

The assumptions of the simulation are shown below :

1. The rotational movement of the spindle performs a complete circular movement.
2. The tool rotation center is a circle center.
3. The tool rotation speed is sufficiently faster than the feed speed, and the trajectory of the tool tip per rotation is a circle.

4. The relative movement of the tool and the workpiece is completely transferred to the machining surface. (The shape of the bottom envelope of each curve of the tool tip trajectory is left on the machined surface.)

5. Systems other than motion error work ideally.

Simulation formula:

Circle center (fly cutter rotation center) motion formula:

$$f(t) = A \sin\left(\frac{2\pi}{\lambda} F_t\right) + A \sin\left(\frac{4\pi}{\lambda} F_t\right) \quad (4.2)$$

in which $F_t = nf$, $n = 1, 2, 3, 4, \dots$, n is revolution number, f is feed per revolution ($f = F/N$, where F is feed rate, N is spindle speed), A is error amplitude, λ is the periodical fluctuation length, $(F_t, f(t))$ is the circle center coordinate.

Fly cutter tool tip motion formula:

$$Y = Y_C - \sqrt{R^2 - (X - X_C)^2} \quad (4.3)$$

in which, $(X_C, Y_C) = (F_t, f(t))$, R is fly cutter rotation radius.

Simulation conditions are shown in **Table 4.2**.

Table 4.2 Simulation conditions

A [μm]	0.1, 0.2, 0.3, 0.4, 0.5, 0.6, 0.7
F [mm/min]	5, 10, 20, 40, 65, 80, 100
R [mm]	13
N [rev/min]	2500

Simulation result:

Circle center motion simulation result

Here just showed the circle center motion simulation result when feed rate was 40 mm/min, as shown in **Fig. 4.14**.

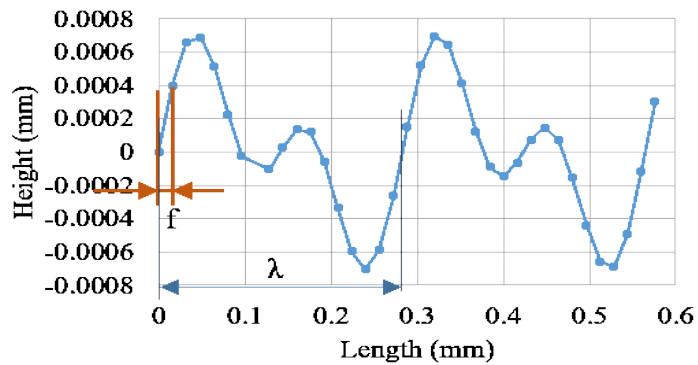


Fig. 4.14 Circle center motion simulation result ($F = 40$ mm/min).

Fly cutter tool tip motion simulation result

The relationship between B and A, feed rate is as shown Fig. 4.15. Height B means the regular fluctuations height (in simulation, residual height is formed by envelope curve). As shown in Fig. 4.16-Fig. 4.27, the height B of machined surface is similar to the simulation values when A is $0.2 \mu\text{m}$. The shape and the height B of regular fluctuations were compared with that obtained by simulations at different feed rate, respectively.

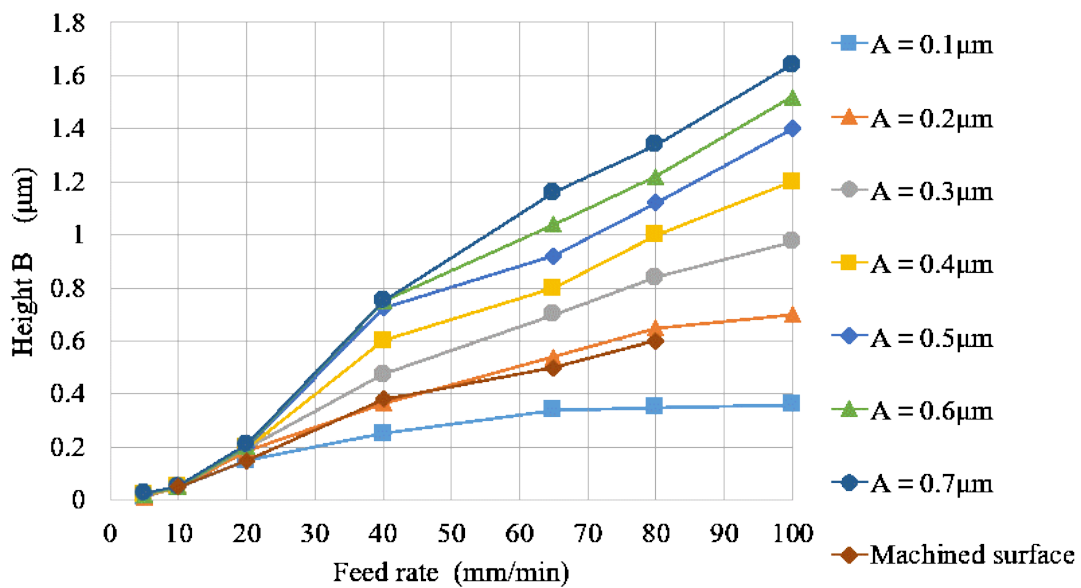


Fig. 4.15 Simulation result ($F = 40$ mm/min).

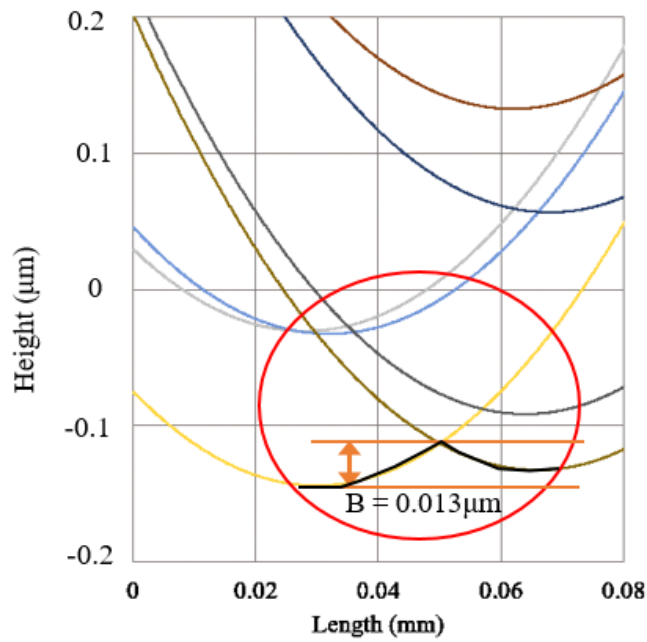
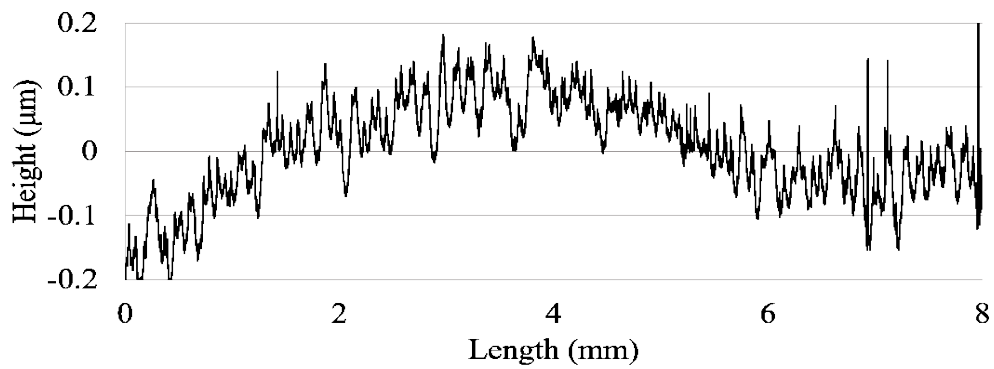
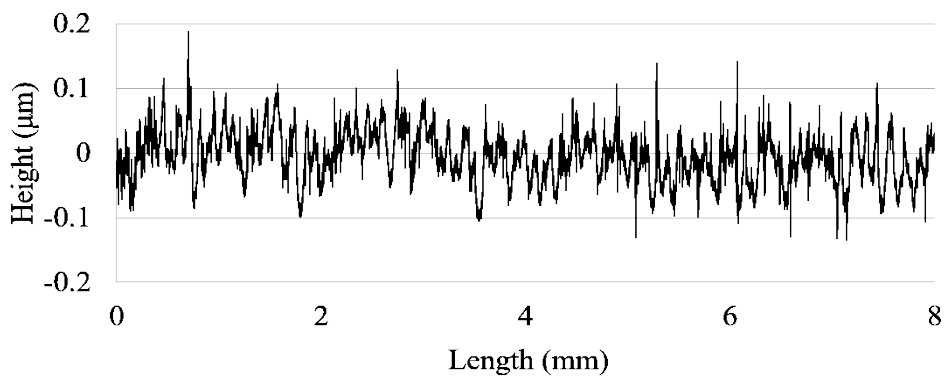


Fig. 4.16 Simulation result ($F = 5 \text{ mm/min}$).



(a) Uncontrolled



(b) Controlled

Fig. 4.17 Profile of the machined surface when feed rate is 5 mm/min .

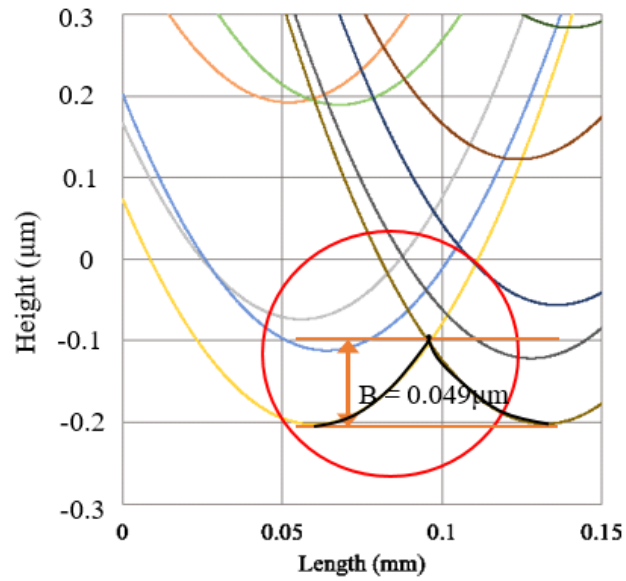
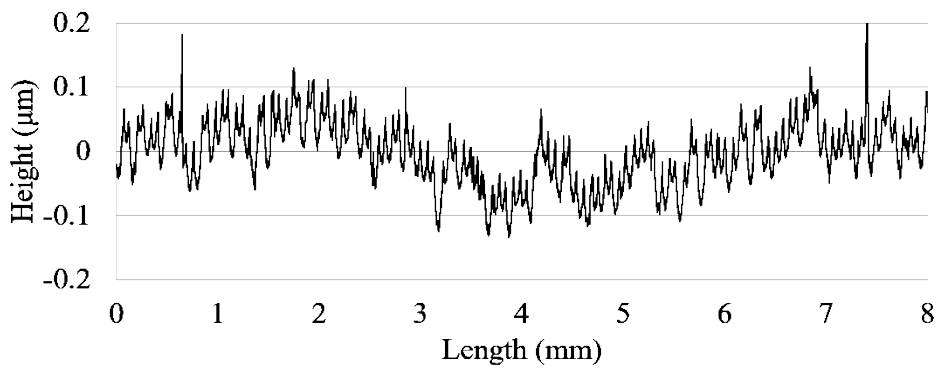
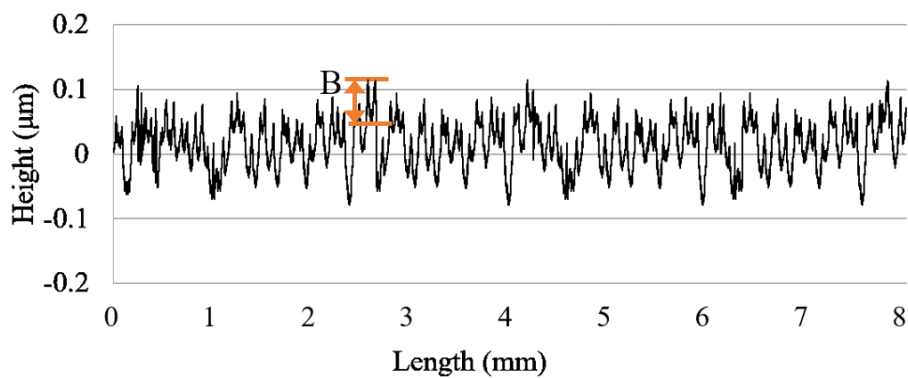


Fig. 4.18 Simulation result ($F = 10$ mm/min).



(a) Uncontrolled



(b) Controlled

Fig. 4.19 Profile of the machined surface when feed rate is 10 mm/min.

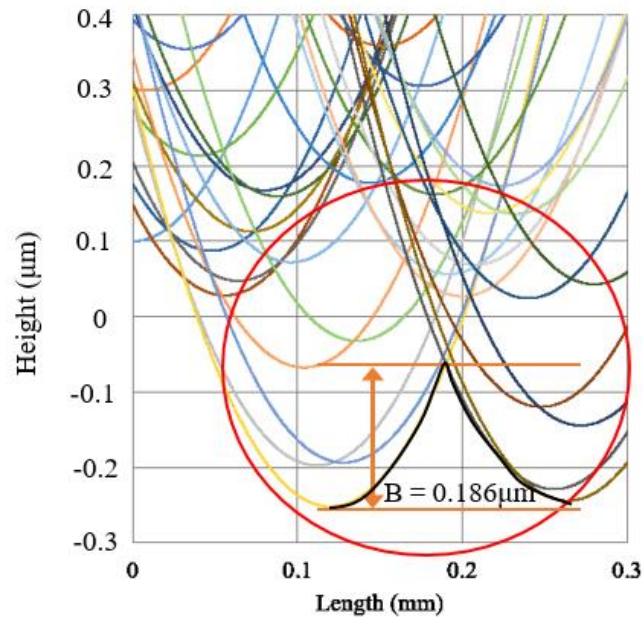
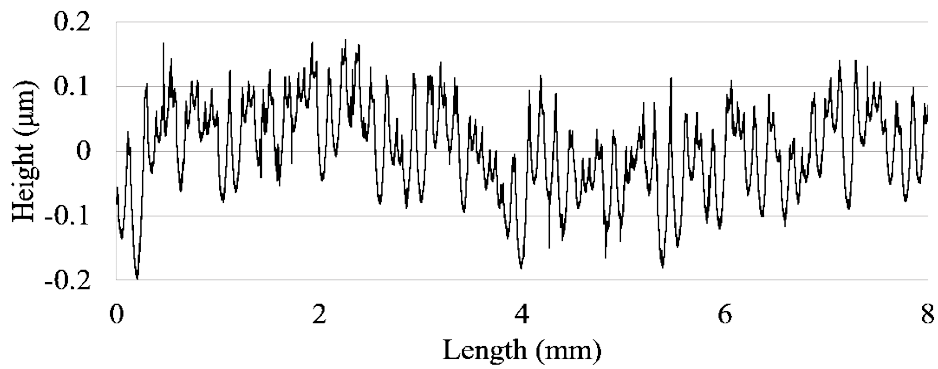
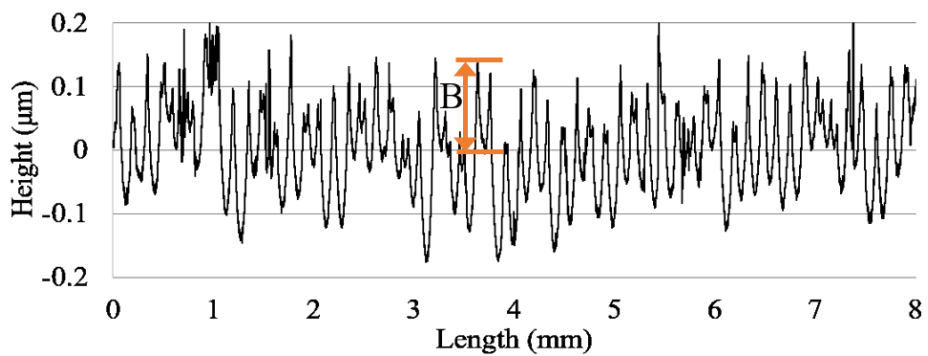


Fig. 4.20 Simulation result ($F = 20 \text{ mm/min}$).



(a) Uncontrolled



(b) Controlled

Fig. 4.21 Profile of the machined surface when feed rate is 20 mm/min .

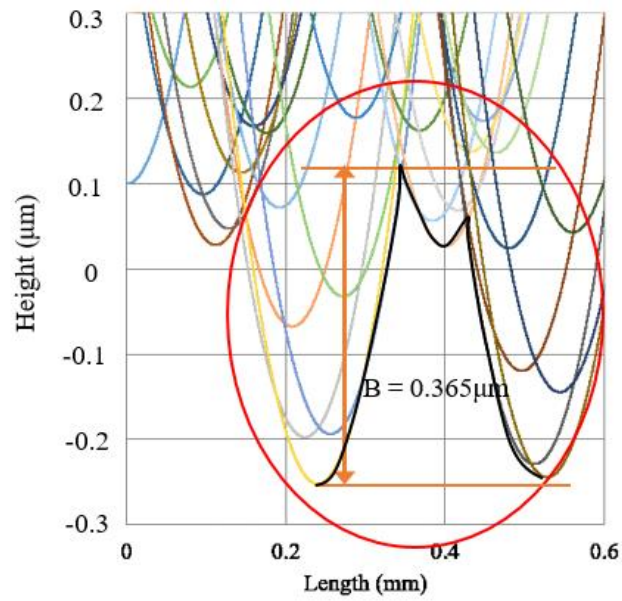
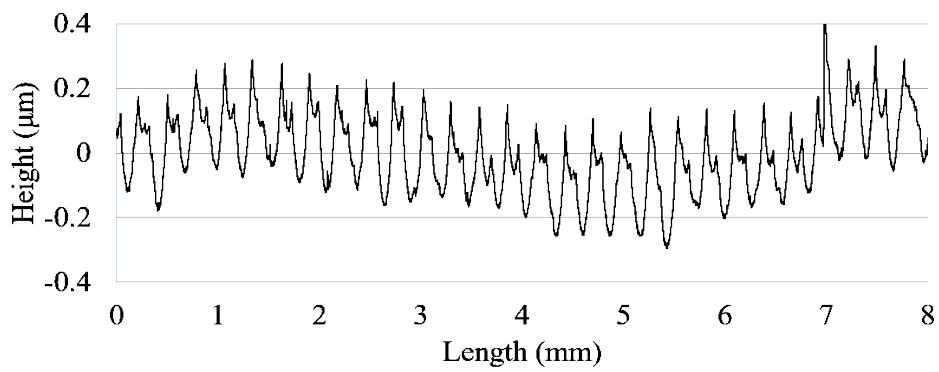
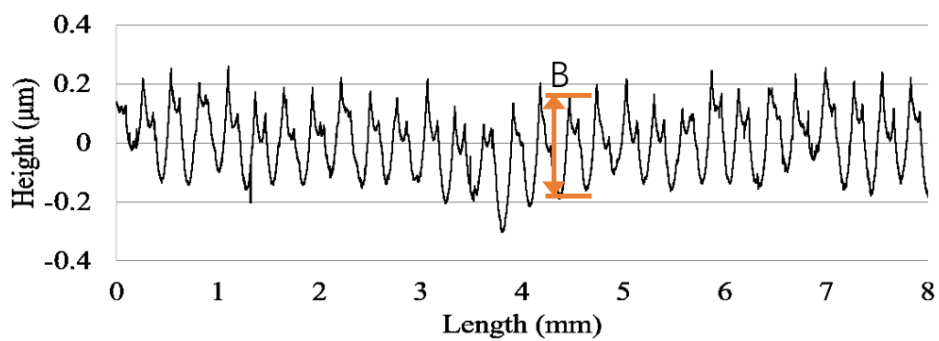


Fig. 4.22 Simulation result ($F = 40$ mm/min).



(a) Uncontrolled.



(b) Controlled.

Fig. 4.23 Profile of the machined surface when feed rate is 40 mm/min.

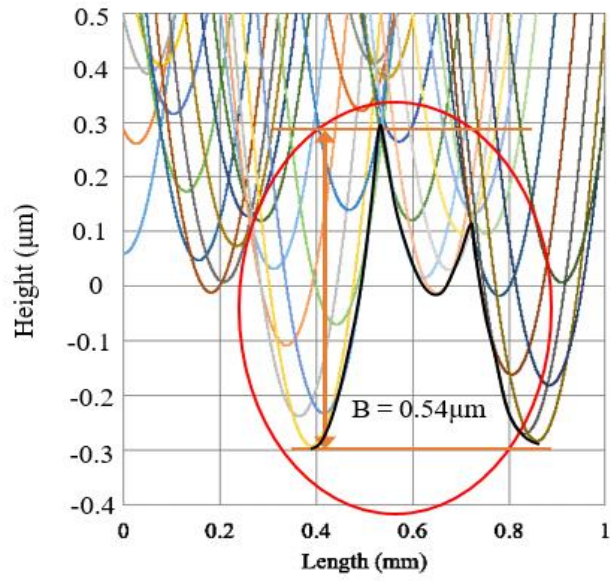
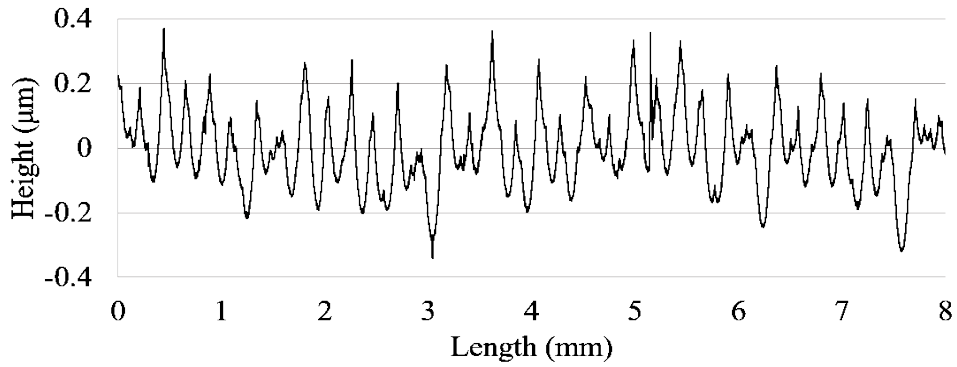
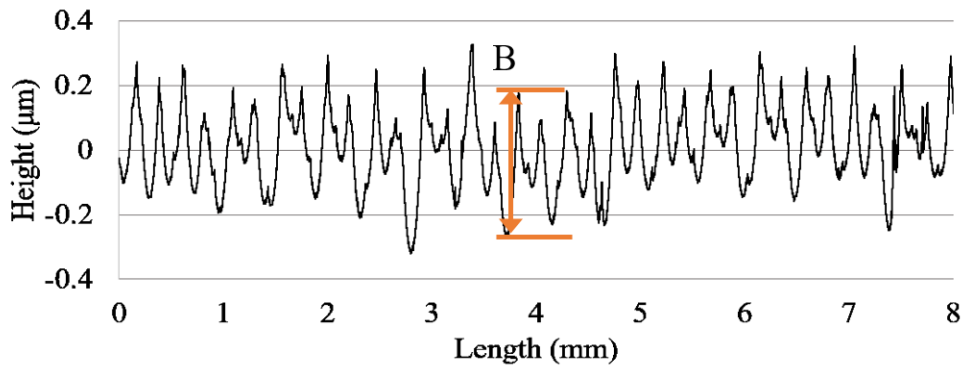


Fig. 4.24 Simulation result ($F = 65 \text{ mm/min}$).



(a) Uncontrolled



(b) Controlled

Fig. 4.25 Profile of the machined surface when feed rate is 65 mm/min .

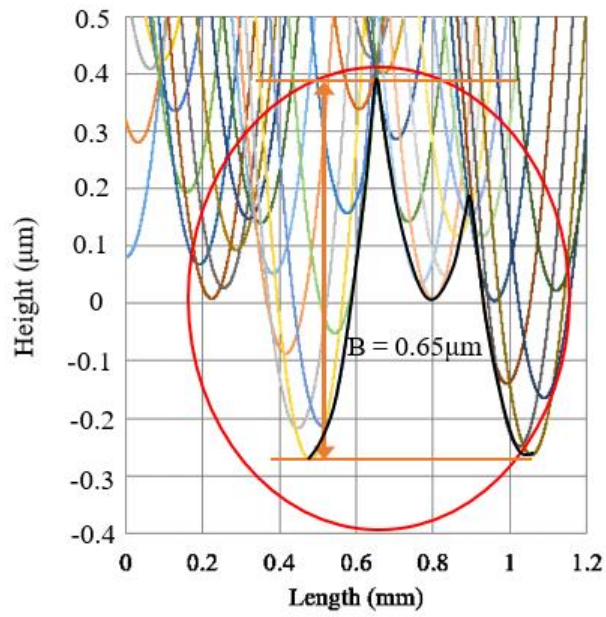
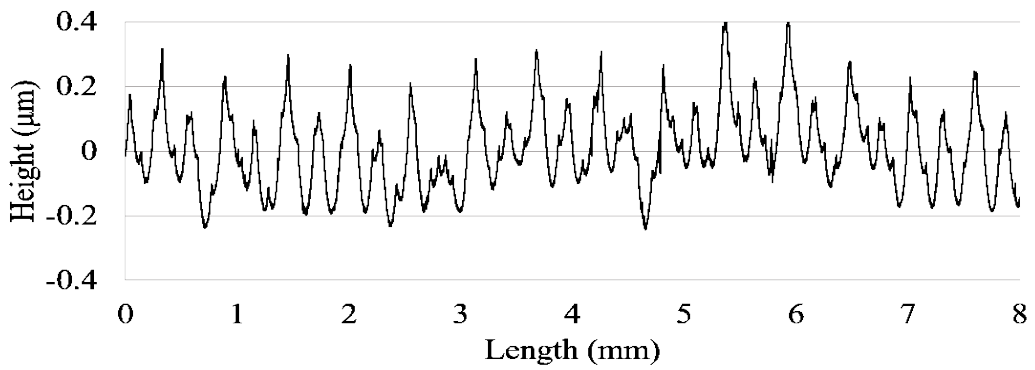
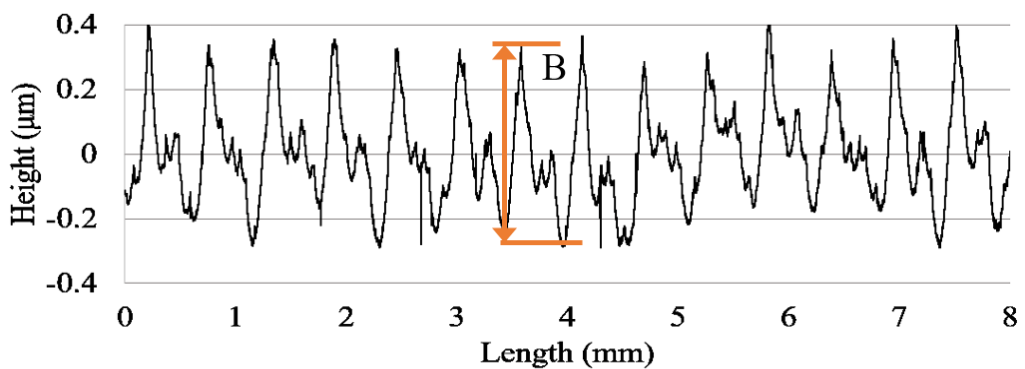


Fig. 4.26 Simulation result ($F = 80 \text{ mm/min}$).



(a) Uncontrolled



(b) Controlled

Fig. 4.27 Profile of the machined surface when feed rate is 80 mm/min .

When feed rate is 5 mm/min, the height B obtained by simulation is 0.013 μm , but the height B value and the shape cannot be found on machined surface since other high frequency errors with amplitude less than 0.1 μm influenced the machined surface, as shown in **Fig.4.16-Fig.4.17**.

However, as shown in **Fig.4.18- Fig.4.27** ($F = 10 \text{ mm/min}, 20 \text{ mm/min}, 40 \text{ mm/min}, 65 \text{ mm/min}, 80 \text{ mm/min}$), the shape and the height B of regular fluctuations are almost the same as that obtained by simulations when A is 0.2 μm . As with the simulation result, the height B of regular fluctuations became higher when the feed rate became higher. According to circle center (fly cutter rotation center) motion formula, the simulation results revealed that there are mainly two kinds of vibration (frequency about 2.4Hz, 4.8Hz) caused the regular fluctuations. These two kinds of vibrations are independent of the control system, since they appeared on machined surface whether using control cutting or not.

During the ultra-precision machining process there are multiple sources of vibration, including spindle vibration [1-4], tool tip vibration [5], self-excited vibration [6], background vibration [7] and material induced vibration [8], etc., all of which have different effects on the surface finish. Tool-tip vibration with high natural frequencies influences surface topography at a nanometric level [9], and usually results in periodic fluctuation of the surface profile in a particular spatial frequency [10] and non-uniform zebra-stripe-like patterns on the machined surface [11]. Spindle vibration is another key factor that has a major influence on surface topography in UPM. For example, in ultra-precision diamond turning, axial vibration produces concave, periodic concentric, spiral and two-fold patterns on the machined surface [12]; and in ultra-precision raster fly cutting (UPRFC), coupled tilting vibration has a principle impact on surface topography by forming ribbon-stripe and irregular patterns on the machined surface [13] (dynamic unbalance of fly cutter has an impact on surface topography).

Therefore, by reducing the effect of those vibrations, such as improving the dynamic unbalance of the fly cutter, it is possible to reduce the height of the periodical regular

fluctuations at a fast feed rate. If those vibrations are suppressed, the machined surface quality can be improved with control cutting at a faster feed rate when considering that the system response speed is fast enough. In that case, the control cutting efficiency can be higher.

But for this current situation, if not suppress the vibrations, by slowing down the feed rate to reduce the influence of periodical regular fluctuations and using control cutting at the same time to improve the form accuracy, a good quality machined surface can be obtained, as shown in **Fig. 4.5 (b)**.

4.3. Conclusions

The experiments of relationship between feed rate and machined surface with controlled cutting and uncontrolled cutting were carried out and the machined surface quality was discussed, conclusions can be drawn as following:

1. Almost all the form accuracy of machined surface were improved with controlled cutting at different feed rate.
2. Periodical regular fluctuations appeared on machined surface became more and more obvious with the increasing of feed rate whether using controlled cutting or not. The regular fluctuations length is proportional to the feed rate, mainly caused by two kinds of vibrations (2.4Hz, 4.8Hz).

Reference

- [1] Zhang SJ, To S, Cheung CF, Wang HT. Dynamic characteristics of an aerostatic bearing spindle and its influence on surface topography in ultra-precision diamond turning. *Int J Mach Tools Manuf* 2012;62:1–12.
- [2] D.L. Martin, A.N. Tabenkin, F.G. Parsons, Precision spindle and bearing error analysis, *International Journal of Machine Tools and Manufacture* 35 (1995) 187–193.
- [3] E.R. Marsh, D.A. Arneson, M.J. van Doren, S.A. Blystone, The effects of spindle dynamics on precision flycutting, in: *Proceedings of the American Society for Precision Engineering 2005 Annual Meeting*, Norfolk, VA, October 2005.
- [4] C.H. An, Y. Zhang, Q. Xu, F.H. Zhang, J.F. Zhang, L.J. Zhang, J.H. Wang, Modeling of dynamic characteristic of the aerostatic bearing spindle in an ultraprecision fly cutting machine, *International Journal of Machine Tools and Manufacture* 50 (2010) 374–385.
- [5] Kim DS, Chang IC, Kim SW. Microscopic topographical analysis of tool vibration effects on diamond turned optical surfaces. *Precis Eng* 2002;26(2):168–74.
- [6] Suzuki N, Kurata Y, Kato T, Hino R, Shamoto E. Identification of transfer function by inverse analysis of self-excited chatter vibration in milling operations. *Precis Eng* 2012;36(4):568–75.
- [7] Lv D, Wang H, Tang Y, Huang Y, Li Z. Influences of vibration on surface formation in rotary ultrasonic machining of glass BK7. *Precis Eng* 2013;37(4):839–48.
- [8] Lee W, To S, Cheung CF. Effect of crystallographic orientation in diamond turning of copper single crystals. *Scr Mater* 2000;42:937–45.
- [9] Zhang SJ, To S, Zhang GQ, Zhu ZW. A review of machine-tool vibration and its influence upon surface generation in ultra-precision machining. *Int J Mach Tools Manuf* 2015;91:34–42.
- [10] Wang H, To S, Chan CY, Cheung CF, Lee WB. A study of regularly spaced shear

bands and morphology of serrated chip formation in micro-cutting process. *Scr Mater* 2010;63:227–30.

[11]Zhang SJ, To S. A theoretical and experimental investigation into multimode tool vibration with surface generation in ultra-precision diamond turning. *Int J Mach Tools Manuf* 2013;72:32–6.

[12]Zhang SJ, To S, Wang HT. A theoretical and experimental investigation into five-DOF dynamic characteristics of an aerostatic bearing spindle in ultra-precision diamond turning. *Int J Mach Tools Manuf* 2013;71:1–10.

[13]ZHANG, S. J.; TO, S. A theoretical and experimental study of surface generation under spindle vibration in ultra-precision raster milling. *International Journal of Machine Tools and Manufacture*, 2013, 75: 36-45.

Chapter 5 Disturbance removal experiment

5.1. Experimental condition

Base on the principle of CCRS, not only the table motion error but also the disturbance from outside should be able to be suppressed. To prove it, in this experiment, artificial disturbance was added between the fly cutter and the workpiece, and the difference of machined surface with controlled cutting and without controlled cutting was compared and discussed.

Assembling of the experimental equipment was the same as in the experiment of the feed rate. The movement (square wave shape) of the feed path shown in **Fig. 5.1** generated by an ordinary milling machine was considered as a disturbance. In the case of controlled cutting at a feed rate of 5 mm / min, good quality machined surfaces can be machined, so feed rate 5 mm/min was adopted for this experiment. In this control processing system, the control length range of PZT actuator is about 10 μm , and there is also a table motion error during the control processing, so the height a of square wave is set to 5 μm . The width b of the square wave was set to 0.25 mm and 0.5 mm so that the influence of square wave disturbance can be seen well on the machined surface after uncontrolled cutting. The other experimental conditions were the same as the experimental conditions of the feed rate.

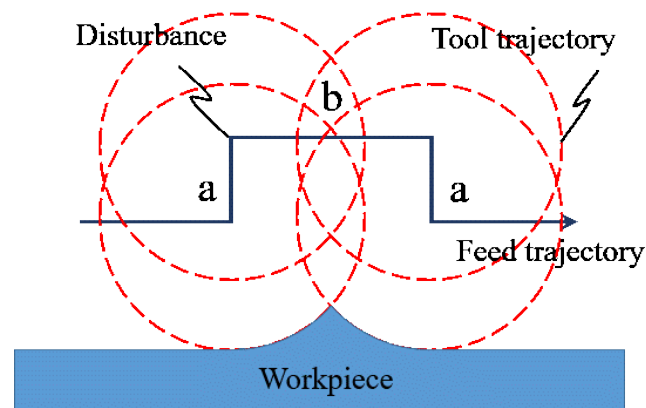
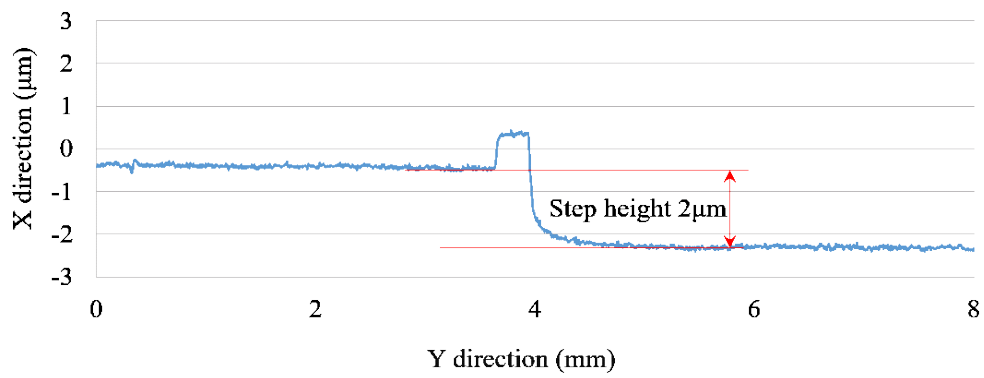


Fig. 5.1 Method of add artificial disturbance.

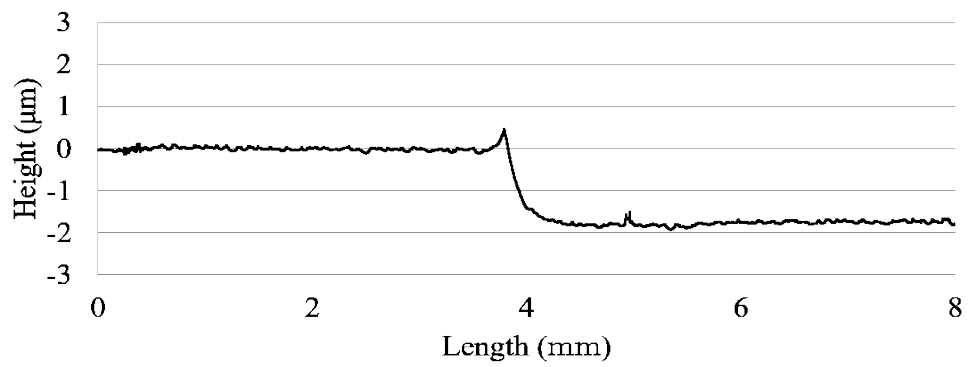
5.2 Experimental results and discussion

As can be seen from the movement of the table in **Fig. 5.2 (a)** and **(c)** and **Fig. 5.3 (a)** and **(c)**, the moving distance of the table in the X direction, that is, the distance the fly cutter leaves the work piece is much smaller than 5 μm of the value a . Besides, since the difference between the distance to go away and the distance to go back is very large, it was known that there was a large table motion error in the used ordinary milling machine. Since the separation distance and the return distance are not equal, in the case of uncontrolled cutting, as shown in **Fig. 5.2 (b)** and **Fig. 5.3 (b)**, a step height of about 2 μm was left on the machined surface. In the case of $b = 0.25 \text{ mm}$ due to the influence of the square wave disturbance, S_z was about 2 μm and in the case of $b = 0.5 \text{ mm}$, S_z was about 3 μm . While after controlled cutting, as shown in **Fig. 5.2 (d)** and **Fig. 5.3 (d)**, the step heights of about 2 μm which appeared on the machined surface by uncontrolled cutting were both suppressed within 0.6 μm by control cutting. The step was not able to be completely compensated because the gains of HIPOSS and LK-H008W did not match completely. After that, as shown in **Fig. 5.2 (d)** and **Fig. 5.3 (d)**, a dent shape was left on the machined surface after controlled cutting. The reason of the dent shape was that the PZT actuator could not respond to became short rapidly due to the control delay of this control system, so when the fly cutter approached the workpiece suddenly, the fly cutter cut the workpiece deeply.

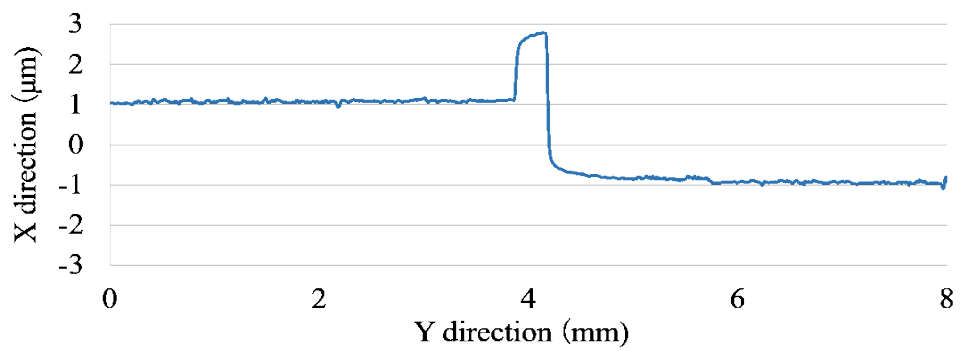
Therefore, based on above, by adjusting the gain and improving the system respond speed, the machined surface quality with controlled cutting will be better.



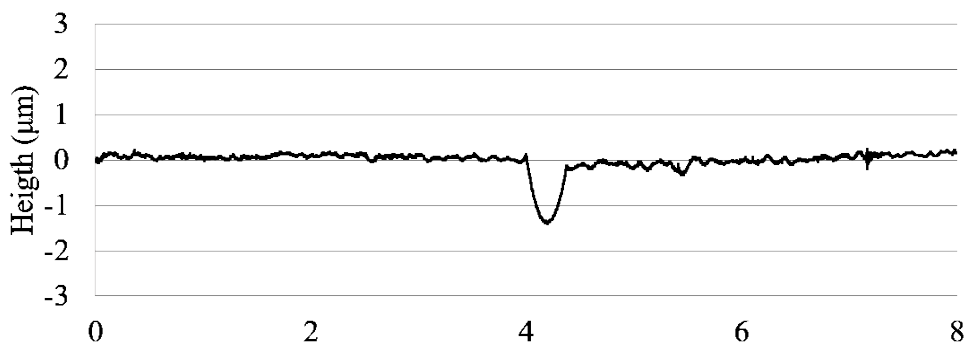
(a) Disturbance in uncontrolled cutting (table movement).



(b) Profile of machined surface after uncontrolled cutting.

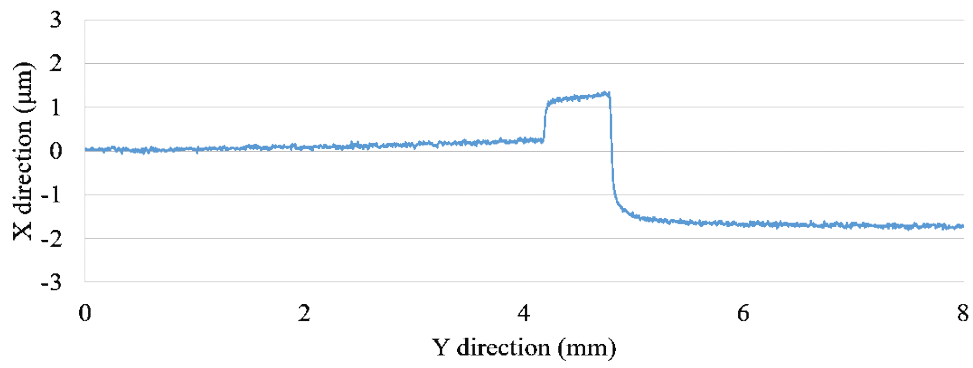


(c) Disturbance in controlled cutting (table movement).

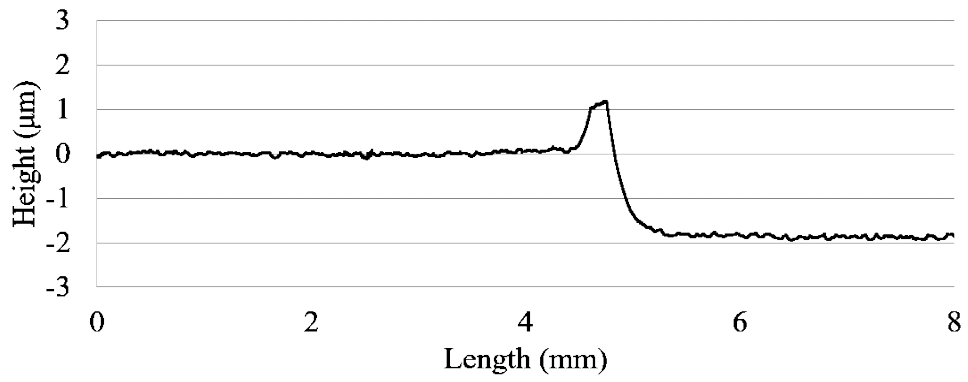


(d) Profile of machined surface after controlled cutting.

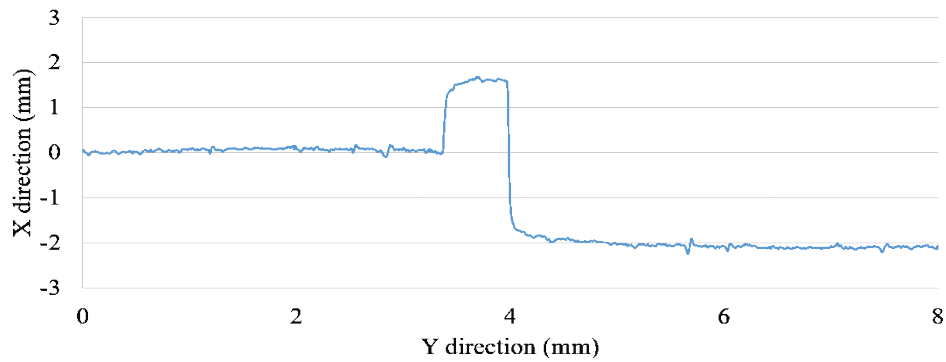
Fig. 5.2 Disturbance removal experiment result of $b = 0.25$ mm.



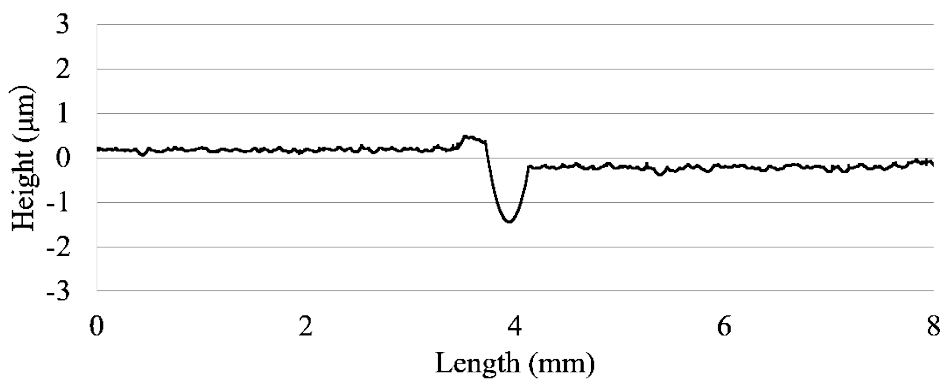
(a) Disturbance in uncontrolled cutting (table movement).



(b) Profile of machined surface after uncontrolled cutting.



(c) Disturbance in controlled cutting (table movement).



(d) Profile of machined surface after controlled cutting.

Fig. 5.3 Disturbance removal experiment result of $b = 0.5$ mm.

5.3. Conclusions

In order to prove the disturbance from outside should be suppressed by the control cutting system, artificial disturbance was added between the fly cutter and the workpiece, and the difference of machined surface with controlled cutting and without controlled cutting was compared and discussed. Conclusions are as follows:

1. The step heights of about $2 \mu\text{m}$ appeared on the machined surface by uncontrolled cutting were both suppressed within $0.6 \mu\text{m}$ by control cutting. The step was not

able to be completely compensated because the gains of HIPOSS and LK-H008W did not match completely.

2. The cause of the dent shape on the machined surface after controlled cutting was that the PZT actuator could not respond to become short rapidly due to the control delay of this control system.

Chapter 6 Experiment for improving precision of circular machining

6.1. Configuration and principle

In this experiment, it was confirmed that the experiment of circular arc machining by uncontrolled machining and control machining was conducted, and the effectiveness of improving the circular arc machining accuracy of the ordinary milling machine was confirmed.

The principle of arc machining by CCRS is shown in **Fig. 6.1**. During circular arc machining, gap sensor regarded as one with the fly cutter detect arc motion error of the spindle by scanning the cylindrical concave mirror, and then feed the signal back to PZT actuator to compensate the arc machining error of the ordinary milling machine.

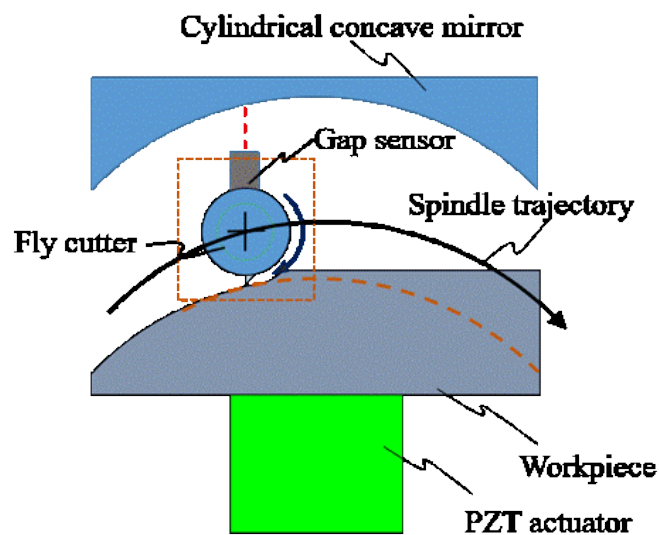


Fig. 6.1 Principle of arc machining by CCRS.

Since the range of precisely measurable angles of the gap sensor LK-H008W is within 2 degrees, here, a cylindrical concave mirror with a radius of curvature of 500 mm was used as a reference surface for this experiment. **Fig. 6.2** shows the size of the

cylindrical concave mirror used in this experiment and **Table 6.1** shows the parameter of the cylindrical concave mirror.

Because the range of the control cutting system can be compensated is about 10 μm , the distance measured with LK-H008W during control (the adjustment of the angle of the cylindrical concave mirror is important) needs to be maintained within 10 μm .

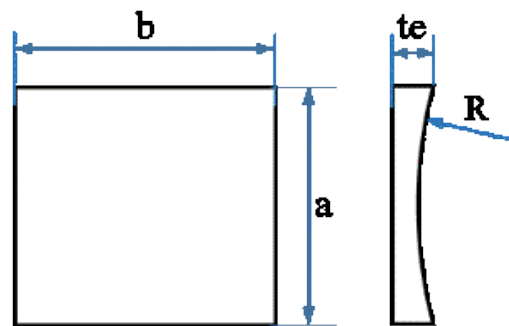
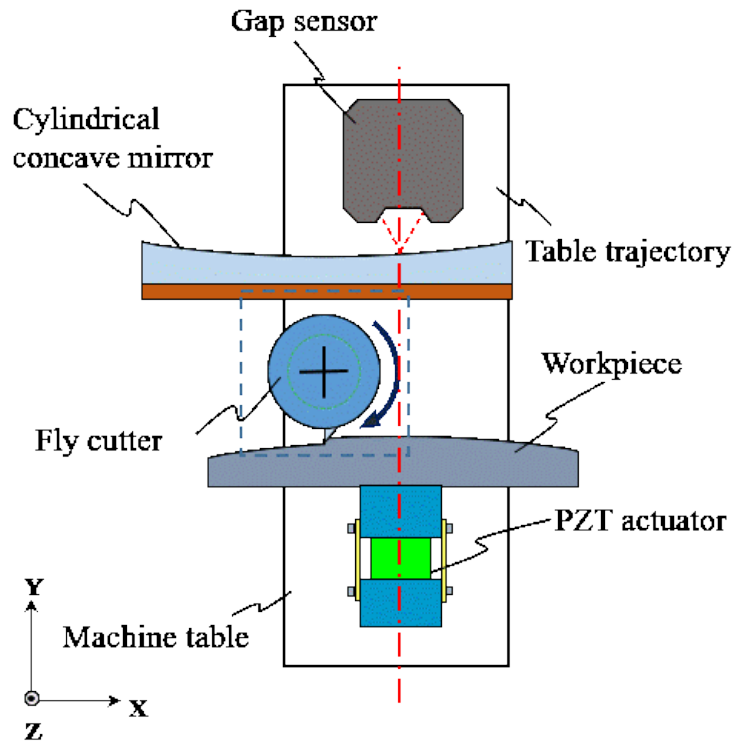


Fig. 6.2 Size of cylindrical concave mirror.

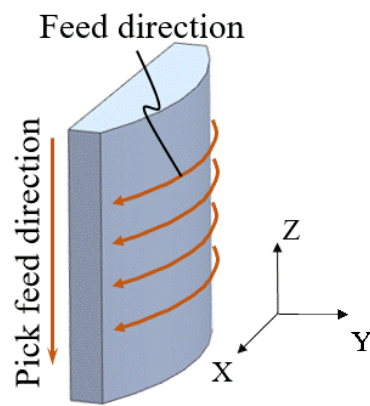
Table 6.1 Parameter of the cylindrical concave mirror

te	5mm
R	500mm
a	30mm
b	30mm

Actually, since the table moves in an arc motion, not the spindle, and the fly cutter and the gap sensor are not integrated, the real experimental setup was shown in **Fig. 6.3 (a)**. **Fig. 6.3 (b)** shows the cutting strategy of arc machining on workpiece surface. Since the cut depth of the fly cutting was 5 μm , we made a rough machining of the arc on workpiece surface before the control cutting experiment.



(a) Principle of circular arc machining by CCRS for actual experimental setup.



(b) Arc cutting method for workpiece.

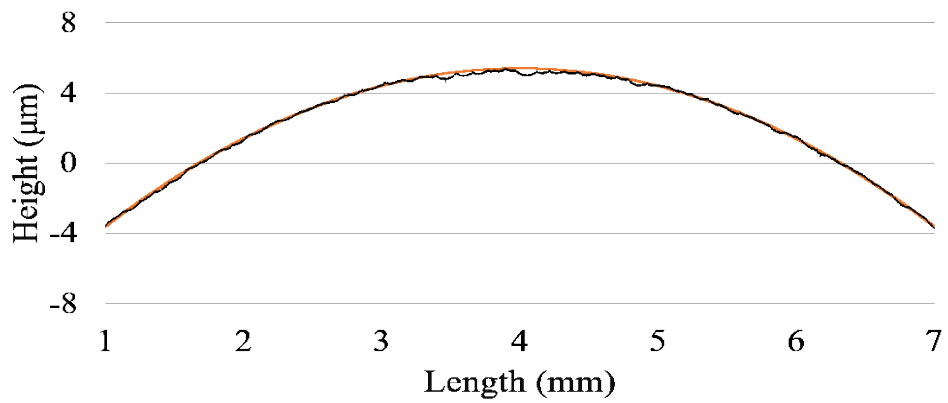
Fig. 6.3 Arc machining by CCRS.

6.2 Experiment result and discussion

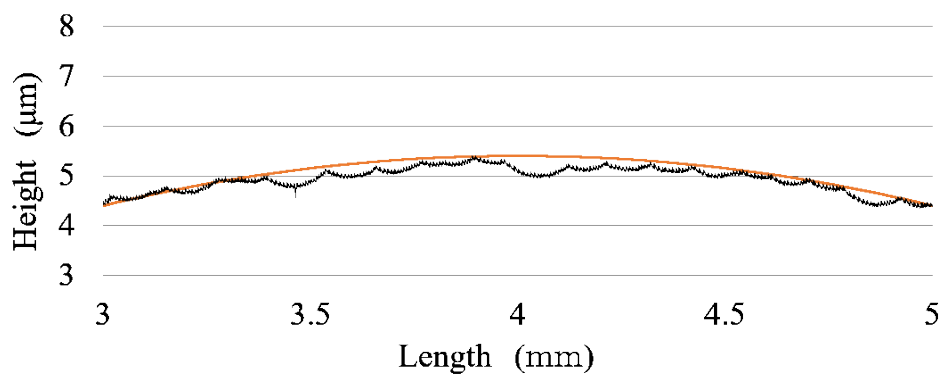
Experimental results are shown in **Fig. 6.4** and **Fig. 6.5**. The orange curve is an arc with an ideal radius of 500 mm. When the evaluation length is 6 mm in **Fig. 6.4 (a)** and **Fig. 6.5 (a)**, the results of machined surface with uncontrolled cutting and controlled cutting seem to be almost the same, but in **Fig. 6.4 (b)** and **Fig. 6.5 (b)** by comparing with the results of enlarged view, the quality of arc machined surface by controlled cutting was improved (The improvement of form accuracy cannot be seen in **Fig. 6.5**, due to that the sensitivity of gap sensor is different at a different measuring angle. For improvement of arc machining form accuracy, the next work is to control within the range of measuring angles where the gap sensor the sensitivity is better).

In order to evaluate the accuracy of the machined surface of arc machining obtained by uncontrolled cutting and controlled cutting, the arc shape was taken from the machined surface with a roughness meter as shown in **Fig. 6.6** and then evaluated with the standard deviation S_p and the maximum height roughness S_z . The values of machined surface were $S_p = 0.0727 \mu\text{m}$ and $S_z = 0.4 \mu\text{m}$ after uncontrolled cutting, while the values became to $S_p = 0.0373 \mu\text{m}$ and $S_z = 0.18 \mu\text{m}$ after controlled cutting. It showed that accuracy of arc machining was improved more than half.

In order to further improve the precision of circular arc machining with this control cutting system, it is necessary to reduce the noise measured by LK-H008W during machining and adjust the gain to match between HIPOSS and LK-H008W.

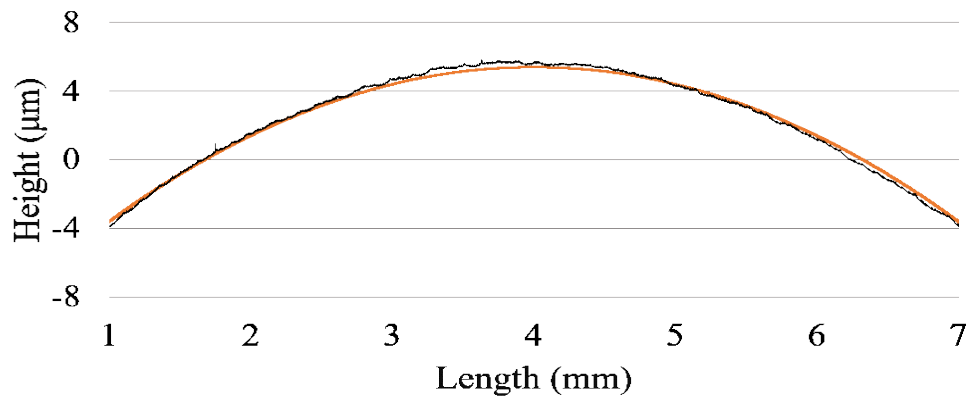


(a) Profile of arc machining surface after uncontrolled cutting.

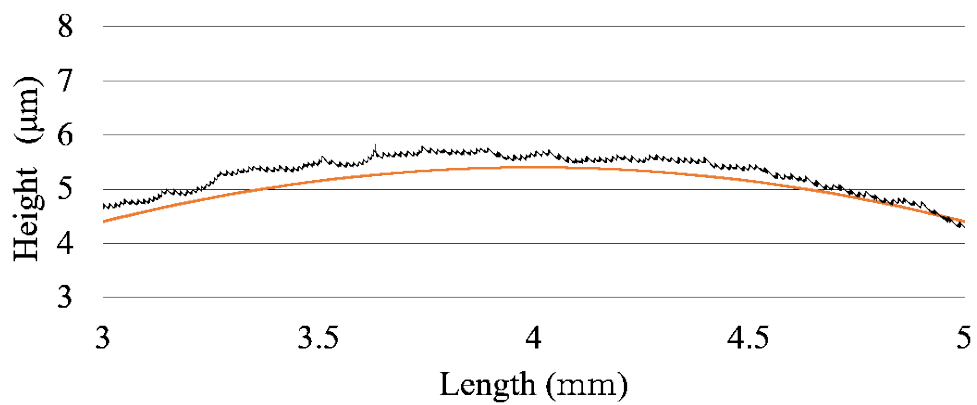


(b) Enlarged view of (a).

Fig. 6.4 Uncontrolled.

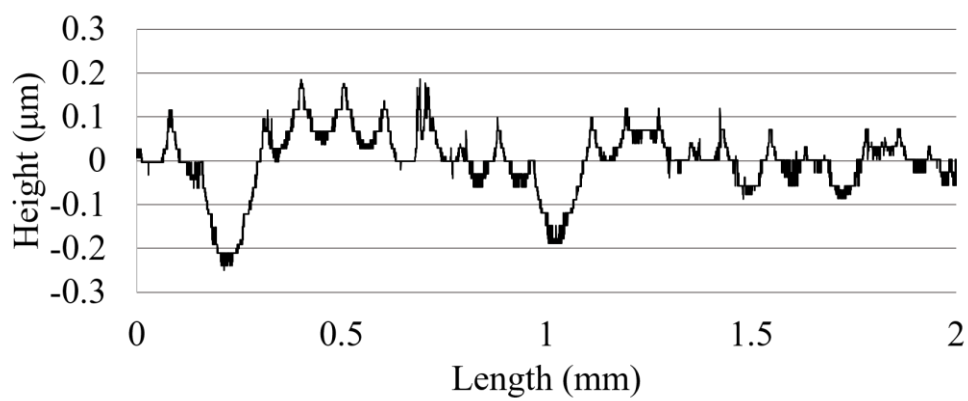


(a) Profile of arc machining surface after controlled cutting.

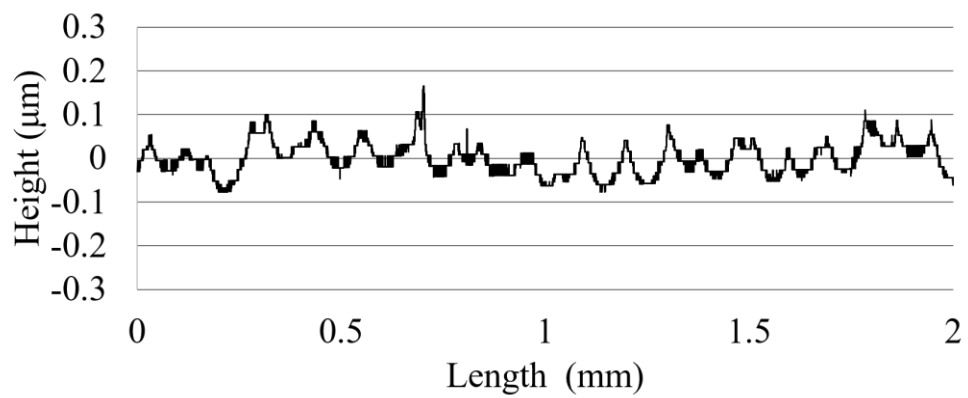


(b) Enlarged view of (a).

Fig. 6.5 Controlled.



(a) Profile of arc machining surface after uncontrolled cutting.



(b) Profile of arc machining surface after controlled cutting.

Fig. 6.6 Profile of machined surface after filtering out arc shape.

6.3. Conclusions

The experiments of circular arc machining by uncontrolled machining and control machining were carried out, and the effectiveness of improving the circular arc machining accuracy of the general-purpose milling machine was confirmed. The conclusions are as follows:

1. After taking the arc shape from the machined surface with roughness meter, the values of machined surface were $Sp = 0.0727 \mu\text{m}$ and $Sz = 0.4 \mu\text{m}$ after uncontrolled cutting, while the values became to $Sp = 0.0373 \mu\text{m}$ and $Sz = 0.18 \mu\text{m}$ after controlled cutting. It showed that accuracy of arc machining should be improved by controlled cutting.

Chapter 7 Summary and future work

In this research, in order to improve the machining accuracy of ordinary milling machine, a control cutting system, diamond fly cutting using CCRS was proposed. The machined surface with and without controlled cutting was evaluated. From the results, it can be seen that using this control system can improve the machining accuracy of ordinary milling machine.

Conclusions obtained in this study are as follows.

7.1 Conclusions of each chapter

Chapter 1

The background and purpose of this research were described.

Chapter 2

In this chapter, the components in control cutting system were introduced, including micro displacement servo (MDS), optical sensors for in-process measurement, diamond tool and fly cutter, mirror and mirror jig, displacement detector, PZT amplifier, HIPOSS amplifier and LK-H008W controller. Static rigidity of MDS were tested, and it was considered that there was no influence of distortion due to cutting resistance. Both of two gap sensors will take about 30 minutes to reach a relatively stable state. Therefore, this control cutting system needs to be warmed over half an hour.

The LabVIEW control program used for control cutting system was developed. The system was tested and adjusted, including time spent to reach steady state, calibration, gain adjustment, transient characteristics.

Chapter 3

In this chapter, the good quality machined surface was obtained (unlike shaping, no high-frequency component left on machined surface), when feed rate and pick feed is small even without controlled cutting. Because the noise detected by LK-H008W affect the surface quality in control cutting process, the different cutoff frequency was set by low-pass filter and then discussed the quality of machined surface in feed direction.

The high-frequency component that degrades the machined surface finish during shaping was suppressed by fly cutting.

The accuracy of the machined surface can be improved on an ordinary milling machine by this control cutting system (to obtain S_z less than $0.2 \mu\text{m}$).

Since the noise detected by gap sensor as instruction value influence the machined surface, it is considered that further noise suppression will increase the quality of the machined surface. Of course, the gain of the two gap sensors need to be matched before experiment.

Chapter 4

In this chapter, the machined surface was machined at different feed rate with and without controlled cutting and the machined quality was discussed.

From the result of machined surface profile, all the form accuracy of machined surface was improved at different feed rate with controlled cutting. However, periodical regular fluctuations appeared on machined surface became more and more obvious with the increasing of feed rate whether using controlled cutting or not. The periodical regular fluctuations were not affected by the table motion error and feed per revolution. The periodical regular fluctuations were probably mostly affected and formed by different vibrations (2.4Hz, 4.8Hz), such as fly cutter tool tip vibration, machine table vibration, spindle vibration, etc.

If suppressed the vibrations, such as by improving the dynamic unbalance of fly cutter, the machined surface quality by controlled cutting is expected to be improved even more. In that case, controlled cutting can works at a faster feed rate when

considering that the system response speed is fast enough and the control cutting efficiency can be higher.

If not suppress the vibrations, by slowing down feed rate, the peak-to-valley height of the regular fluctuations can be reduced, and then we can obtain a good quality machined surface by improving form accuracy using controlled cutting.

Chapter 5

Base on the principle of CCRS, not only the table motion error but also the disturbance from outside should be able to be suppressed. To prove it, in this experiment, artificial disturbance was added between the fly cutter and the workpiece, and the difference of machined surface with controlled cutting and without controlled cutting was compared and discussed.

The step height about 2 μm (affected by artificial disturbance) which appeared on the machined surface by uncontrolled cutting was suppressed to less than 0.6 μm by control cutting. The step was not able to be completely compensated because the gains of HIPOSS and LK-H008W did not match completely.

The cause of the dent shape on the machined surface after controlled cutting was that the PZT actuator could not respond to became short rapidly due to the control delay of this control system.

By adjusting the gain and improving the system respond speed, the machined surface quality with controlled cutting will be better.

Chapter 6

In this chapter, the experiment of circular arc machining by uncontrolled machining and control machining was conducted, and the effectiveness of improving the circular arc machining accuracy of the general-purpose milling machine was confirmed.

After taking the arc shape from the machined surface with roughness meter, the values of machined surface were $S_p = 0.0727 \mu\text{m}$ and $S_z = 0.4 \mu\text{m}$ after uncontrolled

cutting, while the values became to $S_p = 0.0373 \mu\text{m}$ and $S_z = 0.18 \mu\text{m}$ after controlled cutting. It showed that accuracy of arc machining was improved more than half. In order to further improve the precision of circular arc machining with this control cutting system, it is necessary to adjust the gain to match between HIPOSS and LK-H008W.

7.2 Future work

For chapter 3

Although the gain of I-PD in the control program is determined by the critical sensitivity method, there is no fixed formulation, so time and patience are necessary to determine the optimum value. I chose what I am currently using the one with the best follow-up among several kinds of trials, but it seems that it is not optimal. Therefore, in order to improve the followability of the control, it is necessary to finely adjust the condition and to adjust the gain again in next work.

Besides, the transformation coefficient also has an effect on machined surface by control cutting. (In control cutting process, by multiplying the signal value of LK-H008W by the transformation coefficient obtained in control program, accurate feedback control becomes possible). So in next work, a more accurate transformation coefficient value need to be obtained to improve the machined surface accuracy.

Furthermore, the noise measured by LK-H008W directly affect the machined surface by control cutting, since the output value of LK-H008W used as instruction value.

Based on above, it is necessary to be proved that the small waviness left on machine surface with control at feed rate 5mm/min is affected by gain, transformation coefficient and noise.

For chapter 4

In feed rate experiment, periodical regular fluctuations, which worse machined

surface, appeared obviously on machined surface with the increasing of feed rate, even if using control cutting. Therefore, this directly affect control cutting machining efficiency.

Although it is considered that periodical regular fluctuations were mainly caused by the dynamic unbalance of fly cutter, this inference need to be proved in next work. Slow down spindle speed at a same feed rate, and then measure the length of the regular fluctuations. If the length become longer correspondingly, this prove that dynamic unbalance of fly cutter caused periodical regular fluctuations. Therefore, by improving dynamic unbalance of fly cutter, we can improve the control cutting machining efficiency at a higher feed rate.

For chapter 5

In disturbance removal experiment, the dent shape had a big influence on Sz. Because the dent shape was caused by control delay of control system, in next work, we can improve responding speed of control system to reduce the depth of dent shape. In my study, two different AD/DA conversion boards were used and they cannot very compatible through Labview. So we can use a more compatible AD/DA conversion board to improve responding speed of control system.

For chapter 6

As mentioned above, in order to further improve the precision of circular arc machining with this control cutting system, it is necessary to reduce the noise measured by LK-H008W during machining and adjust the gain to match between HIPOSS and LK-H008W. For improvement of arc machining form accuracy, the next work is to control within the range of measuring angles where the gap sensor the sensitivity is better.

Acknowledgments

This thesis is a summary of the research conducted at Nagasaki University Graduate School of Engineering Doctoral Degree from 2016 to 2019.

First and foremost, I would like to express deepest appreciation and gratitude to my honorable research supervisor, Dr. Takanori Yazawa Professor, Nagasaki University Graduate School of Engineering, for his untiring guidance, constructive criticism and generous help in leading this research study with the truest professional manner until its successful completion.

Thanks Dr. Yasuhiko Ougiya associate Professor, Dr. Tatsuhiro Kojima associate Professor, Dr. Tatsuki Otsubo assistant Professor and Reiko Yamada Technical staff of Nagasaki University Graduate School of Engineering, and Dr. Tomonori Kato associate Professor of Fukuoka Institute of Technology Graduate School of Engineering for their useful advices on experiments. Giving thanks to Hideo Ito and other members of Precision Production Technology Laboratory for their cooperation and encouragement.

Highly appreciate General Manager of Nagasaki University practice factory, Hidetiki Kuda, and other technical staffs, who cooperated with me in all aspects such as installing experimental equipment.

I would like to express my deepest appreciation to Mr. Guochen Gu who cooperated with each other at the laboratory and conducted research together.

It's very important to express my indebtedness and love to my parents and my families, all of you give me courage, strength and confidence during my time away from home, which make me mature and sensible. Your unconditional forgiveness, loves and supports encourage me to never give up, and let me march forward courageously.

Finally, but by no means least, I express my deepest appreciation to Asian Student Scholarship Fund and Rotary Yoneyama Memorial Foundation, for awarding me the scholarship, which help me complete my desired research studies and have a chance to enjoy challenging with new experiences.